MECHANISM FOR INFLAMMATORY CYTOKINE-PROMOTED BREAST CANCER PROGRESSION: OSM-INDUCED LOXL2 LEADS TO EXTRACELLULAR MATRIX REMODELING OF COLLAGEN I AND SUBSEQUENT METASTASIS

by

Simion C. Dinca

A dissertation

submitted in partial fulfillment

of the requirements for the degree of

Doctor of Philosophy in Biomolecular Sciences

Boise State University

May 2023

BOISE STATE UNIVERSITY GRADUATE COLLEGE

DEFENSE COMMITTEE AND FINAL READING APPROVALS

of the dissertation submitted by

Simion C. Dinca

Dissertation Title: Mechanism For Inflammatory Cytokine-Promoted Breast Cancer Progression: OSM-Induced LOXL2 Leads To Extracellular Matrix Remodeling of Collagen I and Subsequent Metastasis

Date of Final Oral Examination: 17 March 2023

The following individuals read and discussed the dissertation submitted by student Simion C. Dinca, and they evaluated the student's presentation and response to questions during the final oral examination. They found that the student passed the final oral examination.

Cheryl L. Jorcyk, Ph.D.	Chair, Supervisory Committee
Daniel Fologea, Ph.D.	Member, Supervisory Committee
Richard S. Beard, Ph.D.	Member, Supervisory Committee
Julie Oxford, Ph.D.	Member, Supervisory Committee

The final reading approval of the dissertation was granted by Cheryl L. Jorcyk, Ph.D., Chair of the Supervisory Committee. The dissertation was approved by the Graduate College.

DEDICATION

I would like to dedicate the following dissertation with endless amounts of loving gratitude to my entire wonderful family, and particularly my parents Monica & Laurian Dinca. Thank you all so much for all the love and support you have shown and continue to show me, it did not go unnoticed. Thank you for always being there for me and believing in me, especially when I didn't believe in myself; without you I would not be where I am today on my journey through life. I appreciate everything and love you all!

Most of all, I want to dedicate this accomplishment with all my heart to my amazing late grandparents that greatly impacted my life, Simion Miti, Alexandrina Miti and Gicu Dinca; I know that you are all here in spirit watching over me. Cancer took you all away too soon, robbing us of so many memories. The suffering I witnessed; the unfairness, anger, and pain I felt as a kid losing the 3 of you to cancer all by the start of high school; inspired me to want to make a difference when I got older so that no one else would know the pain of losing their loved ones to this sinister disease. Thank you so much for the positive values you all instilled in me in the time we did have together; you will always be near and dear to my heart; I love you and miss you all so much!

ACKNOWLEDGMENTS

First and foremost, I would like to thank my PI, dissertation advisor, and overall fantastic mentor Dr. Cheryl L. Jorcyk for recognizing my potential and investing the time and resources necessary to foster my growth as a cellular and molecular cancer biologist. I am beyond grateful for the opportunity Dr. Jorcyk provided me; she believed in and took a chance on me, and in response I have accomplish more than I possibly could have expected. Throughout my Master's and Doctoral studies, Dr. Jorcyk has been an invaluable pillar of support that was always there to giving me encouragement when I needed it, yet she was also able to assess my progress with blunt honesty as she identified my areas of weakness and implemented strategies for improvement. Dr. Jorcyk pushed me to strive for excellence and to be the best version of myself, to be confident in my abilities and to embrace failure as an opportunity for growth, to be both self-reliant and capable of working with or collaborating with others, to never shy away from asking questions, and to always think critically about my scientific pursuits.

I would also like to extend my gratitude to professors in the Biomolecular Science department; Dr. Richard Beard, Dr. Daniel Fologea, Dr. Ken Cornell, Dr. Allan Albig, and Dr. Julia Oxford for broadening my breadth of scientific knowledge outside the realm of cancer cell and molecular biology. Further thanks, for the various ways each has contributed to my success and helped with my research over the years from: providing supplies and equipment, assisting with troubleshooting and development of experimental protocols, broadening the scope of my scientific knowledge, challenging me to approach

research with a chemistry and physics perspective, to sharing grant and manuscript writing tips and editing my drafts.

Of these professors, I want to give a special thanks to Dr. Oxford, Dr. Dr. Beard, and Dr. Fologea for accepting the responsibility of being members of my committee. I am grateful for the useful suggestions and ideas for improvement they have all taken time to provide regarding my dissertation research. They have all been fantastic choices in this role and I look forward to presenting my dissertation research and defense to them.

I would like to thank the Biomolecular Sciences (BMOL) Graduate Program for implementing a curriculum that covers a broad range of biomolecular topics with equal focus on the biology, chemistry, and physics of each topic and teaching me to look at research from a multidisciplinary point of view. Specifically, Beth Gee (BMOL Program Coordinator), Dr. Denise Wingett (BMOL Program Director), and office assistant Noah Souza for always being there to support BMOL graduate students like me, for keeping me up to date with deadlines and requirements, and for announcing opportunities for scientific growth and development. I also want to thank all the great graduate students in the BMOL program for the good times we shared and the difficult times we supported one another through, I am especially thankful for the friendships that I have formed with many of them, I know they all will be fantastic future scientists. I would also like to thank the Department of Biological Sciences front office for the notifications about order arrivals especially the sensitive ones. Additionally, I must thank Nicole Teregeyo and Sally Heckathorn, preventing delays to my research by assisting me with a variety of approval forms, order acquisitions, and assisting with outgoing shipments; and for always expressing such nice, cheery, and helpful attitudes whenever I have been around.

I would like to also acknowledge and thank all the wonderful Biomolecular Research Center (BRC) and Biomedical Research Vivarium (BRV) staff for assisting me with my research goals and allowing me access to equipment in order to facilitate the completion of my research. To Laura Bond, for all of the contributions she made as a secondary author on my journal publications; extracting and analyzing patient databases and performing statistical tests, in addition to the lessons she taught me involving those skills. To Dr. Shin Pu, for working with me on my proposed proteomic experiments and running my samples through a (LC/MS) mass spectrometer. To Dr. Cindy Peck, for the confocal microscopy training she provided and for the assistance she provided in troubleshooting ways for me to image collagen I fibers. Lastly, to Bev Montgomery and Chelsea Garrison, for the assistance both of them provided when it was required and for ensuring my in vivo experiments were successfully implemented by taking good care of the mice I purchased.

I would especially like to acknowledge and say thank you to my collaborators from the University of Haifa in Israel, Dr. Dalit Barkan and Dr. Keren Weidenfeld, for utilizing my research in applying for the NSF's Binational Scientific Foundation (BSF) grant we were later awarded, the grant provided a stipend for me and a significant budget for my M.S. / Ph.D. research over the last 4 years. I'm also thankful for their contributions as secondary authors on my publications and for allowing me the opportunity to do the same. Additionally, I want to thank the Graduate College for covering the part of my stipend that the BSF grant did not cover so that I could be a full time Research Assistant.

I would also like to thank my contacts at Pharmaxis Incorporated, Dr. Wolfgang Jarolimek and Dr. Lara Perryman, for working with me and providing excellent small molecule inhibitors (SMIs) that inhibit LOXL2 enzymatic function to successfully complete my research, all free of charge.

Last, but certainly not least, I am thankful for Dr. Jorcyk's Laboratory of Inflammatory Cytokines in Tumor Invasion and Metastasis and all those who have been part of our little lab family throughout my time in the program. Thank you to the current lab members Cody Wolf, Terrell Engmann, Maria Pou, Dena Duran, Jessie Northrup, Jessica Desjardin, Zahra Akbari, Andrea Feci, and Sierra Haile for providing a helping hand when I needed it, for going out as a lab to celebrate special occasions, and for the great banter I have been privy to daily. There have been too many students, both graduate and undergraduate, that have come and gone to individually thank; but I appreciate getting to know all of those great people and I'd like to thank them all for sharing in this experience with me and for involving themselves in this invaluable research. Having said this, there are a few previous lab members that need recognition for their positive impact on me. I want to thank Dr.'s Ken Tawara and Hunter Covert, the senior graduate Ph.D. students when I started, for helping me get my footing in the lab, answering all my many questions, sharing their wisdom, and being invaluable to my growth in the lab. To conclude my recognitions, I'd like to thank Daniel Greiner and Cody Wolf, for the valuable contributions they both made as secondary authors in my published research, for brainstorming their ideas with me, sharing their experiences and with various protocols, and pushing me to be the hard worker that I am today. Each of them has also made contributors to and are presented in those works.

ABSTRACT

Breast cancer has the highest prevalence of cancers in women in the USA; approximately 1 in 8 women will receive a diagnosis in their lifetime. Invasive ductal carcinoma (IDC) is the most commonly diagnosed breast cancer and presents a serious problem if it metastasizes, decreasing 5-year patient survival from ~98% to ~29%. Tumor cells grow in an environment that is known as the tumor microenvironment (TME). Due to inflammation, the TME of IDC is often saturated with neutrophil- and macrophage-derived proinflammatory cytokines including oncostatin M (OSM) and interleukin-1beta (IL-1β), both of which promote favorable conditions for metastasis. Modifications in the organization, density, and alignment of collagen I fibers present in extracellular matrix (ECM) of the TME directly impact IDC cell motility and invasiveness, both factors in metastasis. Lysyl oxidase like-2 (LOXL2) is an enzymatic protein secreted by fibroblast and IDC cells that catalyzes the crosslinking of collagen I fibers in the ECM. Increased collagen crosslinking alters the characteristics mentioned above, worsening patient prognosis and promoting metastasis. Proposed is a novel mechanism for proinflammatory cytokine-promoted ECM remodeling and subsequent metastasis in IDC. OSM signaling induces enzymatically active LOXL2 expression and extracellular secretion, leading to significant remodeling of ECM collagen I fibers that promotes significantly increased invasion, tumor growth, and metastasis. LOXL2-mediated ECM remodeling is also critical for OSM promoted IDC tumor growth and metastatic progression. Combined, these results demonstrate that OSM-induced LOXL2 has serious implications for IDC

tumor progression and metastasis. Further studies and understanding of the mechanisms at play in this association will hopefully lead to better therapeutic discoveries to prevent metastases.

TABLE OF CONTENTS

LIST OF TABLES

LIST OF FIGURES

LIST OF ABBREVIATIONS

BME	Basement membrane
βAPN	Beta-aminopropionitrile
BLI	Bioluminescent imaging
BSA	Bovine serum albumin
CAFs	Cancer-associated fibroblasts
CSC	Cancer stem cell
CTC	Circulating tumor cell
CI	Confidence interval
DMFS	Distant metastasis-free survival
DCIS	Ductal carcinoma *in situ*
ELISA	Enzyme-linked immunosorbent assay
EMT	Epithelial-to-mesenchymal transition
ER	Estrogen receptor
ERα	Estrogen receptor alpha
ECM	Extracellular matrix
FBS	Fetal bovine serum
FCIII	Fetal Clone III
G418	Geneticin
HR	Hormone receptor
HER2	Human epidermal growth factor receptor 2

IVC	Individually ventilated caging system
IACUC	Institutional Animal Care and Use Committee
IBC	Invasive breast cancer
IL-1β	Interleukin-1beta
IL-6	Interleukin-6
IDC	Invasive ductal carcinoma
JAK1/2	Janus kinase-1 or -2
MAPK	Mitogen activated protein kinase
MET	Mesenchymal to epithelial transition
MMP	Matrix metalloproteinase
NFκB	Nuclear factor kappa B
LIF	Leukemia inhibitory factor
LOX	Lysyl oxidase
LOXL1,3,4	Lysyl oxidase like-1 or 3 or 4
LOXL2	Lysyl oxidase like-2
LTQ	Lysyl tyrosylquinone
OSM	Oncostatin M
OSMR	Oncostatin M receptor
OS	Overall survival
PBS	Phosphate Buffered Saline
PI3K	Phosphoinositide 3-kinase
PVC	Polyvinyl chloride
PVDF	Polyvinylidene fluoride

PR	Progesterone receptor
ROS	Reactive oxidative species
qRT-PCR	Real time quantitative reverse transcription-polymerase chain reaction
RFS	Recurrence-free survival
ROI	Region of interest
STAT3	Signal transducer and activator of transcription 3
SMI	Small molecule inhibitor
TCGA	The Cancer Genome Atlas
TNBC	Triple negative breast cancer
TME	Tumor microenvironment
TAMs	Tumor-associated macrophages
TANs	Tumor-associated neutrophils
VEGF	Vascular endothelial growth factor

CHAPTER ONE: INTRODUCTION

The emphasis of this dissertation research is on mechanisms that promote tumor progression and metastasis in the most common type of breast cancer affecting women. Under Dr. Cheryl Jorcyk's mentorship, my research was primarily focused on how: i) ductal carcinoma cells alter extracellular matrix (ECM) in the breast tumor microenvironment (TME); ii) proinflammatory cytokine signaling, initiated primarily by oncostatin M (OSM) but also by interleukin-1beta (IL-1β), affect collagen and stromal ECM tissue remodeling; and iii) the subsequent alterations to the ECM promote breast cancer tumorgenicity, progression, and metastasis. Understanding the mechanism of OSM signal transduction involved in lysyl oxidase-like 2 (LOXL2) induction, and the synergistic relationship between OSM and IL-1β signaling pathways, which combine to significantly increase of LOXL2 expression, is valuable for breast cancer research. This introductory chapter serves as an overview of relevant topics, knowledge of which will be useful for understanding the research presented and discussed later in the dissertation. The following sections of the introduction contain pertinent background information regarding the subject matter highlighted in the section headings. Ideally, with this overview, readers of all backgrounds will be able to comprehend the significance of the data presented and how it fits into the bigger picture.

Cancer

Cancer is not new to humanity; in fact, it was Hippocrates (460-375 BC), the Father of Medicine himself, that coined the term cancer while studying the disease, and

named it after the Greek word for ‘crab’. [1] Cancer is an umbrella term used to classify a collection of cellular diseases that can be characterized by their uncontrolled cell proliferation, abnormal cell shape or morphology, irregular functionality, and most importantly the ability to spread both locally and distally to other tissues. Prior to bypassing the constraints maintaining localized growth, aberrant cells clinically regarded as neoplastic cells, are said to be pre-cancerous. If left undiagnosed or untreated, pre-cancerous neoplastic cells will eventually bypass the limiting constraints and spread out locally, invading neighboring tissues. This action renders the cells to be defined as malignant, which are officially considered cancerous. True malignant cancer involves, but is not limited to, the degradation of the encapsulating basement membrane (BME) by matrix metalloproteinases (MMPs), undergoing epithelial-to-mesenchymal transition (EMT) to promote cell detachment and motility, and stimulating the growth of nearby vasculature by secreting proangiogenic factors such as VEGF. Once the malignant neoplasm has spread to distant tissues through the circulatory and/or lymphatic systems, it receives the metastatic cancer label. The spread, formation, and subsequent growth of these metastases greatly reduces the odds of survival.

Cancers originate from normal cells that for various reasons progressively evolve into neoplasms, which will continue to acquire the hallmark capabilities that lead to neoplasm malignancy and ultimately metastasis. Some of these hallmarks are mentioned above, and they can also be found highlighted in **(Figure 1.1)**. [2] Overall there are a variety of biological factors that promote cancer progression; of noted importance are mutations to DNA, epigenetic destabilization, alterations to the tumor microenvironment (TME), and the activation of inflammatory response. [3, 4] The majority of cancers arise

from the epithelial cells that form glands, ducts, and the epithelium of organs; these are called carcinomas. In comparatively rare cases, there are instances of cancers forming from vascular endothelial cells, bone-forming cells, immune cells, as well as other cell types.

Due to the complexity of the disease, cancer remains one of the leading causes of death in the United States (US) and the world. As of 2020, cancer is the second leading cause of death, just behind heart disease, but the gap between these two has been steadily shrinking. [5, 6] In fact, as of 2023, the lifetime probability of receiving a cancer diagnosis is approximately 2 in 5 (~40.9%) for males and 1 in 3 (~39.1%) for women, with people over the age of 70 contributing the most. [7] Males receive more new cases and have higher incidence and mortality rates of cancer than women. This can largely be attributed to males' propensity for riskier jobs, worse health consciousness, and higher chances for exposure to dangerous environmental conditions. [7, 8] With the probability of getting cancer being so high, many cases occur annually. For 2023, in the US, it is estimated that 1,958,310 new patients will be diagnosed with some form of cancer, and 609,820 cancer-related deaths are projected. [7] The most commonly diagnosed forms of cancer in the USA by incidence rate per 100,000 individuals are breast, lung, prostate, and colorectal cancers, with other forms of cancer having less than 100,000 new cases a year. [7] These four cancers are also the most diagnoses worldwide. [9] As would be expected, these cancers also lead to the largest number of total deaths and incidence of death annually but in a slightly different order, with lung cancer being first, followed by breast, prostate, colorectal, and pancreatic cancer. Though these cancers have the highest number of deaths associated with them, the forms of cancer that have the lowest odds of

survival (over a 5-year period) in order are pancreatic, liver, esophageal, lung, stomach, brain, and ovarian; all of which are below 50% 5-year survival. Pancreatic cancer, unfortunately, is the deadliest with a 12% chance to live 5 years post diagnosis. [7] The healthcare costs for patients who are afflicted with cancer are large, with a national expenditure of over $125 billion each year since 2010. This increased to $183 billion for 2015, making it the fourth most costly chronic disease according to the CDC; behind heart disease, diabetes, and dementia. [10, 11] Estimates are that by the year 2030, the burden of healthcare expenses for all cancers will become 30% greater, with an expected annual cost of $246 billion to the US alone. The field of cancer research is by far the broadest field amongst diseases researched today, due in large part to the many different types of cancers that can arise and the heterogeneity of the associated cells. Therefore, treatments that work for some may not work for others, leaving plenty of possibilities for future cancer biologists to make an impact on the lives of those affected. Specifically, breast cancer is of utmost importance due to its prevalence in women in the US and around the world. Though the advancements in the field of breast cancer research have led to great strides in early detection and treatment options, there is still much work to be done especially when it comes to preventing, and treating, metastatic breast cancer.

Breast Cancer

Breast cancer is by far the most commonly diagnosed cancer in women in the US. The number of new cases for 2022 is approximately 287,850 for invasive breast cancer (IBC) and 51,400 for ductal carcinoma in situ (DCIS), which is a precancerous neoplastic growth that can lead to IBC if unattended. [12, 13] These cases, along with cases diagnosed in previous years, amount to the most devastating statistic for women; the

death of 43,250 grandmothers, mothers, wives, and sisters, all breast cancer victims claimed in 2022. [14] Men are fortunate to make up a very small proportion, at little more than 1%, of the total breast cancer cases each year. The estimated number of males that were diagnosed with some form of breast cancer in 2022 was around 2,710, and 530 deaths were estimated to have taken place. [14] Keeping in mind the fact that breast cancer predominantly affects women, it is truly depressing that for over a decade breast cancer has had the highest incidence rate, had the most overall diagnoses, and the 2nd leading cause of cancer-related deaths in the US annually. Sadly, this trend is expected to continue in 2023. [14]

Breast cancer research is currently booming, and there have been a lot of advancements in the last 20 years that have led to significant improvements in treatment options and the overall health of patients battling with IBC diagnoses. IBC use to predominantly be treated with radiation therapy and mastectomies, where doctors would surgically remove all or part of the breast tissue in order to remove the cancerous tissue. [13, 15-17] Thankfully, new developments have led to better therapeutic options, such as hormonal inhibitors and targeted therapies, that in addition to being effective against cancer, are far less invasive and traumatizing to patients as previous surgical techniques. [13, 18-20] Though surgery is still usually required, these other options have helped with not only improving patient outcomes but also improve quality of life once in remission. These new ways of treating IBC have led to a significant increase in positive prognoses for patients and have greatly improved the odds of survival (from 75% to 90% over a 5-year period). [7, 14] There are limits; however, and far too many breast cancer patients ultimately succumb to and die from this disease. Contributing to this is the fact that IBCs

develop immunity to drugs over time, and the tumor stage, or extent of tumor spread of IBC when it is first detected. IBC is classified into 4 stages with each stage correlating stepwise to increased neoplasticity, irregularity, and aggressiveness of the IBC cells. At stage III the tumor, or amalgamate of cancerous tissue, has spread to other areas of breast tissue **(Figure 1.2)**. [21] However, the overall survivability of IBC can still very high at this stage. It is when IBC becomes metastatic, or stage IV, that odds of survival plummet. In fact, if caught before reaching the metastatic stage of IBC progression, patient five-year survival is greater than 98%. If left undetected or untreated; however, IBC will eventually metastasis and when this occurs the chances of surviving drops precipitously to less than 29%. [8, 14, 22] Contributing to the metastatic phenotype, IBC exists in an inflammatory microenvironment, saturated by growth factors and proinflammatory cytokines released from tumor-infiltrating macrophages and neutrophils present in the stromal extracellular matrix (ECM). [23-25] Additionally, this leads to alterations in signal transduction and gene expression in the cancer cells that ultimately promotes immunity to the various cancer medications currently in use, contributing to aggressively invasive and untreatable forms of IBC. Due to the negative impact metastatic lesions have on patient survival, it is critical to understand the different types of IBC and the mechanisms they utilize to combat therapeutics and promote metastasis.

Types of Breast Cancer and Hormone Receptor Status

Breast cancer can arise from a few different breast cell types, leading to distinct types of breast cancer. The tissues that are most likely to become cancerous are the milk transporting ductal tissues that start at the base of the milk producing lobular glands and terminate at the nipple, and the lobules of the glands themselves **(Figure 1.3)**. [26, 27]

The milk is produced in response to hormonal stimuli, which play a major role in IBC progression. [28, 29] Prior to becoming cancerous, the tissue must first go through the process of neoplasia (new growth) until it forms precancerous tissues, classified as a pre-invasive neoplasm called ductal carcinoma in situ (DCIS) or lobular carcinoma in situ (LCIS), these then become invasive ductal carcinomas (IDC) and invasive lobular carcinomas (ILC) respectively **(Figure 1.4)**. [12, 21, 30, 31] When discussing breast cancer, it is the ductal tissue that is commonly thought of, because it is most likely to become cancerous and ultimately invasive, with IDC making up about 80% to 85% of all diagnosed breast cancers. [13] Lobular carcinomas make up the second most diagnosed form of breast cancers, with about 10% to 15% of the total diagnosed cases. [32, 33] In addition to these, some rare forms of breast cancer make up the remaining 5% of diagnosed cases. Included amongst these is inflammatory breast cancer, constituting 1% to 3% of cases. It results from ductal or lobular cancer cell blockage of lymphatic vessels causing excessive inflammation. It is very aggressive and results in up to 10% of annual breast cancer deaths. [34] There is also Paget's disease, a cancer involving anogenital tissue of the nipple, and phyllodes tumors that form from stromal tissue, but these are usually benign. [35, 36] As described, breast cancer is not just one type of tissue becoming cancerous or one route of pathology; therefore, research must be done on each separately to help address the nuances of each situation. Due to the much higher burden that ductal and lobular carcinomas have on overall breast cancer diagnoses, they are often the most studied form of IBC. To further complicate diagnoses, in addition to breast cancer types, genomic expression analysis of patient derived tumor biopsies across the 4 stages of disease progression revealed four biomarkers whose expression determines the

breast cancer subtype. [37] This, in addition to recurrence with observed resistance to initial treatments, provides evidence that breast cancer tumors are highly variable and are mostly heterogenic in makeup. [38]

Genomic expression studies performed on IBC cells have led to the identification of four major breast cancer subtypes in both IDC and ILC, that are distinguished by and correlate to the expression profile of four biomarkers: three receptors and a proliferation marker. IDC and ILC are organized into four subgroups based on the expression of two hormone receptors (HR), estrogen receptor (ER) and progesterone receptor (PR), an epidermal growth factor receptor called ErbB2 receptor (HER2), and the proliferation marker Ki67; all of which are important for determining cancers pathology. [13, 21, 39] The three receptors are critical for breast cancer cells to transduce signaling stimuli necessary to thrive and acquire hallmark characteristics for cancer progression. Entire classes of therapeutic treatments have been developed to block these receptors and prevent ligands from binding to them, thus inhibiting signal transduction and subsequent gene regulation that promotes breast cancer progression. [13, 14, 21, 26] However, as IBC progresses in patients, the breast cancer cells undergo mutations and new signaling pathways become activated to gain or enhance tumorigenic properties, eventually bypassing the need for these receptors to function and thrive. Consequently, the names and receptor profiles for the 4 major subtypes of IBC arranged in the order of least invasive to most invasive are listed here. 1) Luminal A breast cancer is hormone receptor positive (HR+), meaning it is positive for both ER and PR, and it is negative for HER2 expression (HER2-). Therefore, luminal A breast cancer is ER+ PR+ HER2-. 2) Luminal B breast cancer is ER+ PR+ HER2+/- Ki67+. 3) HER2-enriched breast cancer is ER-

PR- HER2+, with high levels of HER2 receptor expression. 4) Triple negative breast cancer (TNBC) lacks the expression of all 3 receptors and is labeled ER- PR- HER2-. [13, 26] TNBC can be further divided into basal-like A or B, mesenchymal, and mesenchymal stem-like subtypes. [18] Breakdown of IBC diagnoses approximate for luminal A, luminal B, HER-enriched and TNBC are 40%, 20%, 10-15% and 15-20% respectively **(Figure 1.5)**. [13, 18, 19, 26, 40, 41] Starting with luminal A IDC and progressively going through the IDC subtypes will there are several notable patterns observed. There is a shift from an epithelial to a mesenchymal phenotype, cells are less differentiated and more stem-like, increased chance of recurrence, and overall patient survival decreases. Identifying which of the 4 subtype characteristics the IDC tumor in patients have, or determining the subtype for IDC cell lines studied *in vitro*, is critical in advancing breast cancer research. This is due to the differences both phenotypically and genotypically associated with each subtype; therefore, each responds in a unique manner to chemokine, cytokine, and hormone stimulation. There has been some overlap observed between the subtypes, this is usually found in the subtypes that are adjacent to each other on the list.

Due to these differences, most of the time each subtype of breast cancer will require different treatment strategies and therapeutic drugs to combat the IDC for each of the subtypes, especially since a large class of breast cancer drugs do not work on TNBC since they inhibit hormone and HER2 receptor inhibitors for luminal A, luminal B and HER2-positive IDC. [17, 19, 20, 42] Many breast cancers tend to start out as luminal A and progress in a stepwise manner down to mesenchymal-like TNBC. [13, 18, 26, 38] This can also be the situation when IDC patients have a relapse and cancer comes back

after remission. Unfortunately, this generally results in more aggressive IDC cancer that has gained the hallmark characteristics of a more mesenchymal subtype. This development, known as IDC tumor cell progression, can ultimately lead to the metastatic lesions discovered in distant organs. Understanding how IDC progression works is of the highest priority in cancer research since this is the mechanism that leads to the formation of metastatic IDC. In the next section we will focus on IDC

Invasive Ductal Carcinoma Progression to Metastasis

As highlighted in the previous chapter, invasive ductal carcinoma or IDC is the most common form of breast cancer in women, accounting for over 80% of all breast cancer diagnoses. Due to the prevalence of IDC in the total patient population, my research and; therefore, the remainder of this dissertation will be focused specifically on the IDC form of breast cancer. Starting at the base of the lobular tissue, these ductal tissues extend from the nodes to the nipple of the breast facilitating the transfer of breast milk. [26-29] How normal ductal cells progress to IDC is described below. [43] 1) From healthy and fully differentiated epithelial ductal cells, an event, either spontaneous mutation or carcinogen exposure leads to the formation of neoplastic epithelial cells. 2) When that happens, the ductal epithelium begins a process of hyperplasia or increased proliferation, which progresses to apical hyperplasia as proliferation gets more pronounced. 3) Progressing further, the cells become less differentiated and display more abnormal morphology as cells spread inside the duct, forming a pre-invasive, basement membrane (BME) confined neoplasm known as DCIS. [30, 40] 4) As each cell divides mutations will build up until oncogenes gain function capable of basement membrane degradation allowing tissue infiltration, progressing to cancerous IDC **(Figure 1.4)**. [13,

31] 5) Cells continue to proliferate attaining gain of function oncogene and loss of function tumor suppressor gene mutations until becoming malignant and metastasizing. [12, 44] When IDC metastasizes, it does so by directly spreading to nearby tissues or infiltrating lymphatic tissue and vasculature, utilizing these circulatory systems to circulate throughout the body forming distant metastases **(Figure 1.6)**. [13] Dysregulation of the proinflammatory pathways, loss of reliance on hormone receptors, and mesenchymal phenotype transitions are are just some of the important oncogenic functions involved in IDC becoming malignant.

The following sections will cover various mechanisms involved in promoting metastasis that studies in Dr. Jorcyk's lab are predicated on. This includes proinflammatory cytokine promoted changes in IDC morphology by mediating epithelial-to-mesenchymal transition (EMT) in cancer cells, degradation of the BME and remodeling of stromal extracellular matrix (ECM) in the TME, losing cell-to-cell junctions and contact inhibition, and activation of proangiogenic factor secretion. These are facilitated by important biological processes and cellular interactions manipulated to assist tumor progression and ultimately metastasis.

Tumor Microenvironment

The tumor cells themselves are not alone in the propagation and progression of the cancer. One of the largest contributors to the overall maturation of the tumor cell tissues is the tumor microenvironment (TME). Conditions of the local environment in which a cell resides can vary widely depending on several factors such as: i) extracellular matrix (ECM) composition of the stroma and basement membrane (BME), [45-48] ii) cells that are involved in nearby signaling which can be hijacked by the tumor cells, [25,

49-54] and iii) inflammatory response and proinflammatory cytokine signaling, just to name a few. [25, 54-56] In recent years, the TME has been recognized for its involvement and significant impact on IDC tumor cell progression and activation of signaling pathways that affect phenotype, genotype, and morphology. [57-61] The composition, characteristics, and the cellular backdrop of the ECM forming the TME affect interactions with membrane bound proteins on tumor cells. For example, β-integrins and cluster of differentiation-44 (CD44) proteins membrane proteins actively promote inflammatory cytokine secretion and oncogene expression that impact tumor progression. [48, 62-67] Molecules found within the TME can promote changes in normal tissue leading to neoplasia, this includes hydrogen peroxide and other reactive oxidative species (ROS) formed in redox reactions. In high concentrations the unstable free radicals trigger oxidative reactions altering protein function and damaging DNA. [68, 69] The TME also contains fibroblasts and immune cells such as macrophages and neutrophils that normally respond to wound healing and inflammation stimuli. They response to stimuli from IDC tumor cells in a similar manner promoting recruitment to the TME. The IDC tumor cells will secrete chemokines and cytokines that reprogram/ polarize the cells forming cancer associated fibroblasts (CAFs), tumor associated macrophages (TAMs), and tumor associated neutrophils (TANs). In this state they will secrete enzymes, growth factors, cytokines, and chemokines that promote tumor progression and increase tumorigenicity **(Figure 1.7)**. [25, 67, 69-74] The TME is dynamically involved in breast cancer progression, with rapid and dramatic responses to stimuli that take advantage of cellular responses to inflammatory factors and promote epithelial-to mesenchymal transitions (EMT). [75-78] The inflammation and ECM

composing the TME that are important for my research and that impact IDC growth, progression, invasion, and metastasis are highlighted in greater detail below.

Inflammation and Inflammatory Cytokines

Inflammation is critical to IDC tumor cell progression because of the impact it has on various critical functions associated with worsening prognosis. [76, 79-81] Formation of ROS is one important factor in the proinflammatory response in cells, which then combine to promote cytokine expression, DNA damage and increases rate of mutation. [68, 69, 79] IDC inflammation occurs due to many factors that are both extrinsic and intrinsic, and is often associated with immune cells such as macrophages, monocytes, and neutrophils. [24, 25, 82, 83] Inflammatory cytokines such as interleukin-6 (IL-6) and other cytokines in the gp130 family, such as OSM, are known for their role in both acute and chronic inflammation and in promoting cancer progression. [84-86] In addition to IL-6-family of proinflammatory cytokines, the interleukin-1 (IL-1)-family which includes interleukin-1beta (IL-1β) also have a similar duality in their roles in inflammatory response and tumor progression. [87] The current paradigm in inflammation and cytokine-induced ductal tumor development is IL-6 signaling promotes progression and metastasis. [88-91] However, research shows that IL-6's sister cytokine OSM also promotes invasion and metastasis in a manner independent of IL-6. [23, 54, 92, 93] The roles that both OSM and IL-1β play in association with the tumorigenesis and the promotion of metastatic IDC are discussed in the following sections. These are not the only families of cytokines but they are central to the research our lab performs involving IDC progression and metastasis.

Oncostatin M

OSM is a pleiotropic IL-6-related cytokine that is essential for the inflammatory response and is produced by activated T-cells, macrophages, monocytes, and neutrophils. [54, 94, 95] OSM is secreted and can bind to type I collagen and other ECM fibers, remaining active for extended periods of time which promotes signaling in invasive cells. [96] Signaling is prompted when OSM binds to the gp130 receptor subunit, which leads to the recruitment and dimerization with the OSM receptor β (OSMRβ) subunit forming the receptor complex (OSMR). [97, 98] OSM signaling can also occur when OSM bound gp130 subunit dimerizes with the leukemia inhibitory factor beta (LIFRβ) subunit forming the receptor complex (LIFR); [99] however, OSM has an affinity for OSMR that is orders of magnitude greater. [100] This action then leads to the phosphorylation and activation of the JAK/STAT, PI3K/AKT, and MAPK/ERK signaling pathways. [101] Once activated, these pathways alter gene expression so that breast cancer cells progressively become more motile, invasive, and metastatic.

Currently, it is thought that OSM promotes invasion and metastasis by stimulating an epithelial-to-mesenchymal transition (EMT) in breast ductal carcinoma cells through the up- or down-regulation of specific genes that disturb cell polarity, reduce differentiation, and promote motility **(Figure 1.8)**. [102-105] EMT is stimulated through destabilized localization of E-cadherin or its downregulation, as well as an increase in Vimentin, Snail-1, and N-cadherin gene expression. [106, 107] Our lab, as well as others, have demonstrated that OSM induces the upregulation of: i) vascular endothelial growth factor (VEGF) that leads to angiogenesis, [108] ii) circulating tumor cell (CTC) numbers, [55] and iii) lung and bone metastases *in vivo*. [23] Previous research highlights the

important and role that OSM signaling plays in IDC progression and metastasis. However, though OSM can activate CAFs, the impact OSM signaling has on ECM remodeling of the IDC cell tumor microenvironment (TME), has yet to be explored. [60]

Interleukin-1Beta

Another important proinflammatory cytokine family for IDC progression in patients is called the interleukin-1 (IL-1) family. One of the members in this family, interleukin-1beta (IL-1β), is of interest to research preformed in our lab. As a proinflammatory cytokine in the IL-1 family, it binds to a receptor complex composed of IL-1 receptor type I (IL-1RI) and IL-1 receptor accessory protein (IL-1RAcP). [109] IL-1β induces the NFκB signaling pathway and similar to OSM and other IL-6-family proinflammatory cytokines the MAPK signaling pathway. [110] NFκB pathway activation has been shown to increase breast cancer cell proliferation and invasion by increasing CD44 expression, which promotes cell migration, survival, and increased stem cell-like characteristics. [111] Additionally, IL-1β stimulates the secretion of proteases such as MMPs that degrade the ECM basement membrane allowing tumor cells to spread and metastasize. [112-114] NFκB signaling has also been shown to be associated with the development of breast cancer stem cells, which can repopulate regions of metastasis after the tissue is thought to have been eliminated therapeutically. [87] Similar to attempts at creating therapeutics that inhibit IL-6-family cytokines, drugs against IL-1β have been developed, and some are currently on the market, however, none are FDA approved for breast cancer or any other cancer patients due to no appreciable improvement in prognosis compared to current therapies.

The Extracellular Matrix

The ECM is broken down between stromal connective tissue, cellular basement membranes, and the various ligament and cartilages in humans. The extracellular matrix (ECM) plays an integral role in tumor progression, as remodeling the ECM of the tumor microenvironment is critical for ductal carcinoma invasion and metastasis. [47, 48, 61, 70, 115, 116] For invasive ductal carcinomas and other cancers originating in the epithelium to progress towards malignancy they must first degrade and bypass the basement membrane (BME), a specialized layer of ECM primarily composed of collagen IV that forms a barrier between the epithelial layer and the stromal tissue separating the organs. [117, 118] After the BME is degraded, IDC cells are capable of invading nearby tissues and intravasating vasculature by migrating through the stromal ECM. [46, 47, 59, 119-122] To promote the spread into the stroma and beyond, IDC cells and associated CAFs modify collagen and elastin fibers, and other structural proteins in the stromal ECM. This involves secreting peptomers of structural proteins and/or protein enzymes such as lysyl oxidases to enzymatically catalyze remodeling that affects orientation, density, and stiffness promoting invasion and metastasis. [116, 119, 123-125] Alignment of stromal collagen I fibers facilitate directed tumor cell motility, and increases their velocity, to reach nearby vasculature and/or tissue, as opposed to haphazard motility that occurs when randomly oriented. [126-128] These changes in ECM characteristics are analyzed to get a better picture of the mechanisms and enzymes involved and lead to the remodeling and subsequent improvement in metastatic potential.

ECM Proteins and Enzymes

The ECM collectively refers to the milieu of structural proteins that comprise the connective tissues that separate and also envelope cellular tissues, such as the epithelial and endothelial cell layers of organs and vasculature **(Figure 1.9)**. [45, 47, 61, 116] There are several structural proteins that compose the ECM including collagens, elastin, proteoglycans, and glycoproteins. [61, 123] Of these, collagens are the most diverse and found abundantly throughout the ECM. Fibrillar collagens like collagen type I and III are most commonly found in the stromal ECM, with collagen I making up ~80% of the total collagen in the stromal tissue of the breasts. [65, 129, 130] This is a significant fraction of the total ECM as collagens make up ~30% of a human's total protein mass. [131] The BME has a different makeup and is predominantly composed of non-fibrillar collagen IV, making up ~50% of any given basement membrane. [45, 117] The BME is located in between epithelial cell layers and the stroma, forming a barrier between these the stroma and epithelium. The stromal ECM houses a variety of glands, nerves, blood vessels, fibroblasts, and immune cells. Fibroblasts maintain the ECM structure and change density by secreting structural protein peptomers composing collagens, elastin, and glycoproteins. [51, 52] Fibroblasts and IDC cells can also modify the ECM stiffness, density, and orientation through the secretion of enzymes such as MMPs, lysyl oxidases, cathepsins, and plasmin. [72, 132] Lysyl oxidases, specifically LOXL2, is the enzyme my research is predicated on, produced by IDC cells.

Lysyl Oxidase Family

Amine oxidases make up a large contingent of enzymatic proteins that function to catalyze oxidative deamination of differing primary amines. These can be separated into

poly-, di-, and mono-amine oxidases; correlating to the number of amine groups present in the reaction substrate. [133] One such family of monoamine oxidases are known as lysyl oxidases, this family includes lysyl oxidase (LOX) and lysyl oxidase like-1/2/3/4 (LOXL1-4). [134, 135] These are copper dependent enzymes containing a copper binding domain and lysyl tyrosylquinone (LTQ) cofactor site in the catalytic domain, which make up the highly conserved C-terminal. The N-terminal on the other hand varies between family members, with LOXL2/3/4 all containing 4 scavenger receptor cystine-rich domains (SRCR) domains not present in LOX and LOXL1. [136] The catalytic domain promotes the enzymatic activity, initiating the oxidative deamination of peptidyl lysine and hydroxylysine present in collagens and elastin to form allysine and hydroxyallysine. [137] The resulting aldehydes spontaneously react to form a covalent bond between themselves, with hydrogen peroxide (H2O2) as a byproduct. [135] This reaction is essential for the biogenesis of collagen fibrillation and is known as crosslinking, the lysyl oxidase family of enzymes is the only known proteins to initiate this reaction, LOXL2 in particular for my research **(Figure 1.10)**. [138, 139]

The crosslinking reaction leads to the formation of immature crosslinked collagen I abundantly found in the stroma, as well as other fibrous collagens such as collagens III and IV. As they become dimerized at fibrillar polymeric peptides terminal ends due to the spontaneous covalent bonding of the aldehyde formed on the peptidyl lysine and hydroxylysine and bind together in a side-by-side formation like you would lay bricks. [140] This nomenclature has left some earlier scientists confused when regarding crosslinking, as the name implies that the fibers are binding in a cross-like manner and this is not the case, as will be discussed in the next section. Eventually, without the

further need for lysyl oxidases to initiate it, the mature crosslinked form of collagen will result from the immature dimers, these are trimeric crosslinks that promote the maturation of the extracellular matrix. This process needs the initial dimerization catalyzed by LOXL2 to allow for the trimer to form and ECM to mature.

Lysyl oxidases are essential for the continued maintenance of collagen fibers in the stroma, basement membrane, and other fibrous tissues such as skins dermis and sub-dermis, as well as tendons and ligaments in and around our joints. The crosslinking causes collagens basic building blocks, known as fibrils, to associate with one another to form fibers, which can continue being crosslinked in this mechanism which can ultimately lead to the formation of ligaments and the healing of damaged fibrotic tissue. This family of enzymes has not been studied in as much detail as many of the other proteins in the ECM, and new advances are always coming out showing new way these unique proteins are involved in human biological processes. Unfortunately, due to the nature of their ECM remodeling, LOXs have become a critically important factor in cancer research, and specifically breast cancer research. This is in large part due to observations that have shown that denser more fibrotic breast ECM tissues in IDC patients irrefutably leads to a worse prognosis. [141-144] The lysyl oxidase that I have been studying, and the one my research in IDC is predicated upon, is the collagen I and to a lesser extent collagen IV targeting lysyl oxidase-like 2 (LOXL2). In the following section, I will briefly discuss the impact that it has on cancer progression, and why it plays an important role in breast IDC metastatic potential.

Lysyl Oxidase Like-2

LOXL2 is normally highly expressed by fibroblasts or myofibroblasts and epithelial cells express much less of the protein, however, IDC cells activate LOXL2 expression giving them the ability to modify the TME. [119, 125, 145, 146] Lysyl oxidase like-2 (LOXL2) expression has been linked to a worse prognosis in IDC patients, and increased invasion and metastasis of breast tumor cells. [147-149] LOXL2 is also involved in premetastatic niche formation in ECM of distant organs. [150, 151] LOXL2 expression is upregulated in IDC cells and the LOXL2 mRNA is translated into the protein's native conformation. In this state LOXL2 is found in the cytoplasm, measuring ~87 kDa and is inactive with no known cellular function. From its native conformation two different post translational modifications ensue activating LOXL2, which determines LOXL2's ultimate destination and function. It can undergo proteolytical processing and cleavage of the C-term domain resulting in a ~75 kDa LOXL2 protein that is transported into the nucleus. [135, 136] When localized to the nucleus, LOXL2 was observed stimulating invasive and stem-like properties in IDC cells. [152-154] Additionally, LOXL2 promoted EMT through the stabilization and/or upregulation of the transcription factor (TF) Snail-1. [78, 155-157] The native LOXL2 can instead undergo N-linked glycosylation at two asparagine amino acids, located at N593 and N627. [78] This increases the size of LOXL2, appearing as a ~105 kDa protein, which constitutes the enzymatically active form of the protein that is secreted extracellularly and initiates the formation of collagen crosslinks. [78, 134, 135] By catalyzing collagen I crosslinking, LOXL2 secreted by IDC cells can modify the nearby ECM and promotes increased fiber alignment, density, thickness, and stiffness. [119, 158] These effects that LOXL2 has on

stromal ECM collagen promotes dense fibrotic breast tissues, which leads to worse IDC patient prognosis. [141, 142, 159] Modifications to the ECM reduce IDC cell energy consumption during motility and increases velocity, promoting cancer malignancy. [158, 160] In my dissertation research, I was able to show that OSM signaling led to the induction of LOXL2 expression in IDC cells. [146] This significantly impacted collagen I fiber crosslinking and alignment which ultimately resulted in increased invasion and tumor cell metastasis. [146]

Synergistic Interactions

A synergistic interaction occurs when two or more factors combine to increase the expression of a protein of interest beyond what each factor would be capable of individually. [161] When the factors are not synergistic the combined effect on expression is equal to the sum of each individual factors impact on expression, it is an additive interaction. The opposite of a synergistic interaction is known as an antagonistic interaction, or a 'synergetic decrease' in expression resulting from the combination of factors. Several studies have shown evidence that there are overlapping functions between the pSTAT3, pAKT, pERK, and NFκB signaling pathways in IDC ells. This could promote synergistic effects when multiple pathways are activated by cytokines from different families, specifically OSM and IL-1β. In fact, one of our labs previous Ph.D. students Dr. Ken Tawara, showed examples of these synergistic interactions in his research. [162] Indeed, other studies show the potential for synergistic interactions as well. [163] OSM and IL-1β was also observed in my research to synergistically promote LOXL2 expression, highlighted in Chapter 3. The promotion of these synergistic responses in oncogenes are of great importance when it comes to breast cancer

progression and metastasis leading to fold increases several times larger in protein expression than either could affect individually.

Transcription Factor c-Myc

The transcription factor c-Myc is a tightly regulated immediate early response proto-oncogene that plays a significant oncogenic role in IDC and other cancers. [164, 165] As a well-known proto-oncogene, c-Myc plays a pivotal role in cell growth, proliferation, tumorigenesis and cell differentiation. c-Myc also lies at the crossroads of signal transduction pathways found downstream of multiple ligand-receptor complexes, including JAK/STAT, MAPK/ERK, and PI3K/AKT. [164] Because of this c-Myc is often mutated to bypass restrictions that suppress its expression and becoming an oncogene as cancer progresses, a very potent oncogene. [114, 165-167] In fact, c-Myc mutations lead to epigenetic destabilization and throws off the cell cycle modulators such as p21. [168] Binding to the E-Box promoter sequence that is found coded in the DNA, specifically in the promoter sequence of many proteins that c-Myc is responsible for activating or enhancing. [169]

Summary

Our research on IDC suggests that OSM signaling plays a prominent role in cell's ability to remodel the primary constituent of stromal ECM, collagen I. Remodeling occurs as OSM induces the expression and secretion of the matrix remodeling enzyme lysyl oxidase-like 2 (LOXL2) in IDC cells. Understanding how OSM regulates LOXL2 production, and more broadly matrix remodeling of the stroma, will shed light on the effect inflammation has on the TME of IDC patients. Breast cancer patients with dense breasts also have a worse prognosis than those with normal density, suggesting that ECM

remodeling promotes cancer progression. This clinical finding correlates with published breast cancer patient survival data demonstrating that patient survival is significantly diminished when there are elevated levels of LOXL2 expression. This is critical, as our research demonstrates that high OSM and LOXL2 co-expression in IDC patients leads to a drastic decrease in metastasis-free survival. Hence, our research will lead to a better understanding of the dynamic nature of inflammation promoted metastasis.

Chapter One Figures

Figure 1.1 Hallmarks of Cancer Progression.

This illustration highlights the different mechanisms for cancer cell progression to become malignant. There are a total of 10 cellular events or 'hallmarks' that develop in and around a tumor, accumulating as cancerous tumors progress towards malignancy, contributing to the formation of distant metastases. The multicolored icons that form a ring around the central tumor illustration, with arrows pointing inward, are representative and labelled with the 10 hallmarks. Individually, all of these cellular processes are also important to progression and increasing tumor invasive potential. (Taken from [Hanahan 2010] [2]; License granted for Copyright use, no modifications made).

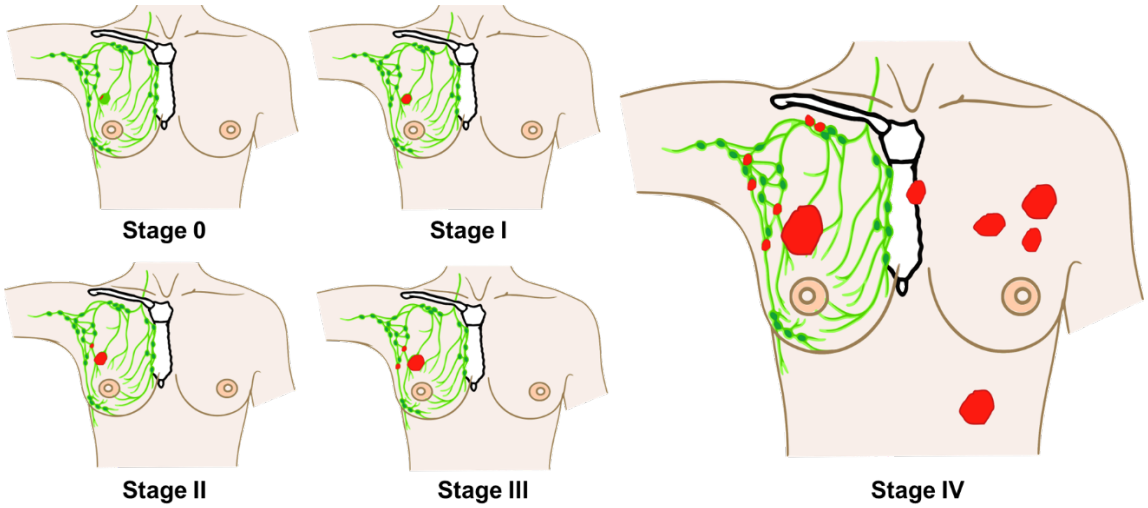

Figure 1.2 Illustration of Local and Distal Spread of Cancerous Tissue Related to Breast Cancer Staging.

There are several methods to classify invasive ductal carcinomas (IDC) progression. The most commonly utilized method that people are familiar with is known as breast cancer staging, where increases in stage corresponds to an increase in level of cancer cell spread. The illustration in this figure depicts the characteristics of each stage of the general staging system. [21] *Stage 0:* this stage designates non-invasive tumors, or DCIS, and can be any size. *Stage I:* refers to early-stage IDC and characterized by small tumor less than 2 cm in diameter that has broken free of basement membrane. *Stage II:* involves IDC characterized by tumor that is 2 cm - 5 cm and spread beginning into neighboring ducts or lobules with possibility of lymph node infiltration to the nearest node. *Stage III*: is associated with IDC that has spread to tissues nearby breast tissue such as skin, chest wall, or ribs; or having infiltrated extensive numbers of lymph nodes. *Stage IV*: this is characterized by IDC that has become malignant with distant metastases present. For a more robust analysis of spread there is also a TNM system, where each letter represents staging for Tumor, Nodes (lymphatic), and Metastases. (Credit to Cancer Research UK/ Wikimedia Commons for original image. Open Access - Creative Commons (CC) 4.0, modified in accordance to CC BY-SA 4.0 guidelines).

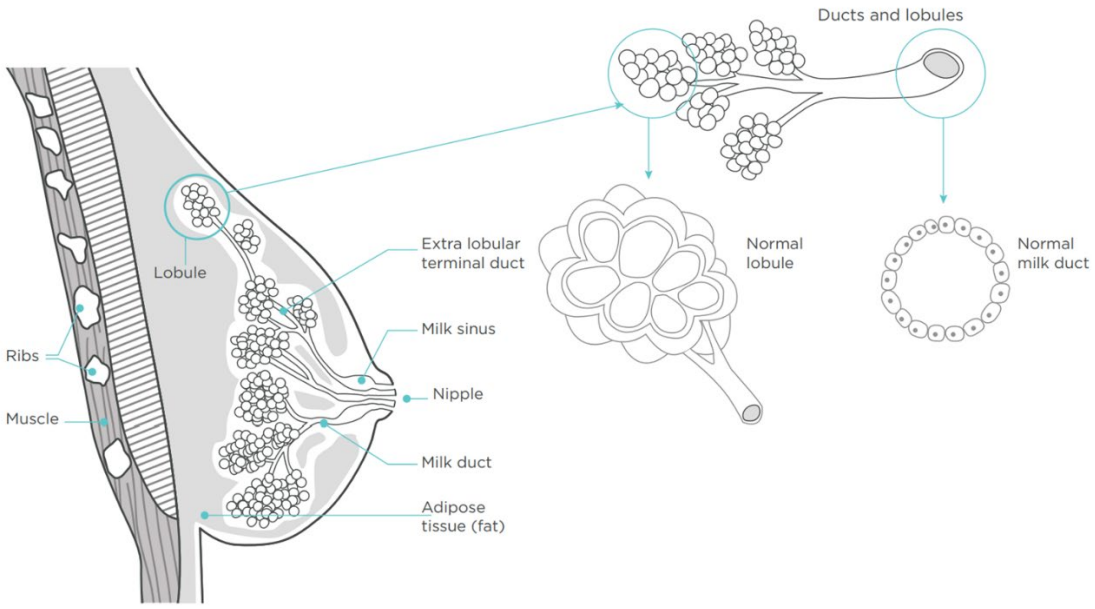

Figure 1.3 Cross-Section Illustration of the Breast Tissue and Close Up of the Lobule and Duct Forming Tissues.

This cross-section of a breast illustrates the lobular and ductal tissues present in the in the breast tissue. As shown the lobules start deep into the tissue and are connected to the nipple by the ducts. These tissues respond to hormone signaling from oxytocin and prolactin during pregnancy and after birth to secrete milk and transport the milk to the nipple. These tissues also respond to estrogen and progesterone hormones, through their respective receptors abbreviated as ER and PR, which promote cellular growth, proliferation, and development of the tissues. These receptors are important in regards to breast cancer progression, where the cells grow and proliferate in excess within the lumen prior to breaking out of their confines, or basement membrane separating epithelial cells from stroma and other tissues. (Public Domain (Copyright expired); Taken from and originally published by Cancer Australia in 2003).

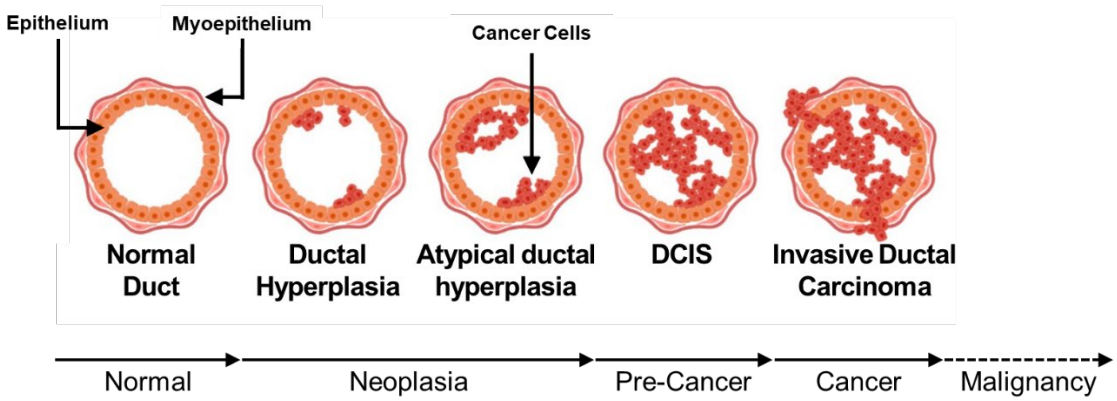

Figure 1.4 Ductal and Lobular Tissues Where Ductal Carcinoma and Lobular Carcinoma Forms.

As highlighted in the illustration, IDC begins in the normal ductal tissue of the breast, where mutations in one or more epithelial cells (or as some believe, stem cells) causes cells to undergo ductal hyperplasia or uncontrolled proliferation of the ductal cells that have undergone mutation [31]. This is followed up by atypical ductal hyperplasia where morphologic and phenotypic changes occur as the cells continue proliferating, receiving characteristics similar to those of IDC cells. During these steps the ductal cells are also known as undergoing neoplasia. As proliferation continues, additional mutations occur and further alterations in cellular features eventually leads to the formation of DCIS, or a not yet invasive tumor confined by the ductal basement membrane (BME). These tumors can be small or large, so long as they are unable to enter the stromal tissue, they are considered pre-cancerous. However, with the right mutations activation of oncogenes that promote the degradation of the BME will eventually occur, making the aberrant proliferating ductal cells into invasive ductal carcinomas (IDC) cells officially becoming cancerous. The last step in the IDC maturation involves more oncogenes that promote cellular infiltration of nearby tissues, vasculature, and lymphatic channels which makes the IDC become malignant resulting in metastasis to various organs. (Taken from [Tower 2019] [31]; Open Access - CC 4.0, modified in accordance to CC 4.0 guidelines).

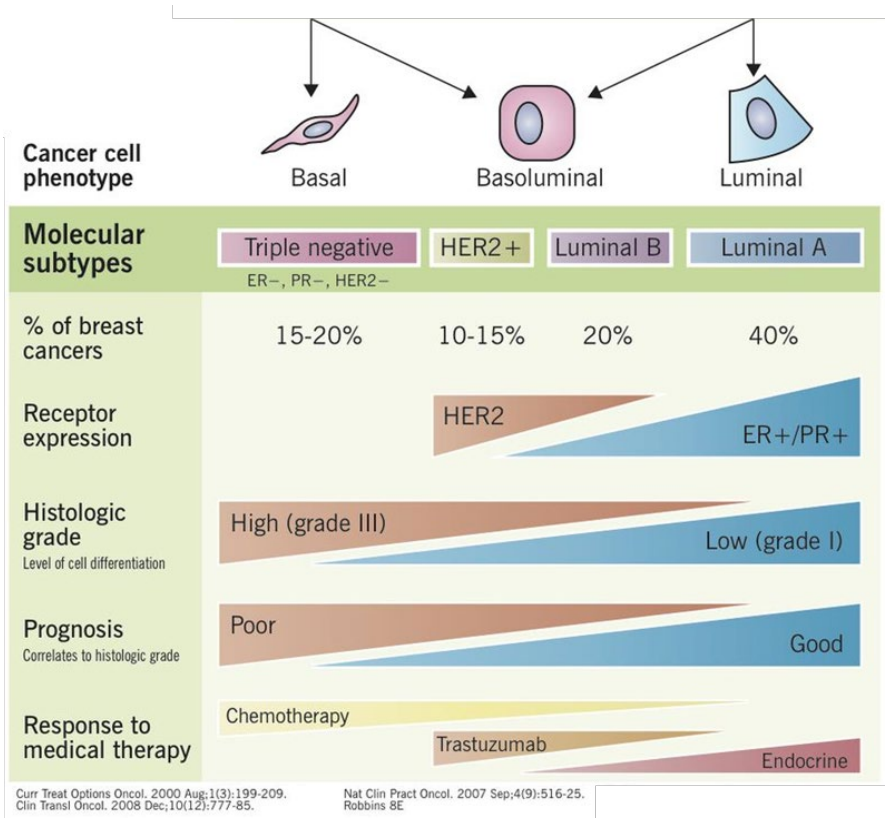

Figure 1.5 Invasive Ductal Carcinoma (IDC) Subtypes, Associated Phenotypes, and Distribution Amongst Patient IDC Cases.

Invasive ductal carcinoma (IDC) is one of several different types of breast cancer, and also the most prevalent in ~80% of patients. However, IDC is not composed of one homogeneous mutation of ductal cells gone awry and is instead a heterogeneous mixture of cells with various mutations and therefore phenotypes. They are categorized into 4 subtypes according to Ki67 proliferation marker, hormone and epidermal growth factor receptor expression: 1) luminal A is ER+ PR+ and HER2- (Ki67 low), 2) luminal B is ER+ PR+ and HER2+/- (Ki67 high), 3) HER2+ is ER- PR- HER2+ (Ki67 high), and 4) triple negative (TNBC) is ER- PR- HER2- (Ki67 high). These are found in patients at 40%, 20%, 10-15%, and 15-20% respectively. From 1 to 4 there is a correlation to higher grading, worse prognosis, and change from epithelial-like to basal-like morphology. (Public Domain; Publications informing the graphic illustration are referenced in at the lower left corner). [26, 40, 41]

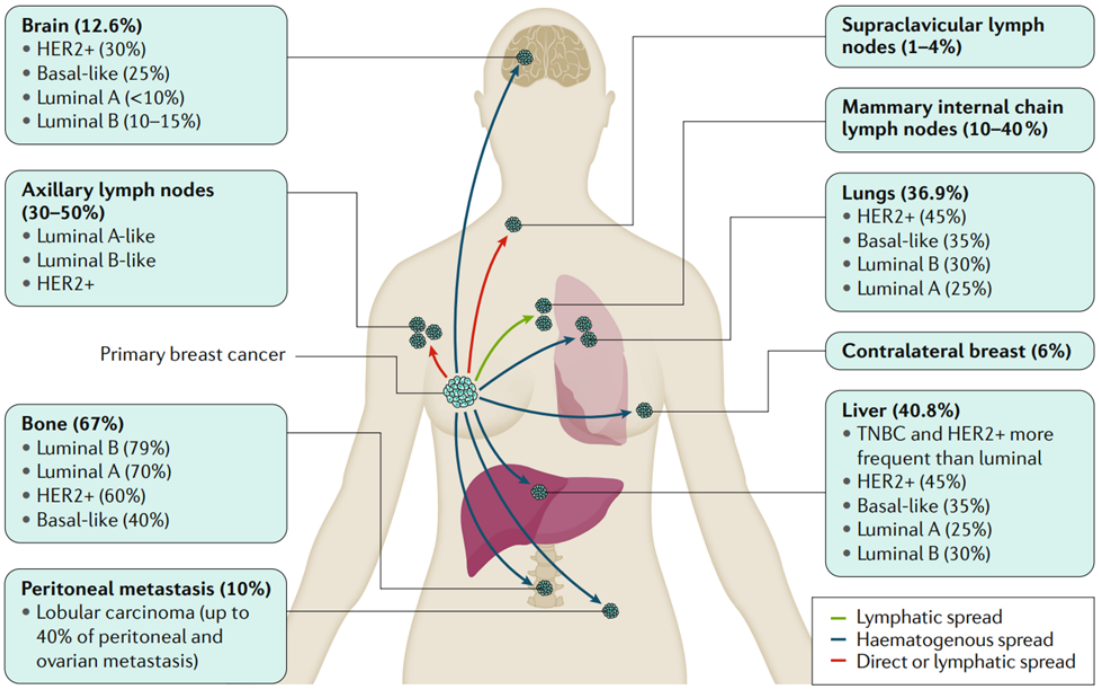

Figure 1.6 Metastasis of IDC with the Most Common Areas and Methods Utilized During Metastasis.

As IDC cell progression continues more oncogene gain of function and tumor suppressor loss of function mutations occur that will ultimately lead to malignancy and metastasis to distant organs. To do this IDC tumor cells will either invade the tissues by directly spreading through the connective tissue or stromal ECM (red arrows) or by the bodies circulatory systems, either thru hematogenous spreading by means of vascular intravasation and extravasation (blue arrows) or by infiltration of the lymphatic system (green arrows). The resulting organs and prevalence in patients (%) for common points of metastasis are labeled in the figure illustration. (Taken from [Harbeck 2019] [13]; License granted for Copyright use, no modifications).

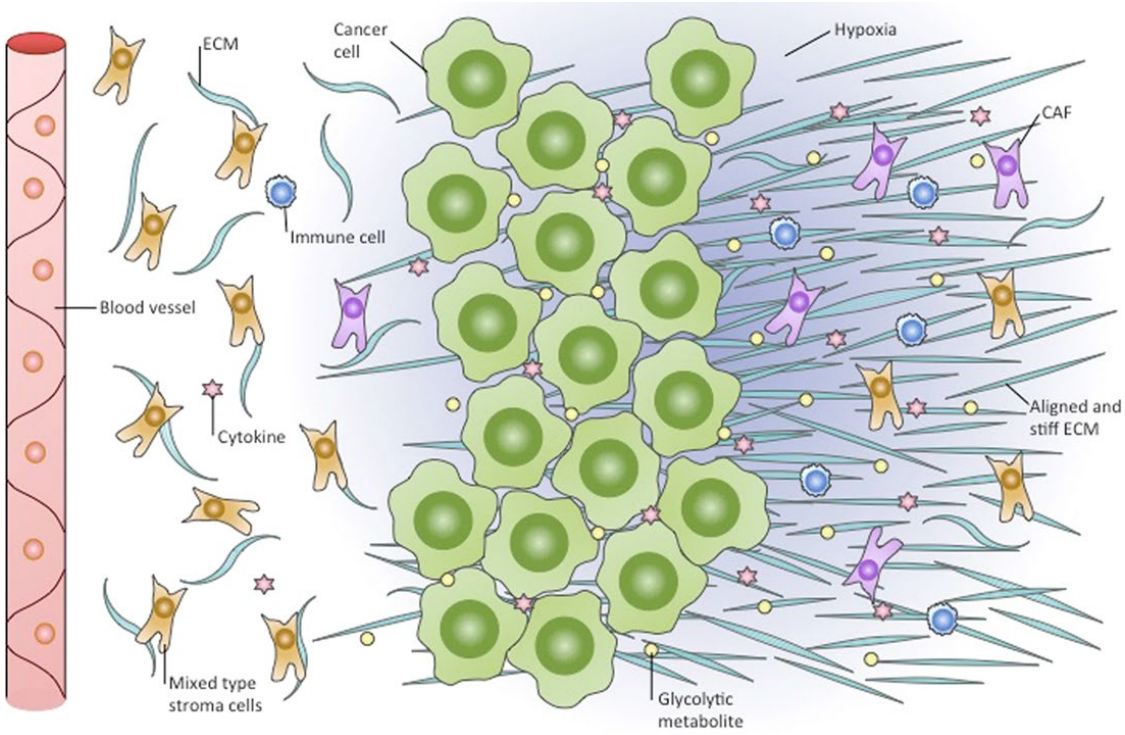

Figure 1.7 IDC Tumor Cell Signaling Converts Stromal Fibroblasts, Macrophages, and Neutrophils into Cancer/Tumor Associated CAF, TAM, and TAN Respectively Promoting Tumorigenesis.

The TME is primarily composed of stromal ECM tissues that the IDC tumor enters once degradation of the BME occurs. Within the stroma there are both fibroblasts and immune cells such as neutrophils and macrophages that respond to epithelial cell signaling stimuli involving wound healing or in response to inflammation. The IDC tumor cells exploit these mechanisms by secreting similar factors promoting fibroblast, macrophage, and neutrophil recruitment to the TME. IDC will continue to secrete chemokines and cytokines that reprogram the cells forming cancer associated fibroblasts (CAFs), tumor associated macrophages (TAMs), and tumor associated neutrophils (TANs). In this state they will secrete enzymes, growth factors, cytokines, and chemokines that promote tumor progression and increase tumorigenicity through epithelial-to-mesenchymal transition (EMT), angiogenesis, and ECM matrix remodeling. IDC tumor cells in a sense corrupt the wound healing and inflammatory response pathways to achieve the ultimate goal of metastasis. (Taken from [Petrova 2018] [70]; Open Access - CC 4.0, modified in accordance to CC 4.0 guidelines).

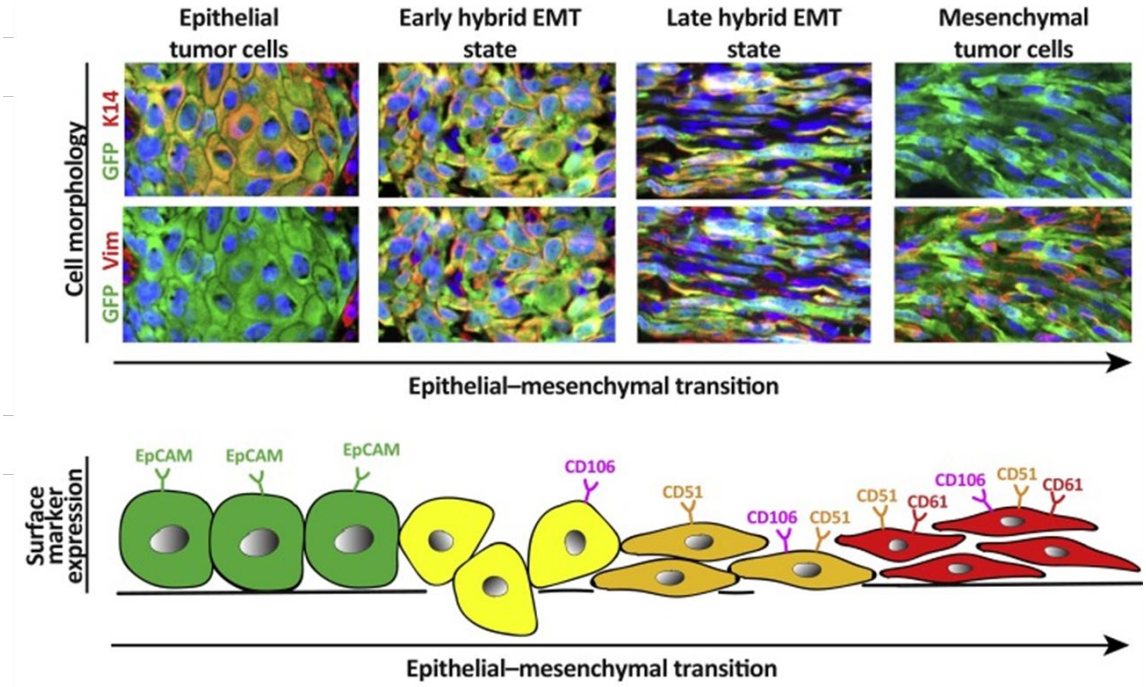

Figure 1.8 A Confocal Image and Illustration Highlighting the Morphological Shift in Cell Phenotypes Undergoing EMT.

IDC tumor cells are able to increase invasive potential through several mechanisms that necessitate the transduction of specific signal pathways like those from inflammatory cytokines. Specifically of great importance, the cytokines are able to stimulate tumor cell motility and mesenchymal phenotype by promoting an epithelial-to-mesenchymal transition (EMT) in the IDC cells. This occurs through the upregulation of Snail-1 transcription factor. The figure shows EMT occurring in stepwise manner through confocal images looking at loss of keratin 14 and increased vimentin (both events are conducive to EMT). The illustration highlights the shift from epithelial to mesenchymal morphology, and cluster differentiation (CD) markers detectable at various points. (Taken from [Pastushenko 2018] [102]; License granted for Copyright use, modified according to Copyright License guidelines).

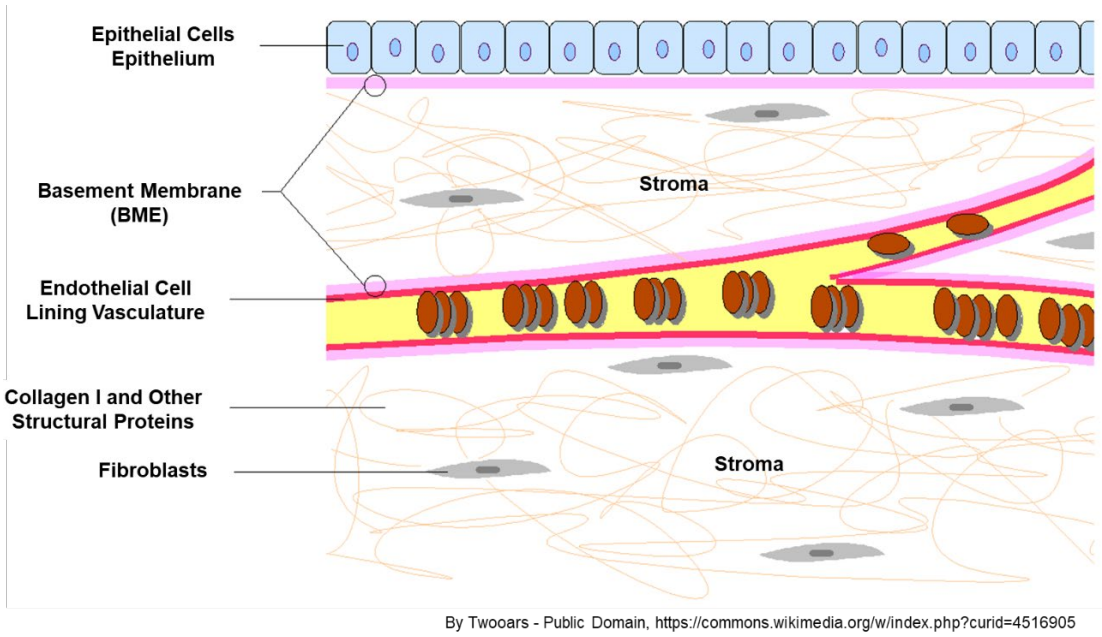

By Twooars - Public Domain, https://commons.wikimedia.org/w/index.php?curid=4516905

Figure 1.9 Epithelial and Endothelial Cell Layers Separated by Stromal ECM and Enveloped by Basement Membrane.

The ECM depicted in this illustration highlights the stroma and BME that comprise the connective tissues that separate and also envelope cells that form the epithelium and endothelium. There are several structural proteins that compose the ECM including collagens, elastin, proteoglycans, and glycoproteins. Of these, collagens are the most critical due to their diversity, making up the majority of ECM proteins. Fibrillar collagens are predominant in the stroma making up ~30-40% of the protein in the stroma. Of these, collagen I makes up ~80% (the rest is mostly collagen III) of the stromal collagen. The BME has a different makeup and is predominantly composed of non-fibrillar collagen IV, making up ~50% of any given basement membrane. The BME is located in between epithelial cell layers and the stroma, forming a barrier between these the stroma and epithelium. In addition to blood vessels and fibroblasts, the stroma also houses a variety of glands, nerves, and immune cells. (Public domain; Author of illustration is credited on right-hand corner of illustration).

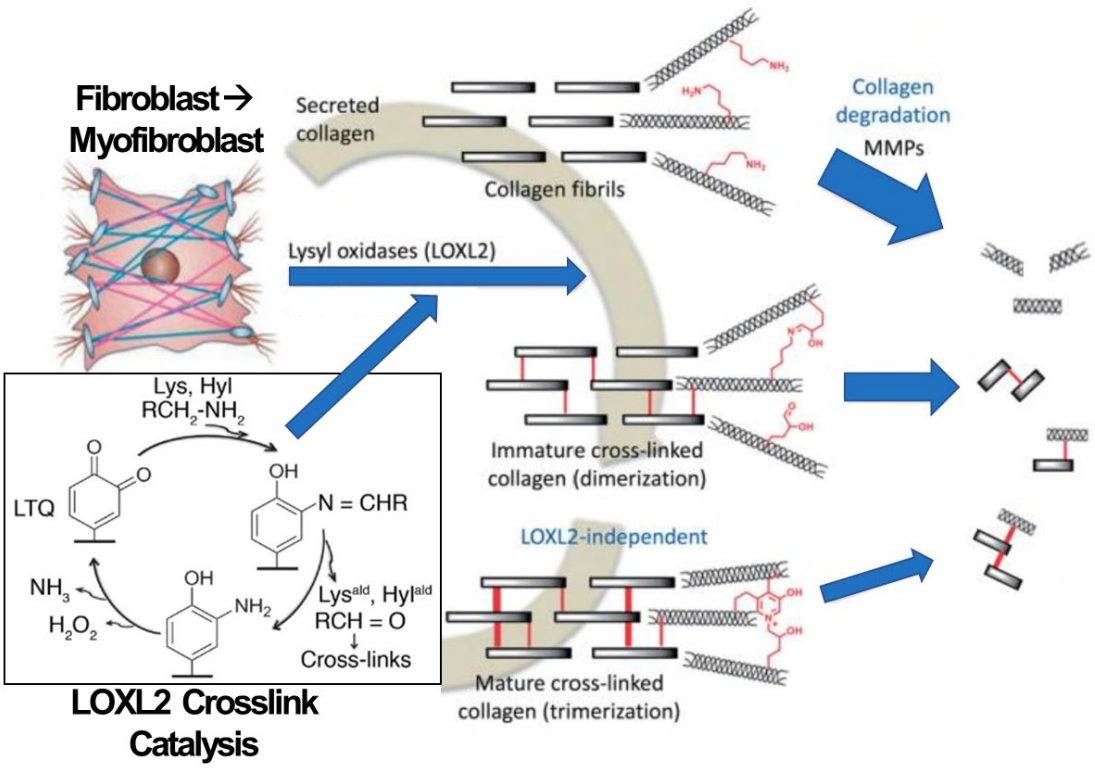

Figure 1.10 Mechanism of LOXL2 Collagen Crosslinking by Enzymatic Catalysis of Fibrillar Collagen Lysine and Hydroxylysine Amino Acid Residues.

This flow chart depicts the main source of LOXL2, fibroblasts that have undergone transition to myofibroblasts. These produce large quantities of this lysyl oxidase enzyme among other secreted proteins. The LOXL2 oxidative enzyme undergoes N-linked glycosylation at two asparagine amino acids and is secreted extracellularly. Collagen crosslinks when the lysyl tyrosylquinone (LTQ) and copper binding domains interact with lysine and hydroxylysine residues present towards the ends of collagen fibrils catalyzing the oxidative deamination of the amino acids to form allysine and hydroxyallysine aldehydes. These spontaneously react to form the covalent crosslinks producing hydrogen peroxide (H_2O_2). The reaction is represented in the figure which shows LTQ recycling to continue crosslinking the next collagen fibers. MMPs are capable of degrading the fibers that have been crosslinked by LOXL2. (Taken from [Findlay 2019, 2020] [138, 139]; License granted for Copyright use, modified according to Copyright License guidelines).

CHAPTER TWO: NOVEL MECHANISM FOR OSM-PROMOTED EXTRACELLULAR MATRIX REMODELING IN BREAST CANCER: LOXL2 UPREGULATION AND SUBSEQUENT ECM ALIGNMENT

Authors & Affiliations

Simion C. Dinca[1], Daniel Greiner[3], Keren Weidenfeld[4], Laura Bond[5], Dalit Barkan[4], Cheryl L. Jorcyk[1, 2, #]

Journal: Breast Cancer Research

Impact Factor: 8.42

1 Boise State University, Biomolecular Sciences Program, 1910 University Drive, MS1515, Boise, ID, 83725 USA

2 Boise State University, Department of Biological Sciences, 1910 University Drive, MS1515, Boise, ID, 83725 USA

3 University of Utah, Department of Oncological Sciences, Salt Lake City, UT USA

4 University of Haifa, Department of Human Biology and Medical Sciences, Haifa, Israel

5 Boise State University, Biomolecular Research Center, 1910 University Drive, MS1515, Boise, ID 83725 USA

Corresponding Author

Abstract

Background

Invasive ductal carcinoma (IDC) is a serious problem for patients as it metastasizes, decreasing 5-year patient survival from >95% to ~27%. The breast tumor microenvironment (TME) is often saturated with proinflammatory cytokines, such as oncostatin M (OSM), which promote epithelial-to-mesenchymal transitions (EMT) in IDC and increased metastasis. The extracellular matrix (ECM) also plays an important role in promoting invasive and metastatic potential of IDC. Specifically, the reorganization and alignment of collagen fibers in stromal ECM leads to directed tumor cell motility, which promotes metastasis. Lysyl oxidase like-2 (LOXL2) catalyzes ECM remodeling by crosslinking of collagen I in the ECM. We propose a novel mechanism whereby OSM induces LOXL2 expression, mediating stromal ECM remodeling of the breast TME.

Methods

Bioinformatics was utilized to determine survival and gene correlation in patients. IDC cell lines were treated with OSM (also IL-6, LIF, and IL-1β) and analyzed for LOXL2 expression by qRT-PCR and immunolabelling techniques. Collagen I contraction assays, 3D invasion assays, and confocal microscopy were performed with and without LOXL2 inhibition to determine the impact of OSM-induced LOXL2 on the ECM. Alignment was analyzed using CurveAlign4.0.

Results

Our studies demonstrate that IDC patients with high LOXL2 and OSM co-expression had worse rates of metastasis-free survival than those with high levels of

either, individually, and LOXL2 expression is positively correlated to OSM/ OSM receptor (OSMR) expression in IDC patients. Furthermore, human IDC cells treated with OSM resulted in a significant increase in LOXL2 mRNA, which led to upregulated protein expression of secreted, glycosylated, and enzymatically active LOXL2. The expression of LOXL2 in IDC cells did not affect OSM-promoted EMT, and LOXL2 was localized to the cytoplasm and/or secreted. OSM-induced LOXL2 promoted an increase in ECM collagen I fiber crosslinking, which led to significant fiber alignment between cells and increased IDC cell invasion.

Conclusion

Aligned collagen fibers in the ECM provide pathways for tumor cells to migrate more easily through the stroma to nearby vasculature and tissue. Taken together, these results provide a new paradigm through which proinflammatory cytokine OSM promotes tumor progression. Understanding the nuances in IDC metastasis will lead to better potential therapeutics to combat against the possibility.

Background

Ductal carcinoma is the most commonly diagnosed form of breast cancer in women. It is classified as either pre-invasive ductal carcinoma *in situ* (DCIS) or invasive ductal carcinoma (IDC). [12] If left undetected or untreated, IDC leads to tumor metastasis, which drops patient five-year survival from >95% to ~27%. [8] Due to the negative impact metastatic lesions have on patient survival, it is critical to understand the mechanisms that promote metastasis. IDC exists in an inflammatory microenvironment, saturated by cytokines released from tumor-infiltrating macrophages and neutrophils present in the stromal extracellular matrix (ECM). [24, 25, 94] Interleukin-6 (IL-6)-

related cytokines, such as oncostatin M (OSM), activate signaling pathways that stimulate the metastasis of IDC cells. [55, 97, 170, 171] Identifying and exploiting novel mechanisms that increase invasive and metastatic potential of IDC is of paramount importance in creating therapeutics to disrupt metastasis.

The current paradigm in inflammation and cytokine-induced ductal tumor development is IL-6 signaling promotes progression and metastasis. [88, 89, 91] However, research shows that IL-6's sister cytokine OSM also promotes invasion and metastasis in a manner independent of IL-6. [23, 84, 85] Signaling is prompted when OSM binds to the gp130 receptor subunit, which leads to the recruitment and dimerization of OSM receptor β and the formation of the receptor complex (OSMR). [97, 170, 171] Currently, it is thought that OSM promotes metastasis by stimulating an epithelial-to-mesenchymal transition (EMT) in breast ductal carcinoma cells through the up- or down-regulation of specific genes that disturb cell polarity, promoting differentiation and motility. [104, 172, 173] EMT is stimulated through destabilized localization of E-cadherin or its downregulation, as well as an increase in Vimentin, Snail-1, and N-cadherin gene expression. [106, 107] Our lab has also demonstrated that OSM induces the upregulation of: i) vascular endothelial growth factor (VEGF) that leads to angiogenesis, [108] ii) circulating tumor cell (CTC) numbers, [55] and iii) lung and bone metastases *in vivo*. [174] Previous research highlights the important and multifaceted role that OSM signaling plays in IDC progression and metastasis. However, the impact OSM signaling has on ECM remodeling in the tumor microenvironment (TME), has yet to be explored.

The extracellular matrix (ECM) plays an integral role in tumor progression, as remodeling the ECM of the tumor microenvironment is critical for ductal carcinoma invasion and metastasis. [46, 57, 58, 175] Invasive ductal carcinoma cells must degrade and break through a specialized ECM (basement membrane, composed primarily of collagen IV, BME) before migrating through the stroma to promote invasion to nearby tissues and vasculature. [44, 118, 120] Proinflammatory cytokines have previously been associated with promoting the expression of BME degrading enzymes. [176-178] Once the BME is degraded, IDC cells modify the surrounding stromal ECM by secreting enzymes that remodel the structural proteins, present in stromal ECM, promoting invasion and metastasis. [47, 122, 124, 145] Here our research suggests that OSM signaling plays a prominent role in IDC cell's ability to remodel the primary constituent of stromal ECM, collagen I. Remodeling occurs as OSM induces the expression and secretion of the matrix remodeling enzyme lysyl oxidase-like 2 (LOXL2) in IDC cells.

Similar to OSM, LOXL2 expression has been linked to a worse prognosis in IDC patients, and increased invasion and metastasis of breast tumor cells. [147, 148, 151, 152, 179, 180] LOXL2 is part of a family of monoamine oxidases known as lysyl oxidases, this family includes lysyl oxidase (LOX) and LOXL1-4. [181, 182] LOXL2 is copper dependent enzyme containing a lysyl tyrosylquinone (LTQ) site in the active domain for turning peptidyl lysine and hydroxylysine into peptidyl allysine and hydroxyallysine on collagen and elastin. [134] These aldehydes spontaneously react to form a covalent bond between themselves, with hydrogen peroxide (H_2O_2) as a byproduct. [135] The covalent bonds formed in this reaction are collectively known as "crosslinking", which leads to changes in ECM structure, density, and stiffness. [150, 183] LOXL2 is present in the cell

cytoplasm before it is glycosylated at amino acids N593 and N627, and it promotes collagen I fiber alignment and crosslinking when secreted. [78, 119] Alignment of stromal collagen I fibers facilitate directed tumor cell motility towards nearby vasculature and/or tissue, as opposed to haphazard motility that occurs with random collagen I fiber alignment. [127, 158] Research also suggests that LOXL2 also has a cell autonomous role. LOXL2 was shown to promote an EMT of breast cancer cells resulting in invasive and stem-like properties of the cancer cells. [152, 154, 156, 157]

There is currently a gap in knowledge regarding the role that proinflammatory cytokines play in ECM remodeling of the TME, specifically the surrounding stroma. Our studies demonstrate that OSM signaling promotes the expression and secretion of enzymatically active LOXL2. We also demonstrate that OSM-induced LOXL2 leads to significantly more crosslinking and alignment of ECM collagen I, the main constituent of the stroma. Further studies show that OSM-induced LOXL2 leads to increased IDC cell invasion in a 3D collagen matrix. Understanding how OSM regulates LOXL2 production, and more broadly matrix remodeling of the stroma, will shed light on the effect inflammation has on the TME of IDC patients. This is critical, as our research demonstrates that high OSM and LOXL2 co-expression in IDC patients leads to a drastic decrease in metastasis-free survival. Hence, our research will lead to a better understanding of the dynamic nature of inflammation promoted metastasis.

Materials and Methods

Cells & Cell Culture

Human breast cancer cell lines used in experiments were purchased from the American Type Culture Collection (ATCC; Manassas, VA). Human luminal A MCF7

and T47D [ER+, PR+, HER2-] and triple negative basal B MDA-MB-231 [ER-, PR-, HER2-] were cultured in RPMI 1640 (Genesee Scientific; San Diego, CA), while BT474 [ER+, PR+, HER2+] and triple negative basal A MDA-MB-468 [ER-, PR-, HER2-] cells were cultured in DMEM (Genesee Scientific). Sk-Br-3 [ER-, PR-, HER2+] breast cancer cells were cultured using McCoy's 5A media (ATCC). All cell media contained 10% v/v Fetal Clone III (Thermo Fisher; Waltham, MA) and 1% v/v penicillin/streptomycin (Genesee Scientific). Cells were cultivated in tissue culture treated T-75 flasks (Genesee Scientific) kept in a Model 3110 (Forma Scientific; Marietta, OH) incubator at 37°C and 5% CO_2. Cells grown to ~75% confluence before plating for experiments. Cells were treated with recombinant human OSM, IL-6, leukemia inhibitory factor (LIF) (25 ng/mL), and/or IL-1β (10 ng/mL) from Peprotech Inc. (Rocky Hill, NJ) at various time intervals depending on the experiment and highlighted in the figures.

Gene Correlation (RNA-Seq)

The Cancer Genome Atlas (TCGA) RSEM counts associated with Breast invasive carcinoma (BRCA), Glioblastoma Multiforme (GBM), Prostate Adenocarcinoma (PRAD) and Ovarian Cancer (OV) were downloaded from the Broad GDAC Firehose repository (https://gdac.broadinstitute.org/). Using python, RSEM count data was standardized to Z-score for comparison and outlier patients above and below 3 standard deviations were removed from the dataset. Genes were then plotted and correlation was assessed by Pearson coefficient using the SciPy package. [184] The line of best fit was determined by linear regression using the Polyfit function in the SciPy package Specific code used for the analysis is available upon request at GitHub.

Patient Metastasis-Free Survival

The data associated with Van de Vijver et. al. [42] was downloaded and coded to ensure key results and figures from the data could be generated. Observed events were coded to be positive outcomes for metastasis, or identified as a death from cancer without metastasis, and a censored event to be any other outcome (by Vijver's definitions). The survival function was censored at 10 years to reduce the influence of the few cases with far longer survival times. Survival plots were created with the Survminer (Kassambara et. al, 2019) and Survival (Therneau, 2015) libraries in R. OSM and LOXL2 cut points were based on the Maximally Selected Rank Statistic, [185] which algorithmically searches the data for optimal cut points.

Real-Time Quantitative Reverse Transcription-Polymerase Chain Reaction (qRT-PCR)

RNA extraction from treated cell cultures was performed using RNA STAT-60 (Tel-Test, Inc.; Friendswood, TX) following the standardized protocol on Tel-Test's website. Isolated RNA concentration and quality was analyzed using a Nano-Dropper2000 (Thermo Scientific; Waltham, MA) and the agarose bleach gel protocol, [186] respectively. Synthesis of cDNA was prepared using High Capacity cDNA Reverse Transcription Kit (Applied Biosystems; Foster City, CA) and 1 μg of sample mRNA. Combining SYBR Green Master Mix (Bio-Rad; Hercules, CA) with sample cDNA, each sample was run in duplicate, at a minimum, on a 96-well plate. Roche Light Cycler 98 and accompanying software was used to determine mRNA expression.

Table 2.1 Oligonucleotide Pairs for Genes Used in qRT-PCR mRNA Analysis

Oligonucleotide	Base Pairs
LOXL2 Forward	(5')-AGGTATCGATGCCCATTCATGA-(3')
LOXL2 Reverse	(3')-GGATCAACTGATAGCTGAATAC-(5')
GAPDH Forward	(5')-GTTAGCTAGGAATAGCGATAGA-(3')
GAPDH Reverse	(3')-AGCATTAGTACAGTTAGCATGC-(5')

Immunoblot Assay

Cells were lysed using RIPA, 1% v/v Protease Inhibitor Cocktail (Sigma Aldrich; St. Louis, MO) and 100x Halt™ Phosphatase Inhibitor (Thermo Fisher). 10 µg of total protein was loaded per well, as determined by Peirce™ BCA Protein Assay Kit (Thermo Fisher). The Chameleon® Duo Protein Ladder (LiCor Biosciences; Lincoln, NE) was used as a protein molecular weight marker. Proteins were separated using Tris-Glycine SDS-PAGE gels and transferred onto nitrocellulose membranes (Thermo Scientific). Subsequently, the membrane was thoroughly dried and rewetted with ddH2O. Five mL of REVERT™ Total Protein (LiCor Biosciences) stain was added before the REVERT wash solution. The rinsing, and the blot was imaged using Odyssey CLx (LiCor Biosciences). The nitrocellulose membrane was blocked using Odyssey PBS Blocking Buffer (LiCor Biosciences) and incubated with the following primary antibodies in addition to 0.2% Tween20: LOX (1:500, Santa Cruz Biotech; Dallas, TX), LOXL1 (1:200, Santa Cruz Biotech), LOXL2 (1:1,000, Genetex; Irvine, CA), LOXL3 (1:200, Santa Cruz Biotech), LOXL4 (1:200, Santa Cruz Biotech), E-Cadherin (1:500, Abcam; Cambridge, UK), Snail-1 (1:1,000, Cell Signaling Technology; Danvers, MA), and GAPDH (1:500, Santa Cruz Biotech). Membranes were further incubated using 800 channel fluorophore conjugated donkey secondary antibodies (1:15,000, LiCor Biosciences), or HRP conjugated secondary antibodies (1:10,000, Jackson ImmunoResearch Laboratories;

West Grove, PA) prior to addition of ECL substrate (Thermo Fisher). The target proteins were then visualized using the Odyssey CLx and quantified using LiCor Image Studio software. Proteins were then normalized either against a REVERT total protein stain or GAPDH expression, and compared against non-treated controls.

De-glycosylation Assay

MCF7 and MDA-MB-468 cells are treated with OSM for 24 hours before samples were lysed with RIPA. 1 μg of Rapid PNGase F (Cell Signaling) enzyme was added to 10 μg of total protein from OSM-treated cell lysates. The assay was performed following the accompanying Rapid PNGase F protocol. LOXL2 proteins were visualized using the immunoblot techniques described above.

RNAi Transfections

Using Qiagen's protocol, the best LOXL2 knockdown in MCF7 cells came from the combination of 5 nM siLOXL2 #2 and 5 nM siLOXL2 #3 (Qiagen; Hilden, GER), called siLOXL2 (2/3), with 3 μL Transfection reagent (Qiagen) for 48 hours. To make the control siControl, 5 nM of scrambled siRNA (Qiagen) with 3 μL transfection reagent was used. The optimal cell density for transfection was 125,000 MCF7 cells in a 6-well plate. The MCF7-shLOXL2 and MCF7-shCTRL cells used in this experiment have previously been published and characterized. [152]

Lysyl Oxidase Activity Assay

MCF7 cells were transfected with siCTRL or siLOXL2 (2/3) for 48 hours then treated with OSM in serum and phenol red-free RPMI 1640 for 24 hours. The conditioned media (CM) was collected and immediately centrifuged at 8,000 g for 10 minutes to remove cellular debris. Lysates were collected to confirm LOXL2

knockdown. Conditioned media (1.75 mL) from each sample was added to separate 3K filter tubes (MilliporeSigma; Burlington, MA), which were centrifuged at 4,000 g in a swinging bucket centrifuge for 30 minutes. The rest of the assay was formulated using the recipe previously published with volumes adjusted to fit within a 96-well fluorescence compatible plate (Thermo Fisher). [187] The plates were read every 30 seconds using a BioTek Mx plate reader with Ex/Em 490/540 and 10 nm bandwidth.

LOXL2 ELISA

The LOXL2 ELISA (R&D Systems; Minneapolis, MN) was performed and analyzed according to the protocol provided by the manufacturer. Protein was concentrated from CM using acetone precipitation. [188] For each condition, one-part CM was mixed with four parts of 100% acetone chilled to -80°C, and placed back into a -80°C freezer overnight. The CM was centrifuged using 13,000 g for 10 minutes at -10°C. The acetone was decanted and the protein precipitates were dried for 20 minutes before being reconstituted with 1x Dilution Reagent (R&D Systems) containing 0.2% Tween20 at 1/3 the original volume. The samples were sonicated prior to addition to ELISA plate for a 3-fold increase in concentration.

Immunofluorescence

Immunofluorescence staining was carried out as previously described. [152] Briefly, cells were cultured in 8 well chamber glass slides, fixed for 5 min with 4% PFA containing 5% sucrose and 0.1% Triton X-100, and re-fixed for an additional 25 min with 4% PFA containing 5% sucrose. The cells were washed 10 min with PBS and an additional 10 min with PBS containing 0.05% Tween 20. Fixed cells were blocked with IF buffer (130 mM NaCl, 7 mM Na_2HPO_4, 3.5 mM NaH_2PO_4, 7.7 mM NaN_3, 0.1%

BSA, 0.2% Triton X-100, 0.05% Tween 20) supplemented with 10% donkey serum for 1 hour and incubated overnight at 4°C with Mouse monoclonal [HECD-1] to E Cadherin (1:500, Abcam). The cells were washed three times with PBS for 15 minutes each, and incubated for 1 hour with donkey anti–mouse conjugated to Alexa Fluor® 647 (1:200, Molecular Probes; Eugene, OR), washed as above, and mounted with VECTASHIELD mounting medium with 4′, 6-diamidino-2-phenylindole (DAPI). For F-actin staining, cells were incubated overnight with Alexa- Fluor® 488 Phalloidin (1:40) (Molecular Probes), washed three times with PBS for 15 minutes each, and mounted with VECTASHIELD mounting medium with DAPI. Immunofluorescent images were captured by Nikon A1R confocal microscope.

Nuclear Fraction Assay

Nuclear/Cytoplasmic fractionation assay was carried out as previously described. [189] Cells were washed twice with PBS, scraped and collected on ice into 1.5 mL microcentrifuge tubes. Tubes were spun with table-top centrifuge, and supernatant was discarded. Fractionation was performed with 0.1% NP40 in PBS. Cell pellets were triturated 5x with ice-cold 0.1% NP40 in PBS (900 µl for 10 cm dish) using P1000 micropipette that was cut at its end. Aliquots of 300 µL of these samples were placed into fresh tubes (designated as ***Total***). The remaining samples were centrifuged for 1 min 16,200 g to pellet nuclei. Aliquots of 300 µL of the supernatant were collected into fresh tubes (designated as ***Cyto***). 100 µl of 4x Laemmli sample buffer was added immediately to ***Total*** and ***Cyto*** samples. Nuclei pellets were resuspended with ice-cold 0.1% NP40 in PBS (1 mL for 10 cm dish), re-pelleted, and resuspended with 180 µL of 1x Laemmli

sample buffer (designated as ***Nuc***). ***Total*** and ***Cyto*** samples were sonicated using microprobes at level 2, twice for 5 seconds.

Collagen I Contraction Assay

Rat-tail collagen I (Corning Incorporated; Corning, NY) was used to form a 1.5 mg/mL collagen I matrix in a 35 mm petri dish with a 14 mm imbedded coverslip. On ice, rat-tail collagen I and 10X RPMI 1640 media (Corning) was diluted 1:10 with 1X PBS and adjusted with 0.1M NaOH to bring the final pH to 7.4. The MCF7 and MDA-MB-468 cells were seeded homogeneously in the matrix before adding 400 μL containing 100,000 cells to each petri dish imbedded coverslip. The matrix solution was incubated 20 minutes at 37C and 5% CO_2. Phenol red-free RPMI 1640 media (Thermo Fisher – Gibco) was added to each sample along with OSM and either 500 μM pan-LOX inhibitor β-aminopropionitrile βAPN (Thermo Fisher) or 200 nM LOXL2/3-specific small molecule inhibitor PXS-5120A (Pharmaxis; New South Wales, AUS) for 48 hours. Images were processed, the area of the matrix was analyzed using ImageJ area measurement tools. [190, 191]

Live Cell Imaging

Live cell imaging was performed using the Leica SP8 white light confocal microscope system with attached Peltier, which maintains cells at 37°C and 5% CO2. 100,000 MCF7 cells were seeded into the same rat-tail collagen matrix described above for the *Collagen I Contraction Assay*. The samples were exposed to recombinant human OSM and 500 μM βAPN for 36 hours prior to imaging. Collagen I fibers were visualized using reflectance mode confocal imaging. [192, 193] Cells were stained with membrane intercalating fluorescent dye Cell Tracker™ Red (Life Technologies; Carlsbad, CA) for

1-hour pre-imaging at a 1:1,000 dilution in serum/phenol-free RPMI 1640. Each image consisted of 15 μm z-stacks split into 44 sections that were taken with four frames stitched together in a 2x2 format at 63x magnification using a water immersion objective.

Collagen I Fiber Analysis

Live cell images of MCF7 cells in collagen I "pucks" were analyzed using CurveAlign4.0 software developed at the University of Wisconsin. [126, 128] Selected regions of interest (ROI) were analyzed -- the areas between the seeded cells and radiating outward perpendicular to the MCF7 cells as illustrated in Supplemental Figure 4. ROIs were utilized because accurate whole image analysis of was not possible due to the varying directions of collagen I fiber alignment. We used sum[(fiber dispersion coefficient) * (# of features (fibers) for each ROI)] / (total sampled features in image) to determine the average level of fiber dispersion for collagen I in each treatment group. For the fiber dispersion coefficient; 0 equals completely random fibers, 1 means all fibers are in alignment.

3-Dimensional Invasion Assay

Utilizing the Oris™ 3D Invasion Assay (Platypus Technologies; Madison, WI), 30,000 MCF7-GFP/Luc breast cancer cells (Genecopoeia; Rockville, MD) were seeded into the same 1.5 mg / mL rat-tail collagen I solution as described in the *Collagen I Contraction Assay* methods. The cells were exposed to 50 ng/mL β-Estradiol (estrogen) (Sigma-Aldrich; St. Louis, MO) in order to promote invasion. In addition, MCF7-GFP/Luc cells were treated with OSM and either 500 μM of pan-LOX inhibitor β-aminopropionitrile (βAPN) or 200 nM of LOXL2/3-specific small molecule inhibitor PXS-5120A for five days, or 120 hours. The rest of the experiment was performed

according to the specifications of the Oris™ 3D Invasion Assay protocol that the assay includes. Images were taken at Day 0, as a control, and Day 5 utilizing an EVOS FL (Life Technologies; Carlsbad, CA) fluorescent microscope with a 4x objective and GFP filter to detect MCF7 cells expressing GFP. ImageJ was used for image processing and cell counting.

Statistical Analysis

Statistical analysis performed using Prism 6.0 software. Significant results were determined by various statistical methods including Student's t-test, One-way ANOVA, Two-way ANOVA, and Log Rank test. Significance is denoted as: n.d. (not detected), n.s. (not significant), $p>0.05$, * $p<0.05$, ** $p<0.01$, *** $p<0.001$ and **** $p<0.0001$.

Results

Elevated OSM and LOXL2 Co-expression is Associated with Faster Onset of Metastasis

To determine whether high co-expression of LOXL2 and OSM mRNA is associated with increased rates of IDC metastasis in patients, we created a distant metastasis-free survival plot using microarray data from the de Vijver (2002) patient study consisting of 295 IDC patients. [42] This database was utilized because the patient population selected for this study and the metadata for metastasis is well characterized. We compared low OSM/ low LOXL2 to low OSM/ high LOXL2, high OSM/ low LOXL2, and high OSM/ high LOXL2 mRNA expression in patients and found that higher levels of OSM and LOXL2 mRNA combined, led to significantly more metastatic events in a 10-year span **(Fig. 1A)**. High expression of each individual gene also led to faster onset of metastasis, but high OSM and high LOXL2 co-expression had a greater significant impact on distant metastasis-free survival.

Our lab, and others, have previously analyzed Oncomine™ and other breast cancer patient databases demonstrating a correlation between reduced recurrence-free survival (RFS) of breast cancer patients with higher expression of LOXL2 [147, 148, 152] and reduced survival rates with higher expression of OSM/OSMR. [86, 162] Taken together, these results confirm that high OSM and LOXL2 co-expression is associated with an overall worse prognosis in IDC patients than high expression of either gene on its own.

LOXL2 Expression is Positively Correlated to OSM Signaling Through OSMR in Invasive Ductal Carcinoma Patients

To assess the correlation between OSM signaling and LOXL2 expression in cancer patients, we analyzed the expression of LOXL2 mRNA in cancer patients and compared it to OSMR mRNA expression. OSM is most often produced by neutrophils and macrophages found in the TME; and in turn, IDC cells, while having the capacity to secrete OSM, normally secrete none to very low levels. [25, 94] Therefore, comparing OSM mRNA expression from tumor samples directly against LOXL2 would not yield a highly relevant correlation. To assess OSM signaling, which occurs by OSM binding to the OSMR complex present on tumor cells, we investigated the expression of the beta subunit of the OSMR complex. Furthermore, this works because increased levels of OSM in the TME promotes the overexpression of OSMRβ mRNA and protein in IDC cells. [93, 194, 195] To assess the correlation between OSMR and LOXL2, we used RNA-Seq data from The Cancer Genome Atlas (TCGA) to assay transcriptional expression of biopsied patient samples in several cancer subtypes. Specifically, LOXL2 was compared against OSMR expression in glioblastoma, breast cancer, prostate cancer, and ovarian

cancer. We observed a weak, yet significant, positive Pearson correlation of 0.263 ($p = 6.97x10^{-20}$) between OSMR expression and LOXL2 expression in breast cancer patients **(Fig. 1B)**. There was also a weak to moderate positive, significant correlation between OSMR and LOXL2 expression in the other cancers investigated. To determine whether the correlation has a potential impact on gene expression we used a least squares linear regression to attain the line of best fit. Then we analyzed the slope and 95% confidence interval (CI) as illustrated in the table accompanying Figure 1B, where a larger slope suggests a greater impact on gene expression. Each cancer analyzed had a positive slope above 0.2 and had a correlation between OSMR and LOXL2 mRNA expression. This data suggests that increasing OSMR mRNA is correlated with increasing LOXL2 transcripts in multiple forms of cancer; including breast cancer.

Next, we analyzed the breast cancer patient data for correlation between OSMR mRNA expression and other lysyl oxidase family members: LOX and LOXL1-4. We performed the same correlation analysis as above, but instead focused on OSMR and lysyl oxidase mRNA expression in breast cancer patients. We observed a significant, moderate to weak positive correlation (0.469 and 0.263) comparing OSMR expression to LOX and LOXL2 expression respectively, as determined by Pearson correlation analysis. While LOXL1/3/4 had significant Pearson correlation coefficients, the Pearson coefficients were considered very weak/negligible because they fall below 0.20. [196] LOX and LOXL2 also generated a line of best fit with a positive slope above 0.2, when compared to OSMR expression, while the slopes for LOXL1/3/4 were approximately zero **(Fig. 1C)**. These results suggest that increasing OSMR gene expression is correlated with increasing LOX and LOXL2 gene expression but not with LOXL1/3/4 expression.

Further analysis of OSM mRNA expression in relation to lysyl oxidase mRNA expression again highlighted a significant correlation between OSM and all lysyl oxidases, except for LOXL4 **(Supp. Fig. 1)**. However, the Pearson correlation coefficient values for all the lysyl oxidases were below 0.25. The slopes for the lines of best fit for LOX and LOXL1-3 were also positive, but had large 95% CI. This data suggests that OSM gene expression is slightly correlated to increased LOX and LOXL1-3 expression. Taken together, these results confirm the positive correlation between OSM signaling and lysyl oxidase mRNA expression in breast cancer patients.

OSM Induces LOXL2 Expression

As the human breast cancer patient data demonstrated a correlation between the proinflammatory cytokine OSM and the collagen cross-linking enzyme LOXL2, we set out to determine whether OSM could promote the expression of LOXL2 at the transcriptional level. qRT-PCR was performed on three IDC cell lines with varying estrogen receptor (ER), progesterone receptor (PR), and ErbB2 (HER2) status: luminal A MCF7 (ER+ PR+ HER2-), basal A MDA-MB-468 (ER- PR- HER2-), and basal B MDA-MB-231 (ER- PR- HER2-). These cell lines were chosen because they represent increasing tumor cell aggressiveness and invasiveness, respectively, [197] and they each express receptors for OSM/IL-6 cytokines. [90, 108] The cells were treated with recombinant human OSM (25 ng/mL), IL-6 (25 ng/mL), or both for 1, 2, 4, 12, 24, and 48 hours and compared against untreated controls. Our cells were treated with cytokine concentrations designed to saturate the IDC cells, as they would be in an actual TME, where cytokines have been shown to be present in high concentrations due to secretion by tumor-associated neutrophils, macrophages, and fibroblasts. [49, 162, 198, 199] qRT-

PCR analysis of MCF7 cells showed that OSM treatment induced an ~3-fold increase in LOXL2 mRNA, relative to the non-treated controls, at 12 and 24 hours, whereas IL-6 treatment produced no significant change in LOXL2 mRNA **(Fig. 1D)**. In MDA-MB-468 cells, OSM induced LOXL2 mRNA by ~2-fold at 24 hours **(Fig. 1E**). In MDA-MB-231 cells, there was no significant change in expression of LOXL2 mRNA with any treatment groups **(Fig. 1F)**. No effect on LOXL2 expression was somewhat expected since ER- MDA-MB-231 cells are already highly invasive, which can limit the impact of OSM signaling on promoting invasive potential. [55] MDA-MB-231 cells produce high levels of LOXL2, as highlighted in the following paragraph, limiting further induction by OSM. These results demonstrate that OSM signaling leads to an increase in LOXL2 mRNA expression in IDC cells.

To determine whether OSM-induced LOXL2 mRNA translates to the protein level, we performed immunoblot blot assays. Analysis was performed on MCF7, MDA-MB-231, MDA-MB-468, BT474 (ER+ PR+ HER2+), and Sk-Br-3 (ER- PR- HER2+) IDC cell lines treated with OSM, IL-6, LIF (all at 25 ng/mL), and IL-1β (10 ng/mL) for 24 hours before cell lysates were collected and compared against untreated controls. Analysis of proinflammatory cytokines in the IL-6 family, as well as IL-1β, was performed to determine whether LOXL2 induction is unique to OSM signaling or has the potential to be broadly applicable to proinflammatory cytokines. In MCF7 cells, OSM induced a greater than 3.5-fold increase in LOXL2 protein expression, a ~2.5-fold increase with IL-1β treatment, but no change with rest of IL-6-family cytokines **(Fig. 2A)**. MDA-MB-468 cells showed a ~2-fold induction of LOXL2 protein expression with OSM treatment, a slight upregulation by IL-1β (not significant), and no change with IL-6

or LIF **(Fig. 2B)**. BT474 cells showed the largest increase in LOXL2 expression with a ~10-fold increase, with LIF also promoting a ~3-fold induction **(Fig. 2C)**. While with the Sk-Br-3 cells, OSM induced the expression of LOXL2 ~2-fold and IL-6 promoted a ~3-fold increase in LOXL2 protein **(Fig. 2D)**. None of the cytokines induced a significant change in LOXL2 protein expression in highly invasive MDA-MB-231 cells that constitutively express very high levels of LOXL2 **(Fig. 2E),** T47D (ER+ PR+ HER2-) cells did not express any LOXL2 protein before or after treatment (data not shown). The bands represent the 105 kDa LOXL2 protein, which we expect correlates to the secreted and enzymatically active form of LOXL2 that is glycosylated at the N593 and N627 amino acids. [78] LOXL2 protein induction was highest after 24 hours, which was supported by In-Cell Western analysis **(Supp. Fig. 2)**. These results confirm that OSM signaling, and to a lesser extent IL-1β signaling, induce LOXL2 protein expression in IDC cells, while other IL-6-family cytokines do not.

Expression of LOXL2 in breast cancer cells is positively correlated with the invasive potential of the breast tumor cells. [145, 147] Therefore, we wanted to determine and compare relative LOXL2 expression between the IDC cell lines treated with OSM. To compare relative expression, immunoblot analysis was performed on lysates from non-treated and OSM-treated cells after 24 hours. We observed a significant step-wise increase in constitutive LOXL2 protein expression from the least (MCF7) to most (MDA-MB-231) aggressive cell line. OSM treatment promoted the expression of LOXL2, bridging the gap in LOXL2 expression between the cell lines **(Fig. 2F)**. Our results suggest that OSM-induced LOXL2 protein expression may be correlated to the development of more aggressive invasive ductal carcinomas due to the incremental

increase in LOXL2 with OSM exposure. Taken together these results confirm OSM-induced LOXL2 at the mRNA level leads to LOXL2 protein expression, which is correlated with increasing aggressiveness of IDC cells.

OSM Induction of Lysyl Oxidases is Unique to LOXL2

To characterize the effects of OSM signaling on the expression of the different family members of lysyl oxidase, we performed immunoblot assays using MCF7 and MDA-MB-468 cells that were treated for 24 hours with OSM. LOX expression was analyzed with IL-6 and LIF treatments, in addition to OSM. Besides LOXL2, the only lysyl oxidase detectable by immunoblot analysis in MCF7 cells was LOXL1. OSM treatment; however, did not alter any of the other lysyl oxidase members **(Fig. 2G)**. These results suggest that OSM induces only LOXL2 expression in the IDC cell lines. Based on these results we chose to further focus on the OSM-LOXL2 axis in IDCs cells using MCF-7 cells as our model system. Though, OSM also exclusively induced the expression of LOXL2 in MDA-MB-468 cells, these cells constitutively expressed LOX protein **(Supp. Fig. 3)**. This high endogenous expression of LOX may represent a confounding variable for functional analysis of LOXL2. Taken together, OSM signaling does not impact the expression of all lysyl oxidases but seems to be unique to LOXL2.

OSM-Induced EMT is Independent of LOXL2 Expression

EMT has been widely implicated in regulating cell invasion and metastasis. [200] OSM signaling and LOXL2 nuclear localization have been implicated in promoting epithelial to mesenchymal transition in ductal carcinoma cells. [77, 104, 152, 154, 172, 173] Indeed, MCF7 cells treated with OSM induced cytoplasmic localization of the epithelial marker E-cadherin (E-Cad) as depicted by immunofluorescence analysis **(Fig.**

3A). Given that OSM induces LOXL2 expression and the latter has been also implicated in promoting EMT, we next explored whether EMT induced by OSM is dependent on LOXL2 expression. To this end MCF7 cells stably expressing shRNA targeting LOXL2 (MCF7-sh-LOXL2) and MCF7 cells stably expressing sh-Non-target (MCF7-sh-Non-target) were treated with OSM and expression of E-Cadherin and Snail, a transcription factor mediating EMT, were determined by immunoblot analysis. Our results demonstrate that knockdown of LOXL2 in MCF7 cells did not inhibit OSM-induced EMT, given that E-Cadherin expression was slighty downregulated and Snail expression was upregulated upon OSM treatment in both MCF7-sh-Non-target and MCF7-sh-LOXL2 cells (**Fig. 3B**). Similarly, in MDA-MB-468, our results demonstrate that knockdown of LOXL2 in MDA-MB-468 cells did not inhibit OSM-induced EMT, given that E-Cadherin expression did not change and Snail expression was upregulated with OSM treatment in both siCTRL and siLOXL2-exposed MDA-MB-468 cells **(Fig. 3C)**.

Notably, we previously demonstrated that nuclear expression of LOXL2 is required to promote EMT in MCF7 cells. [152] Therefore, we determined the cellular localization of LOXL2 upon OSM induction. We envisioned that OSM induced only cytoplasmic expression of LOXL2, thus promoting EMT independent of LOXL2 expression. To this end we performed nuclear and cytosolic fractionation on MCF7 cells treated with OSM, using GAPDH as a cytosolic marker and Snail as a nuclear marker **(Fig. 3D)**. Indeed, OSM induced cytoplasmic expression of LOXL2 while the nuclear fraction did not contain any nuclear LOXL2. This data confirmed that OSM did not induce nuclear LOXL2 expression where it could promote EMT through the stabilization

of Snail. Taken together these results demonstrate that OSM promotes EMT independently of its induction of LOXL2 protein.

OSM Induces a Glycosylated LOXL2 That is Secreted and Enzymatically Active

LOXL2, in addition to its cell autonomous activity, has been well studied for its extracellular activity on ECM proteins. [148, 201] Secreted LOXL2 promotes collagen I fiber crosslinking and affects matrix remodeling, which has been linked to increased metastatic capability in breast cancer. [40-44] Interestingly, immunoblot analysis suggested that OSM-induced expression of the N-linked glycosylated form of the LOXL2 protein (105 kDa) which is secreted into the tumor microenvironment. [78] To confirm that OSM-induced the expression of glycosylated and enzymatically active LOXL2, we determined the N-linked glycosylation status of expressed LOXL2. MCF7 and MDA-MB-468 cell lysates treated with OSM were exposed to the N-linked deglycosylase enzyme, PNGase F, before immunoblot analysis was performed. OSM induced the expression of the 105 kDa LOXL2 protein, which was reduced in size to 87 kDa following the addition of PNGase F in both MCF7 **(Fig. 4A)** and MDA-MB-468 **(Fig. 4B)** cells. To confirm and quantify LOXL2 secretion, we performed an ELISA on MCF7 cells treated with OSM for 36 hours. We observed a significant induction in LOXL2 protein secretion with OSM treatment averaging 877 pg/mL of LOXL2 in solution. In comparison to the non-treated samples that averaged 347.6 pg/mL of LOXL2, we observed an ~2.5-fold induction in LOXL2 secretion **(Fig. 4C)**. Together, these results confirm that the LOXL2 protein expressed through OSM signaling in IDC cells is N-linked glycosylated and secreted.

In order to confirm that the LOXL2 protein induced by OSM is enzymatically active, we performed a lysyl oxidase activity assay on MCF7 cell conditioned media. MCF7 cells were transfected with siLOXL2 or siCTRL, and treated with OSM for 24 hours. In the siLOXL2 group we observed that OSM treated samples had significantly reduced lysyl oxidase activity compared to the siCTRL group **(Fig. 4D)**. We saw a significant ~2-fold increase in lysyl oxidase activity with OSM treatment when comparing against non-treated controls in the siCTRL group. The accompanying immunoblot confirms the knockdown of LOXL2 protein in the MCF7 cell line. Further immunoblot analysis confirmed that there was no impact on LOXL1 protein expression **(Supp. Fig. 4)**. Based on these results, we conclude that OSM-induced LOXL2 is enzymatically active and accounts for all of the lysyl oxidase enzymatic activity present in MCF7 cell conditioned media.

OSM-Induced LOXL2 Leads to ECM Remodeling and Increased Collagen I Fiber Alignment

To assess the effect of OSM-induced LOXL2 on crosslinking collagen I, we performed a collagen contraction assay. MCF7 and MDA-MB-468 cells were seeded into a 1.5 mg/mL rat tail collagen I matrix, and the cells were treated for 48 hours with OSM, a combination of OSM and the pan-LOX inhibitor βAPN (500 μM), or a combination of OSM and the LOXL2/3-specific inhibitor PXS-5120A (200 nM). βAPN, or β-aminopropionitrile, is a small molecule inhibitor (SMI) commonly used as a nonspecific inhibitor for lysyl oxidase proteins; [190, 201] PXS-5120A (PXS-S1A) is a LOXL2 specific inhibitor at a range of concentrations in the nanomolar range. [138, 149] OSM induced a ~2.5-fold increase in collagen I contraction in MCF7 cells, as compared to the

non-treated control, while OSM-induced contraction was blocked by βAPN and PXS-5120A treatment **(Fig. 5A).** In MDA-MB-468 cells, we saw similar ~2-fold increase; however, the overall contraction was substantially reduced compared to MCF7 cells **(Fig. 5B)**. These results demonstrate that OSM-induced LOXL2 increases collagen I contraction, and suggests that OSM promotes crosslinking through induced LOXL2, as collagen I contraction correlates to collagen crosslinking. [190, 191]

To visualize collagen alignment, we performed Live-Cell confocal imaging on MCF7 cells treated with OSM and/or βAPN for 36 hours in the collagen I matrix described above. Prior to imaging, the MCF7 cells were exposed to CellTracker Red (depicted in red), and the collagen I fibers were visualized by resonance scanning of the matrix (depicted in green). As seen visually, OSM promoted collagen I alignment, and inhibition of LOXL2 with βAPN reduced fiber alignment **(Fig. 5C)**. Images were processed by ImageJ in order to highlight fiber density at its greatest intensity **(Fig. 5D)**. CurveAlign4.0 software [126, 128] was used to quantify the alignment of collagen I fibers in-between, and tangential to, MCF7 cells by analyzing alignment in selected regions of interest (ROI) **(Supp. Fig. 5)**. Analysis of the fiber dispersion coefficient in the ROIs using CurveAlign4.0 showed a significant ~2-fold increase in fiber alignment with OSM treatment, as the closer the coefficient is to 1 the more alignment is present. The increase in alignment was significantly reversed with the inhibition of LOXL2, using βAPN **(Fig. 5E)**. These results confirm that OSM-induced LOXL2 leads to collagen I fiber alignment in the ECM.

OSM-Induced LOXL2 Leads to Increased Invasion in 3D Collagen I Matrix

After determining that OSM-induced LOXL2 promotes a significant increase in collagen I fiber alignment, we wanted to examine whether OSM-induced LOXL2 in turn impacts invasion. Research suggests that an increase in collagen I fiber alignment leads to an increase in invasion of breast cancer cells. [127, 158] To assess the impact of OSM-induced LOXL2 on IDC cell invasive potential, we performed a 3D invasion assay on IDC cells. We utilized MCF7 cells that incorporate green fluorescent protein (GFP) for visualization using fluorescent microscopy. MCF7-GFP cells supplemented with β-estradiol (50 ng/mL) were seeded in a collagen I solution with a concentration of 1.5 mg/mL. The cell suspension was then added to wells of a 96-well plate containing a circular "cell-free zone" for cells to invade towards. Cells were treated with OSM, OSM with βAPN (500 uM), or OSM with PXS-5120A (200 nM) and compared against a non-treated control. Images were taken at Day 0, as a control, and the experiment was run until Day 5 **(Fig. 6A)**. We analyzed the fluorescent images using ImageJ to determine the number of cells that entered the "cell-free zone" after Day 5. The total number of MCF7-GFP cells that entered the "cell-free zone" significantly increased with OSM treatment (>3-fold) compared to the non-treated control, and cell invasion was in turn significantly decreased with LOXL2 inhibition, using both βAPN (~ 3-fold) and PXS-5120A (~ 3-fold) SMIs **(Fig 6B)**. These results suggest that OSM-induced LOXL2 is critical to OSM-promoted invasion, and may likely have an impact on metastasis.

Taken together, these results demonstrate that OSM induces sufficient LOXL2 protein expression/secretion to promote remodeling and alignment of collagen I fibers in the ductal carcinoma tumor microenvironment. Due to the alignment of collagen I fibers,

it is expected that OSM-induced LOXL2 will promote ductal carcinoma cell invasion and metastasis as tumor cells migrate along aligned collagen fibers. [47, 127] This was supported by our 3D invasion assay results, which showed that OSM induced an ~3-fold increase in the number of MCF7-GFP cells that invaded the "cell-free zone", when compared to OSM treatment in conjunction with LOXL2 inhibition. Therefore, this research highlights a novel mechanism in ductal carcinoma tumor progression, independent of EMT. Further research is needed to confirm that OSM-induced LOXL2 extracellular matrix remodeling leads to a significant increase in metastasis.

Discussion

The novel findings in our study demonstrate that the proinflammatory cytokine OSM promotes the expression of LOXL2 in breast cancer cells, which significantly impacts collagen I fiber crosslinking, fiber alignment, and invasion **(Fig. 7)**. Clinically, we show that the co-expression of OSM and LOXL2 in patients leads to significantly lower rates of distant metastasis-free survival (DMFS). Our results confirm that proinflammatory cytokine signaling can lead to key alterations in ECM structure through the regulation of LOXL2. These results also suggest that ECM remodeling through OSM-induced LOXL2 may promote metastatic events due to the alignment of collagen I fibers that make up >80% of the stromal collagen. [120] This is further confirmed by our 3D invasion data, where OSM-induced LOXL2 was key for IDC cell invasion. The novelty of these findings opens the doors for new paradigms related to proinflammatory cytokine-promoted invasion and metastasis.

As it is currently understood in the literature, OSM signaling promotes metastasis by initiating EMT, inducing VEGF expression and angiogenesis, and the secretion of

enzymatic proteins that lead to the degradation of the basement membrane surrounding the invasive ductal carcinoma tumor. [104, 106-108, 172, 173] Our research shows that OSM signaling also led to the crosslinking of collagen I fibers, the primary constituent of the stroma, that promotes ECM remodeling in the form of increased fiber alignment due to LOXL2 overexpression. Our research additionally shows that OSM-induced LOXL2 is important for cellular invasion in a 3D matrix similar to the stroma. We tested and analyzed six different cell types (MCF7, MDA-MB-468, BT474, Sk-Br-3, MDA-MB-231, and T47D) of which four showed the capability for OSM-induced LOXL2 expression. Several other cytokines also induced LOXL2 expression but in only one or two cell lines. Only in the T47D cell line was LOXL2 neither expressed nor induced. This knowledge is important, as our lab has previously shown that secreted OSM can bind to type I collagen and other ECM fibers and remain active for extended periods of time, [96] thus creating an proinflammatory environment around the breast tumor. This proinflammatory TME provides OSM to the tumor cells as they traverse the ECM. OSM increases the tumor cell invasive capability by inducing an EMT response and, as we have just shown for the first time, upregulating LOXL2 expression.

As has been demonstrated for OSM signaling, LOXL2, when it localizes to the nucleus, has been shown to promote EMT [78, 152] through the stabilization and/or upregulation of Snail-1. [78, 157] Using cytoplasmic and nuclear fractions, we were able to conclude that OSM-induced cytoplasmic expression of LOXL2, and promoted the secretion of LOXL2. LOXL2 KO experiments confirmed that OSM promotes EMT through Snail-1 upregulation and E-cadherin cytoplasmic localization, in a manner independent of LOXL2 expression. Therefore, while OSM-induced LOXL2 does not play

a role in promoting EMT, it does actively remodel the ECM of the TME by promoting collagen I fiber alignment and IDC cell invasion. As previously published, aligned collagen fibers facilitate directed tumor cell migration towards nearby vasculature, an important early step in metastasis. [47, 127] Thus, OSM-induced LOXL2 has the potential to promote higher rates of metastasis, in addition to OSM-promoted EMT. It was recently documented that knockdown of LOXL2 expression in specific lung adenocarcinoma cell lines decreased collagen fibrillar alignment. [125] The presence of LOXL2 in the ECM was also observed to lead to the formation of stiffer matrices. [150, 183] Stiffer substrates provide metastasizing tumor cells better focal adhesion anchorage and "durotaxis", which leads to easier and faster migration. [62, 202] The ECM remodeling draws a parallel with research that highlights patients with stiff, dense breast tissue have a worse prognosis than those with normal density. [141, 142, 160]

Our analysis of patient data confirmed that IDC patients with high co-expression of OSM and LOXL2 have worse rates of metastasis than either alone. LOXL2-promoted collagen I fiber alignment in addition to OSM-promoted EMT may be responsible for the drastic decrease in DMFS in IDC patients. This data is supported by published research demonstrating that individually, OSM and LOXL2 overexpression in patients correlates with decreased reoccurrence-free survival (RFS) and distant metastasis-free survival (DMFS). [86, 147, 148, 162] Our patient data is further supported by our *in vitro* data. LOXL2 expression correlates with IDC cell aggressiveness, as the more aggressive MDA-MB-231 and MDA-MB-468 triple negative breast cancer cell lines show higher LOXL2 expression than less aggressive ER+/PR+ MCF7 cells. This phenomenon has been confirmed independently by other labs. [145, 147, 148, 151, 179] These results

suggest that LOXL2 regulation is critical for OSM-signaling promoted invasiveness and metastasis in IDC. These results are important, because previous research has shown that OSM promotes metastatic events through EMT, angiogenesis, and basement membrane degradation. Our research in addition suggests that OSM-induced LOXL2 also promotes metastatic events through the alignment of collagen I fibers found abundantly in the stroma, allowing mesenchymal-like tumor cells to efficiently migrate into vasculature and nearby tissue

Conclusion

In summary, we show for the first time that a proinflammatory cytokine (OSM) can promote the expression of ECM remodeling lysyl oxidases, specifically LOXL2, in IDC cells that leads to significant collagen I fiber crosslinking, alignment, and IDC invasion. Because collagen I fiber alignment is associated with increased tumor cell motility rate, and we observed an increase in 3D invasion within a collagen I matrix; OSM-induced LOXL2 may likely have an impact on metastasis. For our future goals, we will perform *in vivo* studies to determine how OSM-induced LOXL2 affects metastasis and *in vitro* experiments to determine the transcription factor and signaling mechanism responsible for the induction of LOXL2 by OSM. There is a major need for novel ways to treat and prevent breast cancer metastasis, and the mechanism behind OSM's induction of LOXL2 could prove to be exploitable in the race for more effective cancer therapies. In addition, OSM expression and signaling is linked to invasion and metastasis in other carcinomas including prostate, cervical, ovarian, kidney, and lung. [105, 203-206] Combined with our correlation data between OSMR and LOXL2 mRNA in glioblastoma, prostate, and ovarian cancer patients, it is possible that OSM induces LOXL2 in multiple

types of cancer and these patients could also benefit from a therapeutic targeting OSM induction of LOXL2.

Chapter Two Figures

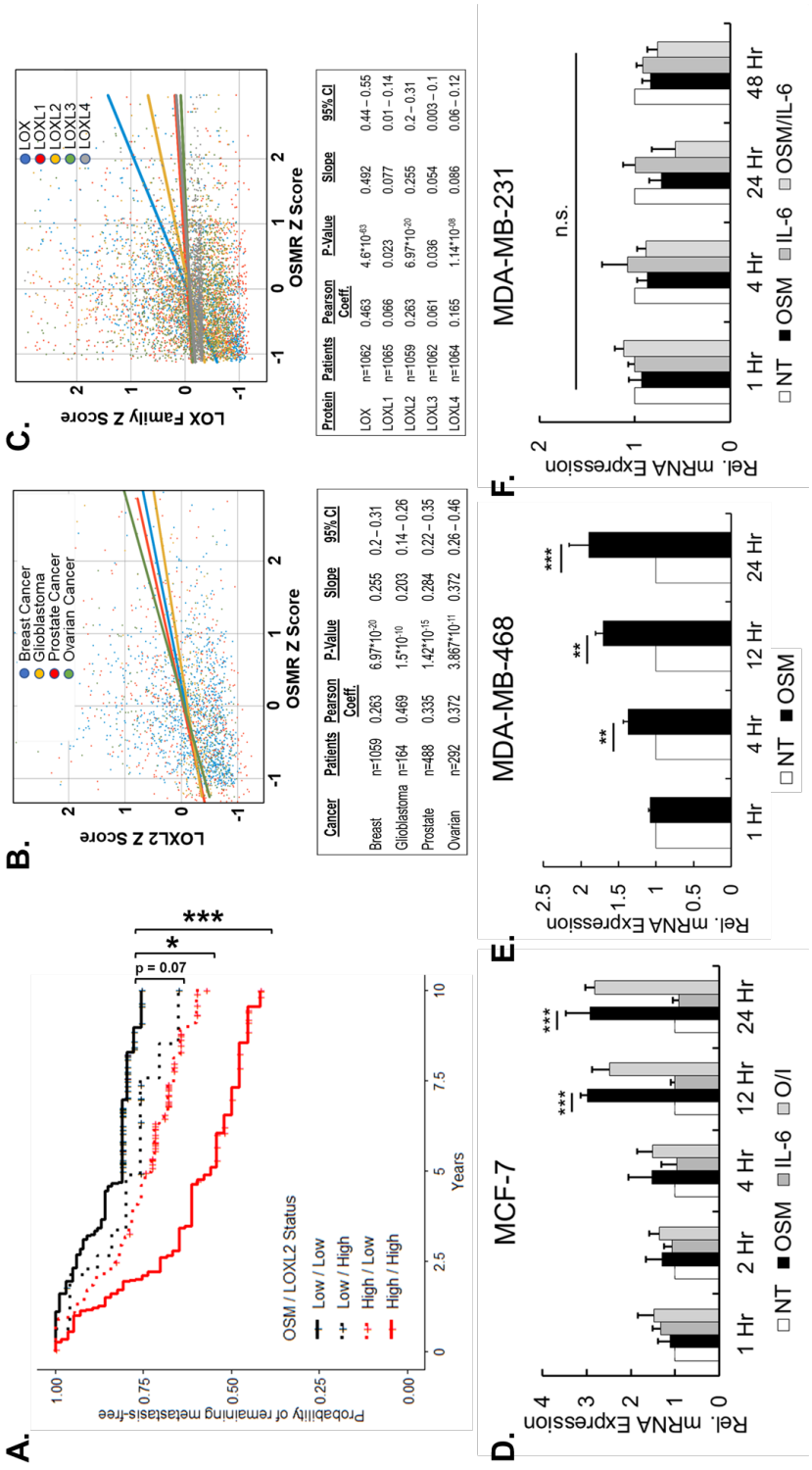

Cancer	Patients	Pearson Coeff.	P-Value	Slope	95% CI
Breast	n=1059	0.263	$6.97*10^{-20}$	0.255	0.2 – 0.31
Glioblastoma	n=164	0.469	$1.5*10^{-10}$	0.203	0.14 – 0.26
Prostate	n=488	0.335	$1.42*10^{-15}$	0.284	0.22 – 0.35
Ovarian	n=292	0.372	$3.867*10^{-11}$	0.372	0.26 – 0.46

Protein	Patients	Pearson Coeff.	P-Value	Slope	95% CI
LOX	n=1062	0.463	$4.6*10^{-63}$	0.492	0.44 – 0.55
LOXL1	n=1065	0.066	0.023	0.077	0.01 – 0.14
LOXL2	n=1059	0.263	$6.97*10^{-20}$	0.255	0.2 – 0.31
LOXL3	n=1062	0.061	0.036	0.054	0.003 – 0.1
LOXL4	n=1064	0.165	$1.14*10^{-08}$	0.086	0.06 – 0.12

Figure 2.1 Co-expression of OSM and LOXL2 Leads to Drastically Decreased Metastasis-Free Survival.

In **A.** Distant metastasis-free survival (DMFS) plotted from de Vijver et. al. (2002) invasive ductal carcinoma patient microarray database comparing low OSM/ low LOXL2 to low OSM/ high LOXL2, high OSM/ low LOXL2, and high OSM/ high LOXL2 mRNA expression (n = 295). We observed a stronger negative impact on DMFS with high OSM and LOXL2 co-expression compared to high expression of OSM or LOXL2 separately (Log Rank Test). **B.** LOXL2 mRNA expression Z-score is positively correlated as measured by Pearson correlation coefficient to the expression of OSM receptor (OSMR) mRNA expression Z-score in cancer patients analyzed from The Cancer Genome Atlas (TCGA) RNA-Seq database, specifically: breast cancer (BRCA), glioblastoma (GBM), prostate cancer (PRAD), and ovarian cancer (OV). Scatter plot consists of Z-score mRNA expression and line of best fit as determined by linear regression; a summary of the data is found in the accompanying table. **C.** The mRNA Z-score of several LOXL2 family members exhibit positive Pearson correlation to OSMR mRNA Z-score in the breast invasive carcinoma dataset from TCGA. **D.** qRT-PCR analysis of MCF7 luminal A invasive ductal carcinoma cells treated with OSM shows LOXL2 mRNA induction starting at 12 hours and peaking at 24 hours; there is no induction with IL-6. **E.** qRT-PCR analysis of MDA-MB-468 basal A invasive ductal carcinoma cells treated with OSM also shows an increase in LOXL2 mRNA expression starting at 4 hours. **F.** qRT-PCR analysis of MDA-MB-231 basal B breast cancer cells, that constitutively express high levels of LOXL2, show no significant induction of LOXL2 mRNA expression by either OSM or IL-6 signaling. (All qRT-PCR experiments n=3+; n.s. $p>0.05$, ** $p<0.01$, *** $p<0.001$; Two-way ANOVA).

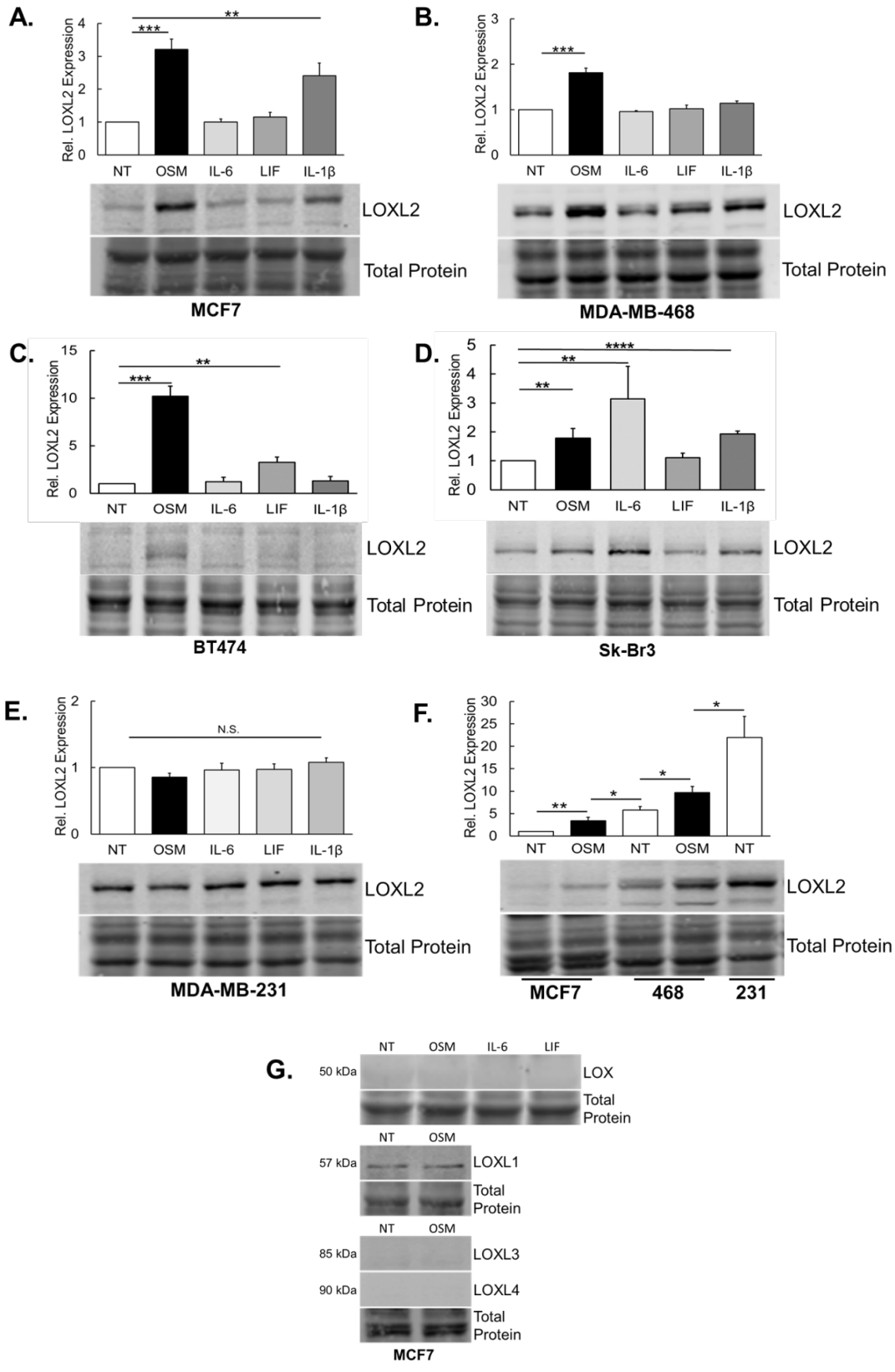

Figure 2.2 OSM Promotes LOXL2 Protein Expression.

All experiments and results pertain to immunoblot assays run with 10 - 20 μg total protein. **A.** MCF7 breast cancer cells were treated with OSM, IL-6, LIF, and IL-1β for 24 hours. Our analysis showed that only OSM and IL-1β promoted a significant upregulation of LOXL2 protein expression. **B.** In analyzing MDA-MB-468 breast cancer cells, the same treatments that are described above were utilized. We observed that only cells treated with OSM had significantly induced LOXL2 protein expression. **C.** BT474 breast cancer cells, under the same conditions, showed a significant increase in LOXL2 expression with OSM and LIF treatments. **D.** In Sk-Br-3 breast cancer cells, we observed a significant increase in LOXL2 expression with OSM and IL-6 treatment. **E.** We again used the same treatments in MDA-MB-231 breast cancer cells. LOXL2 expression was not significantly affected by either OSM, IL-6, LIF, or IL-1β treatment after 24 hours. **F.** Relative LOXL2 protein expression was compared among three breast cancer cell lines treated with OSM. From least invasive (MCF7) to the most (MDA-MB-231), we observed a stepwise increase in LOXL2 protein expression. OSM treatment bridges LOXL2 expression between cells. **G.** MCF7 cells were treated for 24 hours with OSM; OSM, IL-6, and LIF for LOX expression. No changes are observed in lysyl oxidase expression; LOXL1 is constitutively expressed. (All experiments n=3+; n.s. $p>0.05$, ** $p<0.01$, *** $p<0.001$; One-way ANOVA).

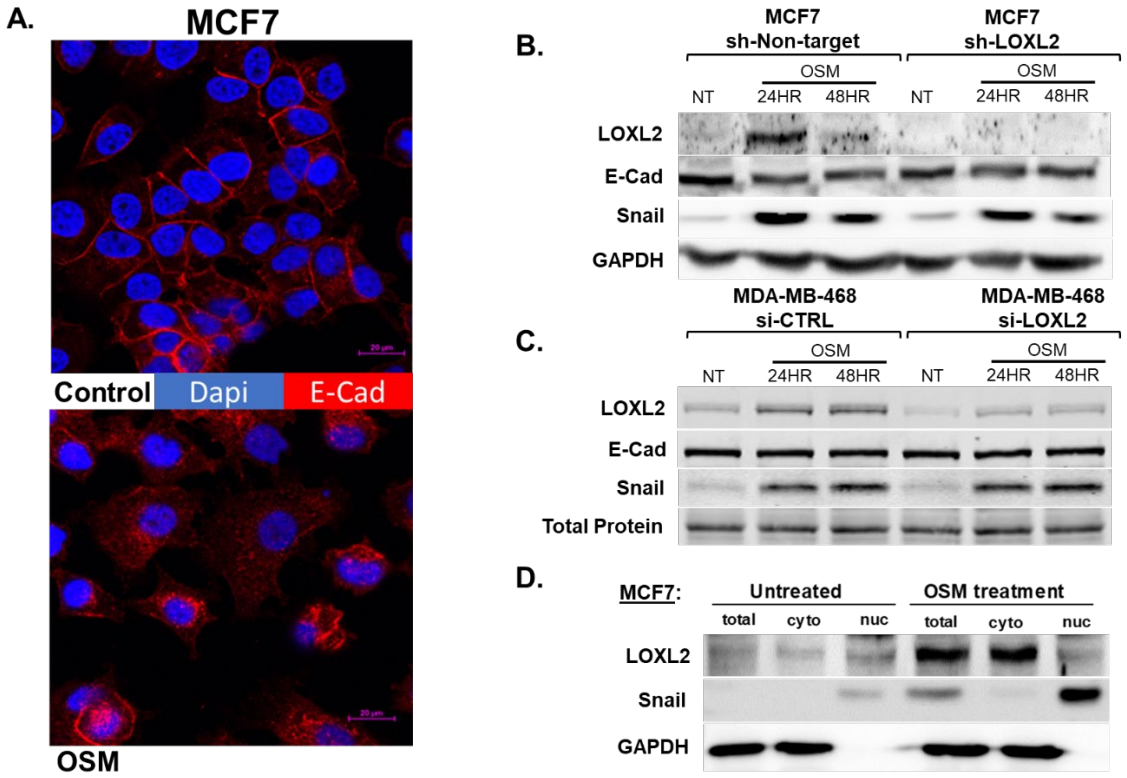

Figure 2.3 OSM Signaling Promotes an EMT That is Independent of LOXL2 Expression.

In **A.** Confocal images of MCF7 cells depict a distinct loss of cellular junctions and a transition from membrane localization to cytoplasmic localization of E-Cadherin with 48-hour OSM treatment, both hallmarks of EMT. E-cadherin (Red), and nuclei (DAPI, blue). Magnification x40 with digital zooming x2; Scale Bar = 20 µm. **B.** Immunoblot of MCF7-sh-Non-Target and MCF7-sh-LOXL2 cells treated with OSM for 24 and 48 hours. Expression of EMT markers, E-Cadherin (E-Cad) and Snail, are compared between these cell lines. The absence of LOXL2 expression in MCF-7 cells had no effect on OSM induced EMT. **C.** Immunoblot of MDA-MB-468 breast cancer cells exposed to siCTRL and siLOXL2 for 48 hours prior to OSM treatment for 24 and 48 hours. Expression of EMT markers, E-Cad and Snail, are compared between siLOXL2 and siCTRL treatments. Inhibited LOXL2 expression in MDA-MB-468 cells had no effect on OSM induced EMT. **D.** Immunoblot of MCF7 cells treated with OSM for 24 hours; post treatment cells are collected and subjected to nuclear-cytoplasmic protein fractionation. LOXL2 protein expression is not present in the nuclear fraction, only in the cytoplasmic fraction. GAPDH protein expression is used to confirm purity of cytoplasmic fraction and Snail

transcriptional factor expression is used to confirm nuclear fraction purity. (All experiments n=3+).

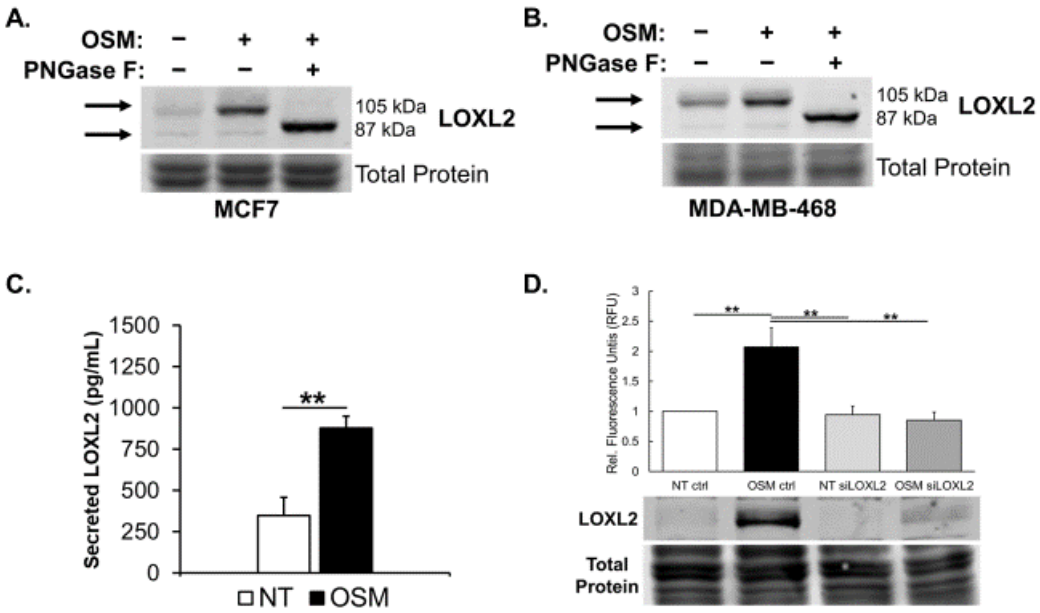

Figure 2.4 OSM-Induced LOXL2 is Glycosylated, Enzymatically Active, and Secreted from IDC Breast Cancer Cells.

In **A.** MCF7 and **B.** MDA-MB-468 cells were treated with OSM for 24 hours to induce the expression of LOXL2. PNGase F, an N-linked glycosylase, is then added to cleave N-linked glycosylation sites. The immunoblot results confirm LOXL2 glycosylation as the LOXL2 protein band size goes from ~105 kDa to ~87 kDa with PNGase F treatment. **C.** Lysyl oxidase activity assay performed on MCF7 cell conditioned media (CM) is analyzed by using an Amplex red based fluorometric assay. Immunoblot analysis is utilized to confirm siLOXL2 knockdown of LOXL2 expression. Results show that 24-hour OSM treatment led to significantly increased lysyl oxidase activity, this is repressed with exposure to siLOXL2. **D.** ELISA is used to quantify LOXL2 protein secreted into CM from MCF7 cells after 36 hours with OSM treatment. The results confirm that OSM signaling induces the expression, and promotes the secretion, of LOXL2 protein. (All experiments n=3+; * $p<0.05$, ** $p<0.01$, *** $p<0.001$; Student's t test & One-way ANOVA).

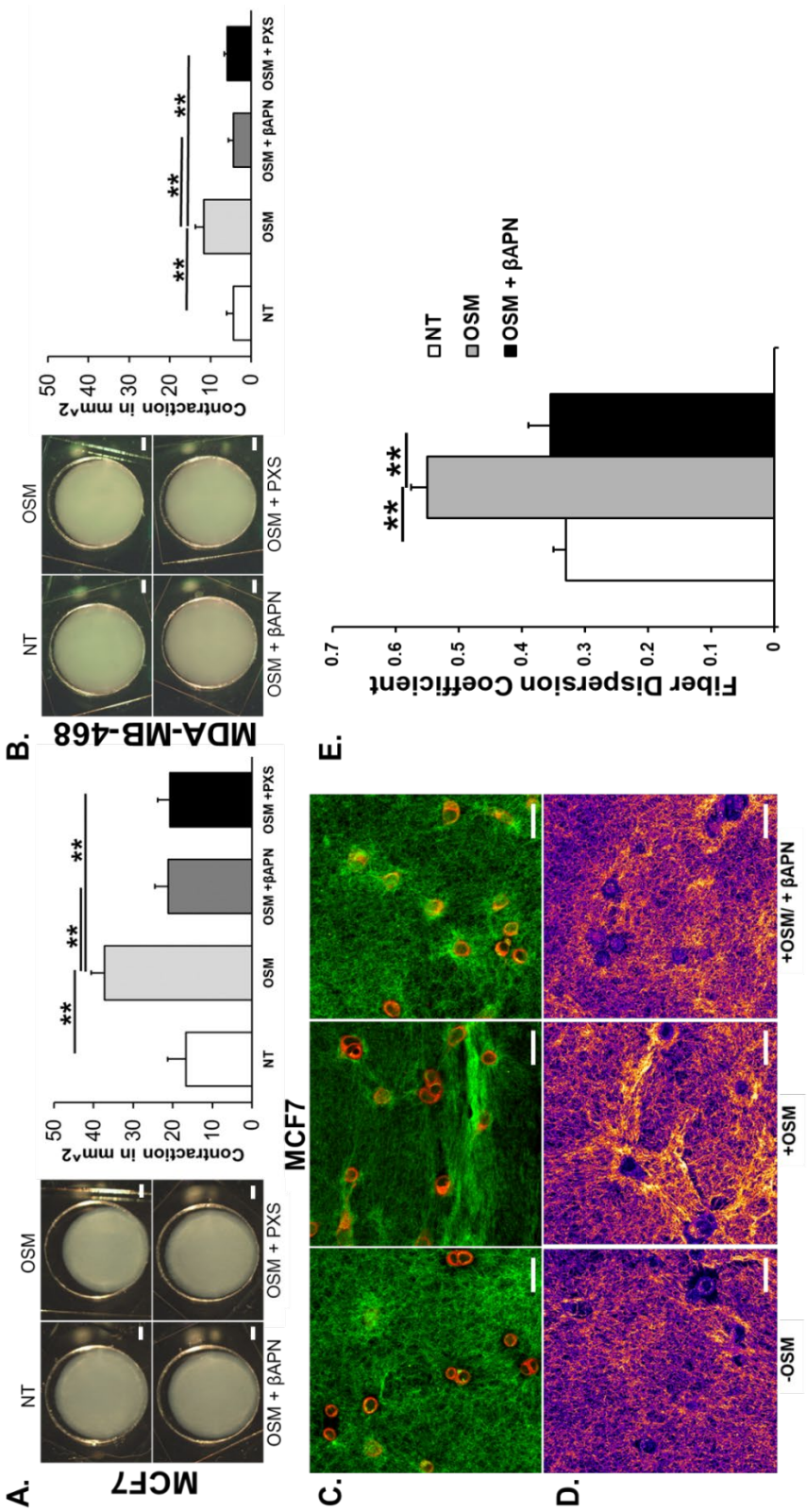

Figure 2.5 OSM-Induced LOXL2 Promotes ECM Crosslinking and Alignment of Collagen I Fibers.

In **A.** Collagen contraction assay was performed using 1.5 mg/mL collagen I matrices or "pucks" seeded with MCF7 cells and treated for 48 hours with OSM or OSM with βAPN (500 μM) or PXS-5120A (200 nM) [LOXL2 inhibitors]. After 48 hours, dissecting microscope images of the collagen I matrix depict significantly more contraction in the OSM-treated samples, which is reversed in the presence of LOXL2 inhibitors. Scale bar = 2 mm. Graph quantifying the change in area of the matrix (in mm^2) due to contraction. Collagen I fiber contraction correlates to fiber crosslinking and is reversed with the inhibition of LOXL2. **B.** The same experiment as above was performed with MDA-MB-468 cells. Representative images after 48 hours and accompanying graph are depicted using the same scale as above. As with MCF7 cells, LOXL2 inhibition prevented contraction due to OSM-induced LOXL2, but overall contraction is not as pronounced. Scale bar = 2 mm. **C.** Confocal images of the collagen "pucks" depict the increase in collagen I fiber (green) alignment between MCF7 cells (red) in collagen I matrices that are treated with OSM for 36 hours. Alignment is not observable with the addition of LOXL2 inhibition using βAPN (500 μM). Magnification x63; Scale bar = 50 μm. **D.** Representative images with areas of greatest collagen I fiber density emphasized using ImageJ image processing. This clearly highlights the increase in fiber density and alignment present with OSM treatment, which reversed by LOXL2 inhibition. **E.** Graph depicting the average fiber dispersion coefficient of collagen I fibers perpendicular to and bridging MCF7 cells in collagen I matrices. Confirms qualitative data that OSM treatment significantly increases alignment which is reversed with LOXL2 inhibition. (All experiments n=3+; ** $p<0.01$, *** $p<0.001$; One-way ANOVA).

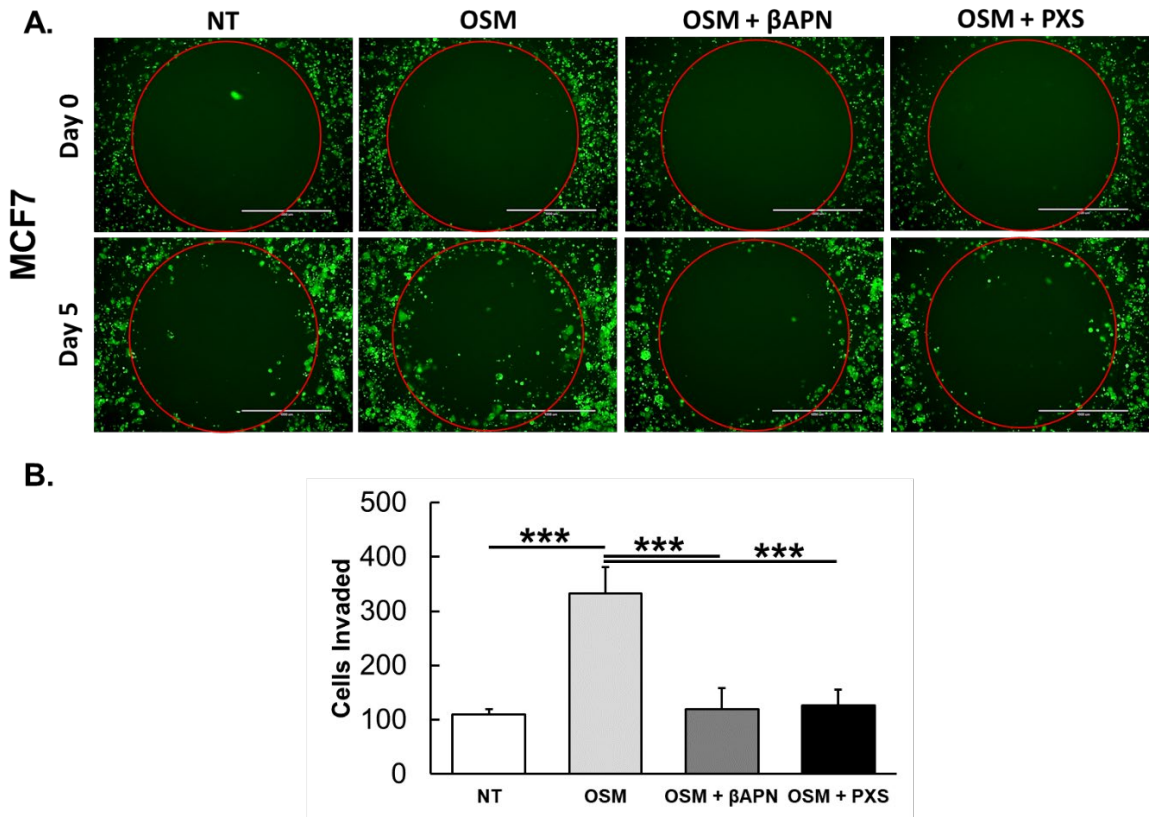

Figure 2.6 OSM-Induced LOXL2 Promotes Invasion in 3D Extracellular Matrix.

In **A.** MCF7-GFP cells were seeded into a 1.5 mg/mL collagen I solution and molded into wells of a 96-well plate containing "cell-free zones". Cells were supplemented with β-estradiol (50 ng/mL) and treated with OSM, OSM with βAPN (500 μM), or OSM with PXS-5120A (200 nM). Fluorescent images were taken at Day 0, and at the conclusion of the experiment on Day 5. We observed an increase in 3D invasion of MCF7 cells treated with OSM that was limited by the inhibition of LOXL2 enzymatic function using βAPN or PXS-5120A. Scale bar = 1,000 μm. **B.** Graph represents the total number of MCF7-GFP cells that invaded into the cell-free space by Day 5, with the various treatments discussed above. OSM treatment significantly increases 3D invasion in MCF7 cells and that is significantly reversed by LOXL2 inhibition. (Experiment n=3; *** $p<0.001$; One-way ANOVA).

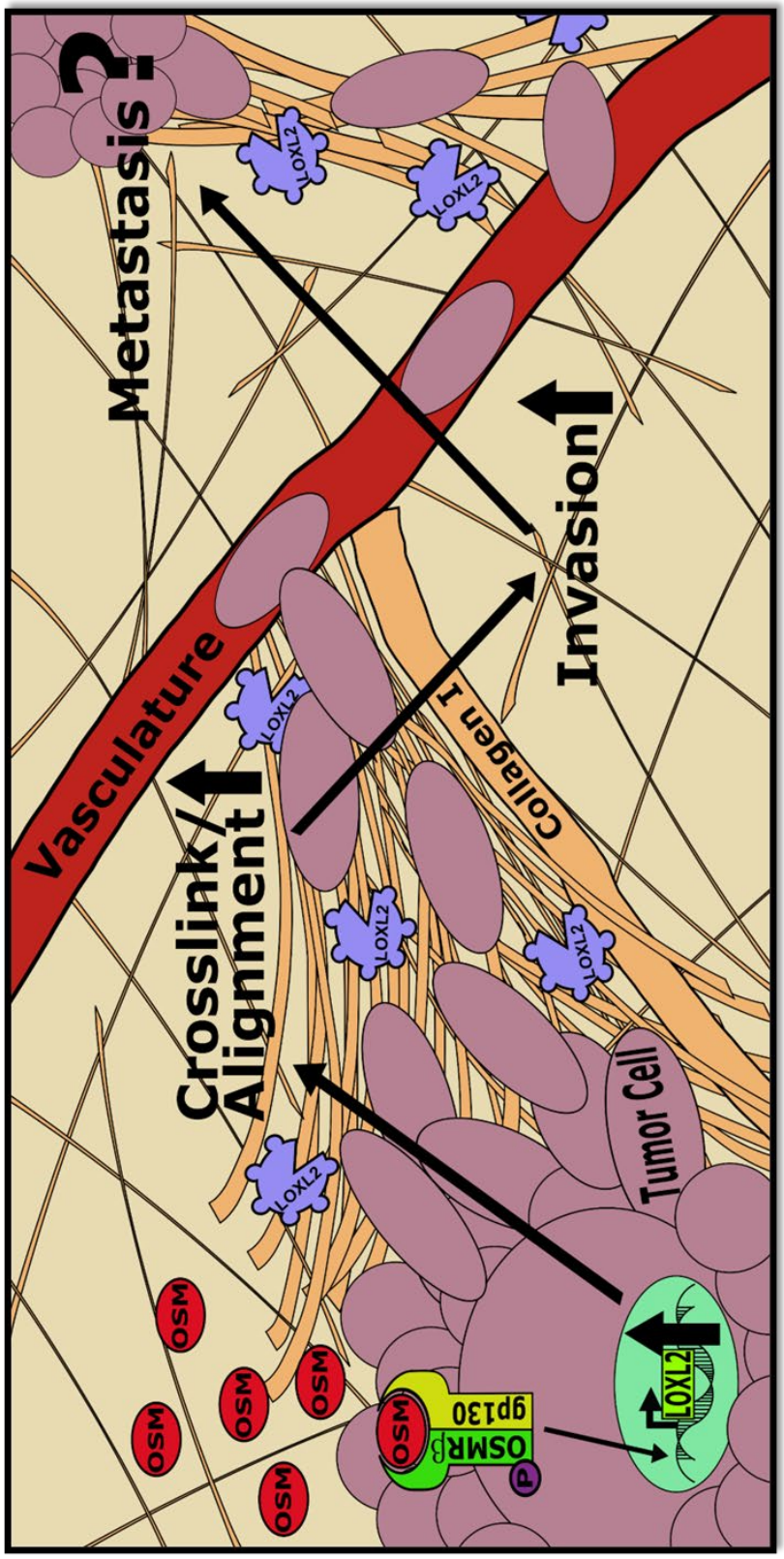

Figure 2.7 Mechanism by Which OSM-Induces LOXL2 and Promotes ECM Remodeling.

OSM binds to gp130, which recruits OSMRβ to form a heterodimer and allow the phosphorylation and activation of downstream signaling pathways, including STAT3, MAPK, and PI3K. OSM signaling promotes EMT in invasive ductal carcinomas and as the data shows LOXL2 expression in its ~105 kDa glycosylated form. The 105 kDa LOXL2 is enzymatically active and secreted into the ECM of the breast tumor microenvironment. In the ECM, LOXL2 promotes crosslinking of the main constituent of the stroma, collagen I, which leads to collagen I fiber alignment. The alignment of collagen I fibers in the stroma provides pathways for cancer cells that have undergone EMT to invade nearby tissue and vasculature. Therefore, these changes to the ECM of the tumor microenvironment likely play a functional role in invasive ductal carcinoma metastasis.

CHAPTER THREE: OSM-INDUCED LOXL2 ECM REMODELING PROMOTES BREAST CANCER METASTASIS; OSM IS SYNERGISTIC WITH IL-1B, AND REQUIRES C-MYC EXPRESSION

Background

In the previous chapter, we presented results that highlighted a novel mechanism involving proinflammatory cytokine promoted IDC cell invasion that had yet to be observed prior to our research. However, proinflammatory cytokines from the interleukin-6 (IL-6)-family and interleukin-1 (IL-1)-family of ligands, such as oncostatin m (OSM) and interleukin-1beta (IL-1β) respectively, have been increasingly studied for their role in IDC progression and ultimately metastasis. The STAT3, MAPK, PI3K, and NF-κB signaling pathways that are activated by these proinflammatory cytokines are known to promote irregular gene expression, especially through oncogene upregulation and tumor suppressor downregulation. Exemplifying this mechanism OSM binds to gp130 receptor subunit, the ligand-receptor pair recruit and dimerize with the OSM receptor beta (OSMRβ) subunit to form an OSMR complex, the interaction results in downstream signaling by activating Janus kinase-1 and 2 (JAK1/2) phosphorylation cascade [170]. The inflammatory response resulting from OSM signaling causes abnormalities in IDC cells that are hallmarks of cancer progression by stimulating cell survival, epithelial-to-mesenchymal transitions (EMT) for motility, oncogenic transcription factors (TF) such as c-Myc, and secretion of angiogenic growth factor VEGF and basement membrane degrading matrix metalloproteases (MMPs). These

effects make up what is currently known about the role of OSM in IDC, forming the paradigm for OSM-promoted tumor progression and metastasis. However, our research will likely persuade further studies involving inflammatory cytokine promoted ECM remodeling which we hope will lead to novel mechanisms that will add to our understanding of IDC progression and metastasis. We observed that OSM, and to a lesser extent IL-1β and IL-6, mediated indirect remodeling of extracellular matrix (ECM) collagen I matrices, which makes up 60 - 80% of the stromal ECM proteins in IDC tumor microenvironments (TME). [146] The remodeling is caused by the overexpression of lysyl oxidase like-2 (LOXL2) induced in response to cytokine signal transduction. LOXL2 enzymatic glycoprotein catalyzes an amine to aldehyde oxidation in the peptidyl lysine residues located towards the end of collagen fibrils and fibers, predominantly in collagen I. This is known as collagen crosslinking which promotes the maturation of the ECM tissues, consequently it also promotes fiber alignment between cancer cells in and detached from the primary tumor throughout the TME. OSM, IL-1β, and other proinflammatory cytokines are secreted by neutrophils and macrophages found in the TME altered by IDC tumors to become tumor associated neutrophils and macrophages. As TANs and TAMs, they aggressively respond to inflammation by producing excessive amounts of growth factors, chemokines, and inflammatory cytokines; including OSM and IL-1β. These then induce LOXL2 expression and cause significant crosslinking, fiber alignment, and IDC invasion through collagen I matrices as observed *in vitro*. [119, 125, 146, 190, 207]

As stated above, OSM-induced LOXL2 promoted significant ECM remodeling and studies have confirmed that collagen I fiber alignment is associated with increased

tumor cell velocity when motile. [126-128, 158] Bearing that in mind, OSM-induced LOXL2 could have an important role to play in OSM-mediated tumor progression and more specifically have an impact on metastasis. To test our hypothesis, a novel mouse model featuring luminal A ER+ MCF7-Luc IDC cells that constitutively express luciferase and full length OSM (MCF7-Luc-flOSM) or only luciferase in empty vector control cells (MCF7-Luc-EVctrl) injected into the 4^{th} mammary fat pad of immunocompromised nude athymic mice was developed. These mice were treated with either PXS-5382, a LOXL2/3 specific small molecule inhibitor (SMI), or vehicle control formulated into chow for consumption. The results from the *in vivo* study and the *ex vivo* bioluminescent images of resected organs subsequently taken at the study's conclusion indicated the presence of metastatic lesions and further analysis confirmed the importance of LOXL2 enzymatic activity on ECM collagens significantly affected OSM mediated metastasis. This confirmed our hypothesis that LOXL2 mediated ECM remodeling indeed plays an important role in IDC metastasis and tumorigenesis in IDC cells. In addition to our *in vivo* study, an analysis of OSM's canonical signaling pathways was performed *in vitro* to determine the method of OSM signal transduction involved in LOXL2 induction. Inhibition of OSM's canonical signaling pathways and the affects observed in LOXL2 expression suggested the presence of the transcription factor c-Myc was necessary as a mediator for OSM signaling. Further *in vitro* research highlighted the synergistic expression of LOXL2 in IDC cells treated with OSM and IL-1β. The impact of these results may lead to a shift in ideology involving cytokine research, where ECM modifications promoted by proinflammatory cytokine-induced LOXL2 or potentially other lysyl oxidases becomes a critical component in IDC tumor progression and

metastasis studies and drug development, similar to the way OSM and IL-6 promoted EMT and angiogenesis are considered.

Materials and Methods

Cells and Cell Culture

Non-transformed human IDC cell lines MCF7 (HTB-22), MDA-MB-468 (HTB-132), and BT474 (HTB-20) utilized were purchased from the American Type Culture Collection (ATCC; Manassas, VA). The firefly luciferase bioluminescent enzyme expressing (-Luc) transformed IDC cell line MCF7-Luc (Bioware MCF-7-Luc-F5) was obtained from PerkinElmer Inc. (Waltham, MA); however, this specific cell line is no longer available, a new cell line is sold instead, Bioware: IVISBrite MCF-7 Red F-Luc. Luminal A MCF7 and MCF7-Luc [ER+, PR+, HER2-] cell lines were cultured in RPMI 1640 with L-glutamine (Genesee Scientific; San Diego, CA), while luminal B BT474 [ER+, PR+, HER2+] and triple negative breast cancer (TNBC) basal-like A MDA-MB-468 [ER-, PR-, HER2-] cell lines were cultured in DMEM with L-glutamine and high glucose (Genesee Scientific). All cell media contained 10% v/v Fetal Clone III (Cytiva Biotechnology-HyClone; Marlborough, MA) and 1% v/v of 100x penicillin/streptomycin (Genesee Scientific). Cells were cultivated in tissue culture (TC) treated T25 and T75 flasks and 6-, 12-, 24-, 96-well plates (Genesee Scientific) kept in a Model 3110 (Forma Scientific; Marietta, OH) incubator at 37°C and 5% CO2. Cells grown to ~75% confluence before plating for experiments. At various time intervals, IDC cells were treated with either 25 ng/mL of 209 aa recombinant human OSM (rhOSM) and/or 10 ng/mL of rhIL-1β (Peprotech Inc.; Rocky Hill, NJ) stored at -20°C in 1x PBS (Genesee

Scientific) with 0.2% bovine serum albumin (BSA) as a carrier protein for cytokine stability (Thermo Fisher; Waltham, MA).

Reagents and Small Molecule Inhibitors

There are five different small molecule inhibitors (SMIs) that were used during experimental procedures, all of which, except the LOXL2 SMI, were dissolved in sterile cell culture grade 100% DMSO (VWR International; Radnor, PA) and then aliquoted and stored at -80°C. These were all from same company: 1) MEK1/MEK2 SMI, preventing pERK phosphorylation, named PD0325901 at 5 mM stock dilution; 2) PI3Kα/δ SMI, preventing pAKT phosphorylation, named GDC-0941 also at 5 mM stock dilution; 3) STAT3 SH2 domain SMI, preventing pSTAT3 phosphorylation, named Stattic at 100 mM stock dilution; and 4) c-MYC/Max protein association and dimerization SMI, prevents c-MYC transcriptional activity, named 10058-F4 at 100 mM stock dilution (Sigma Aldrich; St. Louis, MO). Prior to 15-minute and 24-hour treatment with rhOSM, IDC cell lines were incubated with of these signal pathway SMIs or vehicle control for DMSO for 2 hours. The LOXL2/3 specific SMI that prevents catalysis of collagen I crosslinking by binding to and blocking the active binding site for peptidyl lysine and hydroxylysine amine groups in LOXL2/3 called PXS-5382 (Pharmaxis Ltd.; New South Wales, AUS). This SMI was integrated into a specialized chow formulated for *in vivo* studies, due to its great oral bioavailability, allowing for continuous exposure to LOXL2 inhibition in mice (Research Diets Inc.; New Brunswick, NJ).

One gram of 17β-estradiol (estrogen or E2) (Sigma-Aldrich) was dissolved in 200 proof ethanol to a concentration of 20 mg/mL and sterile filtered with a hydrophobic polyvinylidene fluoride (PVDF) 0.22 μm luer locking syringe filter attachment cased in

PVC plastic that resists degradation from pure ethanol (Millipore Sigma; Burlington, MA). E2 was aliquoted and stored at -20°C until it is needed and then added to bottled drinking water for the mice to achieve 4 mg/L of E2 with the ethanol diluted to very low percentage of 0.02% and won't interfere with mouse health or activity.

For bioluminescent visualization of the MCF7-Luc IDC cell line and derived cell line colonies that were i, IVISBrite D-luciferin potassium salt (Xenolight, PerkinElmer) was dissolved to 100x (15 mg/mL) in sterile 1x PBS (Genesee Scientific) and sterile filtered using a polyether sulfone (PES) 0.22 μm luer lock syringe filter attachment (Millipore Sigma) was used. This solution was diluted 1:100 in culture media to make it 1x (15 μg/mL) for *in vitro* or added directly at a volume of 200 μL for *in vivo* bioluminescent imaging.

Sterile antibiotics, blasticidin and geneticin (G418) (Thermo Fisher), were diluted into sterile 1x PBS at 5 mg/mL and 50 mg/mL respectively. Blasticidin was used for selection during cell transduction at 5 μg/mL and to maintain isolated colonies at 2.5 μg/mL, G418 was used to maintain luciferase expressing cells at 250 μg/mL.

Cell Transduction

For full-length human OSM (flOSM) vector transduction, the luminal A IDC cell line MCF7-Luc was used, which was purchased from PerkinElmer already transformed to express the bioluminescent, enzymatic firefly luciferase protein by the incorporation of a firefly luciferase expression vector with G418 antibiotic resistance. Antibiotic resistance was critical when determining the plasmid for flOSM cDNA integration, so that the resistances were different and did not overlap and prevent colony selection from taking place. The MCF7-Luc cells were transformed to constitutively overexpressing flOSM

(MCF7-Luc-flOSM) or empty vector control (MCF7-Luc-EVctrl) using CMV promoter containing pLenti6.3/TO/V5-DEST plasmid found in the ViraPower™ HiPerform™ T-Rex™ Gateway™ Vector Kit (Thermo Fisher) according to the accompanying protocol. The plasmids contained either the full-length human OSM (flOSM) cDNA sequence, inserted according to protocol in the manual, or were left empty (Evctrl) to control for the effects of transduction in MCF7-Luc cells by lentiviral particles.

A series of volumes (20 µL to 100 µL) for each lentiviral plasmid construct, flOSM and EVctrl, was added to the wells of a TC treated 96-well plate (Genesee Scientific) plated with 15,000 or 30,000 cells in triplicate for each vector and volume combination for a total volume of 200 µL in combination with RPMI 1640 complete media; therefore, MCF7-Luc cells were exposed to lentiviral particles at ratios of 1:10 up to 1:2 for 24 or 48 hours. Cells were washed with 1x PBS and 200 µL of complete RPMI 1640 media was added containing 5 µg/mL of blasticidin, to select for MCF7-Luc cells that expressed flOSM or EVctrl media. Selection media was replaced every 3 to 4 days until there were stable colonies to isolate and subclone. These were maintained by intermittently adding 2.5 µg/mL blasticidin to media. For luciferase expression maintenance in parental MCF7-Luc and MCF7-Luc-flOSM and MCF7-Luc-EVctrl colonies, 250 µg/mL of G418 was added intermittently to media. Selected colonies were established, followed by characterizing the morphology and protein expression of each colony to find suitable cells for *in vivo* studies. RPMI 1640 media was slowly replaced with DMEM media due to excessive detachment observed in the MCF7-Luc-flOSM colonies using RPMI 1640 media at confluency that DMEM prevented.

Lentiviral Particles

The flOSM and EVctrl pLenti6.3/TO/ V5-DEST plasmids were transfected into HEK293FT cells (Thermo Fisher) with the use of ViraPower™ Packaging Mix (Thermo Fisher) and Lipofectamine 2000 (Thermo Fisher) following the protocols provided in ViraPower™ HiPerform™ Lentiviral Expression Systems (Thermo Fisher). All biosafety level 2 (BSL-2) guidelines and protocols were adhered to, including the use of a Class 2 tissue culture hood. After 24-hour incubation, the above transfection media was removed and replaced with fresh media after 1x PBS rinse. Conditioned media (CM) with plasmid containing lentiviral particles that were formed and released by cells was collected 72 hours later. The resulting lentiviral media solution was carefully handled prior to cellular debris being eliminated by CM centrifuged at 300 g for 5 minutes and sterile filtered using a PVDF 0.45 μm luer lock syringe filter (Millipore Sigma). Following CM clean-up the lentiviral solution was titrated following ViraPower™ manufacturer protocol. Once the solution was titrated, the lentiviral CM was safely and sterilely aliquoted into cryovials with screw on caps that had O-rings for an air tight seal (Genesee Scientific) and stored at -80°C.

Mouse Model

This *in vivo* model, and the subsequent procedures implemented throughout and at experimental endpoint, were determined to be humane and necessary receiving approval from the authorized IUCAC board at Boise State University. For this mouse model 40 Foxn1^{nu} homozygous female nude athymic mice were purchased at 7-8 weeks of age (The Jackson Laboratory; Bar Harbour, ME). After a mandatory day of quarantine, the mice were divided into 2 groups of 20 mice and given drinking water supplemented with

estrogen (4 mg/L of 17β-estradiol) for 5 days prior to tumor cell injections and throughout the entire length of the experiment (Sigma-Aldrich; St. Louis, MO). After 5-day pretreatment with E2, mice from each group received a 50 µL injection in the 4th mammary fat pad using a sterile 27G 0.5CC syringe (Becton, Dickinson, and Company or BD; Franklin Lakes, NJ) containing 50% Matrigel (9.1 mg/mL) basement membrane matrix (Corning; Corning, NY) mixed with 50% or 25 µLs of either 2.0x10^6 cells of the human flOSM constitutively overexpressing MCF7-Luc-flOSM cell line or 2.0x10^6 cells of the lentiviral transduction control MCF7-Luc-EVctrl cell line, described in the Cell Transduction section. These mice were placed in their assigned cages, where 5 mice occupied each cage for a total of 8 cages placed on racks, which were connected to an individually ventilated caging system (IVC). After palpable tumors 1 - 2 mm in diameter were detected in mice from both groups 10 days since being injected with the two MCF7-Luc derived cell lines, they received IP injections of 200 µL of 100x luciferin before imaging with IVIS. The mice were further separated, distributed according to tumor bioluminescence to be evenly grouped, from 2 groups of 20 mice into 4 total groups of 10 mice each. A group of 10 mice from both the MCF7-Luc-flOSM and MCF7-Luc-EVctrl injected mice received LOXL2 inhibition through specially formulated chow infused with a PXS-5382 LOXL2 SMI, while the other 10 mice received control chow. The 4 groups were: MCF7-Luc-flOSM (Vehicle), MCF7-Luc-flOSM (PXS), MCF7-Luc-EVctrl (Vehicle), and MCF7-Luc-EVctrl (PXS). Estrogen supplemented water and chow with treatments were restocked as necessary and checked on daily by Vivarium technicians. Cages, bedding and nesting materials, rodent enrichment devices, and chew sticks were replaced weekly or as was required for the health of the mice, especially with the

compromised immunity of nude athymic mice. Upon the conclusion of the experiment, due to waning health of the mice, experimental endpoint procedures were implemented with great care. The resulting measurements and collected tissues were carefully gathered, labelled, analyzed, and stored for future use.

Weight, Tumor Size, Score, and Bioluminescent Imaging

According to our protocols, mice must be weighed, scored for pain, and their tumors measured by millimeter (mm) scaled caliper 3 times a week on Monday, Wednesday, and Friday. The mice were removed from their IVC racks, one cage at a time, and weighed on an animal transfer station (Nuaire; Plymouth, MN) using a gram scale sensitive enough that could measure changes in weight as low as 0.1g. In addition to the weight measurement, mice were also scored from a score of 0 to 2 based on the number and severity of the signs that are proven to correlate to pain experienced by mice. The score provided for the mice is in accordance to The National Centre for the Replacement, Refinement and Reduction of Animals in Research's (NC3R's) Mouse Grimace Scale where symptoms such as nose bulge, eyelid tightening or closing, and several other are signs of pain or distress. [208] A Digital caliper was then used to measure the diameter of the resulting tumors, where length and width diameters were measured in cases where the tumor was not approximately spherical. On Wednesday's, when tumor growth and progression was further assessed, mice would receive 200 µL of 100x (15 mg/mL) of luciferin administered by IP injection using 27G 1CC sterile syringes. The luciferin interacts with the luciferase enzyme constitutively expressed by the transduced MCF7-Luc-flOSM and -EVctrl to produce bioluminescent signature that

is detectable by IVIS Spectrum imager (PerkinElmer). This, and the procedures specified above, were carried out weekly until the conclusion of the experiment.

Endpoint Procedures

At the conclusion of the *in vivo* experiment, endpoint procedures were performed that included final live mouse measurements, anesthesia, blood collection and serum isolation, euthanasia, organ and tumor tissue resections, and *ex vivo* bioluminescent imaging. Prior to sacrifice, final measurements were taken for weight, pain score, and caliper in all of the mice before they received luciferin IP injections to perform final bioluminescent tumor assessment. After imaging, the mice were sacrificed one mouse at a time, starting with the first cage that was imaged. Luciferin was administered for a second time before anesthetization in a gas chamber using 3% of the gaseous anesthetic isoflurane mixed with 24% medical grade oxygen at a flow rate of 0.7 L/min. Anesthetization was continued as mice were moved to a nose cone where terminal intracardiac puncture procedures were performed using 27G 1CC sterile syringes for blood collection. For each mouse, the skin layer was removed around the belly and rib-cage, exposing peritoneum. A syringe was inserted, bevel up, into the base of sternum at a 20° angle under or slightly left of the xyphoid process. The syringe was aspirated slowly and 0.6 mL to 1.0 mL of blood was collected from each mouse, of which half was saved for serum isolation and rest was kept uncoagulated in EDTA tubes (BD Biosciences). Immediately afterwards, each mouse was euthanized by cervical dislocation, followed by dissection and the resection of primary the tumor and all relevant organs, using a different pair of tweezers and surgical scissors for each so organs were not contaminated with primary tumor tissue.

Ex vivo Imaging and Tissue Preservation

The organ tissues that were resected were placed on clear 60 mm petri dishes and used for *ex vivo* bioluminescent imaging analysis using the IVIS Spectrum imager (PerkinElmer). These tissues included the primary tumor, ovaries, lungs, liver, brain, spleen, kidneys, GI tract, spine, and femur bone opposite of the tumor site. First, the organs including the primary tumor was imaged with short, 1 second exposure times, to confirm that bioluminescent signal was present in the mice, after which the tumor was removed from the petri dish. Without the primary tumor to mask potential bioluminescence the organs were imaged again, exposed for 1 minute, followed up by 3 minutes to determine the presence of metastatic lesions through their relatively weak bioluminescent signal. The tumor during this time was split and half of the tissue was snap frozen in liquid nitrogen and placed in -80°C freezer for immunoblot analysis and other proteomics. The rest was fixed in 10% formalin (Thermo Fisher) for future immunohistochemistry analysis. After imaging, the rest of the organs were fixed in 10% formalin as well, added to the same 50 mL conical tube as the tumor section.

Analysis of Tumor Growth and Metastasis

Tumor size and growth over time was determined using the caliper measurements taken 3 times weekly, throughout the course of the *in vivo* study and at the study's conclusion. The primary tumor size was calculated in terms of volume (mm^3) using the accepted formula (length x width^2)/ 2 for all the tumors measured. [209] In instances where mice had two distinct lobes for the primary tumor, each lobe was measured separately as where the calculated volumes and then added together. The metastatic burden on each group of mice was calculated by creating ROIs around organs with

bioluminescent signal and comparing the bioluminescence of the groups. Metastasis was also determined by the fraction of mice where metastatic lesions were present and the fractions of organs in which they were observed.

Immunoblot Assay

Immunoblot processing and imaging followed the same method previously described in CHAPTER TWO and in previous publication. [146] Details for primary antibodies used for this chapter and relevant differences in methodology from previous work follow. 10 μg of total protein for OSM signaling pathway protein phosphorylation analysis and 20 ug for all other proteins analyzed including proteins from primary tumor derived cells were loaded per lane, as determined by Peirce™ BCA Protein Assay Kit (Thermo Fisher). Primary antibodies used to determine protein expression were all targeted for human epitopes associated with LOXL2 (Genetex Inc.; Irvine, CA), OSM (Santa Cruz Biotechnology, Dallas, TX), firefly Luciferase (Sigma Aldrich); ERα, E-Cadherin, Snail-1, c-Myc, p-c-Myc [Ser62], p-c-Myc [Thr58], pERK, pAKT, and pSTAT3 (Cell Signaling Technology; Danvers, MA). All blots are incubated with primary antibodies at [1:1000] dilution, except for OSM [1:500] and pAKT [1:2000].

Quantitative ELISA

Conditioned media (CM) or lived-in cell culture media that contains extracellular proteins and biomolecules secreted by cells over time, was collected from IDC cells and analyzed by ELISA to determine and compare the concentrations of secreted hLOXL2, hOSM, and hVEGF proteins at various times and treatments. These assays were performed and analyzed according to the protocols provided with the DuoSet ELISA Kits (R&D Systems; Minneapolis, MN) specific for each protein. These are all quantitative

ELISAs because the exact weight / volume concentration can be determined from the results, using a standard curve. Lyophilized recombinant hOSM, hLOXL2, and hVEGF came with each kit so that standard curves, ranging from 2000 pg/mL to 31.25 pg/mL for hOSM and hVEGF, and 24 ng/mL to 0.375 ng/mL for LOXL2, could be calculated. Each sample was analyzed in triplicate, duplicate when there were too many samples, and the resulting 450 nm absorbance values were compared against the standard curves created from fitting a 2^{nd} degree polynomial or 4PL sigmoidal curve to get the concentration of each protein.

Cytokine Synergy Analysis

Synergistic interactions are defined as deviations from the additive linear response of the measured outcome, either by up- or down-regulation, between two different treatment vectors. To determine synergistic interactions between OSM and IL-1β, the deviation from additive linear response was calculated as the measured outcome in the presence of both treatments #1 + #2 combined, divided by the sum of the outcomes of treatment #1 only and treatment #2 only. [210] To put this relationship into an equation: (Outcome from Treat #1 + Treat #2 in same reaction) / (Outcome from Treat #1 + Outcome from Treat #2) = When answer is greater than 1 (>1) there is a deviation in the linear response and there is a synergistic interaction; for value that is exactly 1 or close to 1 there is no deviation and is an additive interaction; less than 1 (<1) and it is opposite of synergistic and is an antagonistic interaction. To determine if the deviation from additive response is significant, the mean of $\log_2$(Treat #1) + $\log_2$(Treat #2) is compared against mean of $\log_2$(Treat #1 + #2).

Statistical Analysis

Statistical analysis was performed using Prism 8.0 software. Significant results were determined by various statistical methods including Student's t-test, One-way ANOVA, Repeated Measures (RM) Two-way ANOVA, and Pearson Correlation test. Significance is denoted as: n.s. (not significant), $p>0.05$, * $p<0.05$, ** $p<0.01$, *** $p<0.001$ and **** $p<0.0001$.

Results

IDC Cells Transformed with Either OSM Overexpression or Control Plasmids are Similar to Parental

To determine the *in vivo* effect of OSM-induced LOXL2 ECM remodeling observed in my last publication, we designed an *in vivo* mouse model for IDC tumor growth and metastasis. We started with the poorly metastatic luminal A ER+PR+HER2- human IDC cell line MCF7 containing the luciferase bioluminescence enzyme (MCF7-Luc). To transduce OSM-overexpression in MCF7-Luc cells, we developed lentiviral particles containing the full-length OSM (flOSM) or empty vector control (EVctrl) plasmids with a CMV promoter and blasticidin resistance. Stably propagating colonies expressing flOSM or EVctrl vectors resulted from lentiviral transductions followed by antibiotic selection. The morphology of the colonies was initially assessed and compared against the parental MCF7-Luc cell line. The colonies showing altered morphology were removed from consideration, while those that retained morphologies similar to parental cells were assessed further (data not shown).

Based on both morphology and appropriate OSM secretion, as determined by OSM ELISA of conditioned media (CM) from MCF7-Luc-flOSM colonies after 24

hours, the two most promising colonies were selected (C1 and C2) **(Supp. Figure B.1 and B.2).** Using a human OSM ELISA kit with rhOSM for the standard curve, a quantitative assessment of these colonies showed that MCF7-Luc-flOSM C1 secreted ~70 ng/mL OSM, while C2 secreted ~60 ng/mL OSM. As expected, OSM could not be detected in parental cell CM or media control **(Figure 3.1 A)**. This level of OSM secretion is ~2-3-fold higher than the level of rhOSM we would normally treat cells with (25 ng/mL) *in vitro*.

OSM-induced LOXL2 secretion was evaluated next. CM from C1 and C2 were collected at 72 hours and tested using a human LOXL2 ELISA. C2 secreted ~3X more LOXL2 (7.25 ng/mL) than C1 (2.75 ng/mL). Colonies C1 and C2 were also compared against parental and EVctrl cells. As expected, the parental and EVctrl controls secreted low levels of LOXL2 that increased in response to OSM treatment (25 ng/mL), from 1.5 to 8 ng/mL and 1.25 to 9.75 ng/mL respectively. Comparing control LOXL2 expression in C1 and C2, only C2 secreted significantly ~7X more LOXL2 than non-treated EVctrl **(Figure 3.1 B).** Due to these results C1 was selected as the best colony moving forward. To determine whether OSMR signaling was saturated by the natural overexpression and secretion of OSM by C1 and C2, additional rhOSM (25 ng/mL) was added to the cells for 72 hours. CM was tested by LOXL2 ELISA, and the additional OSM did not increase LOXL2 expression suggesting that the OSMR was saturated by the overexpressed OSM **(Supp. Figure B.3)**.

OSM-induced VEGF secretion was also evaluated in parental, EV control, and C2 cells +/- additional rhOSM (25 ng/mL) by VEGF ELISA **(Figure 3.1 C**). OSM overexpression by C2 cells resulted in a greater than 2-fold higher induction of VEGF

secretion compared to parental and EV control cells. Treatment with additional OSM resulted in the expected increase in secreted VEGF in parental (3-fold) and EV control (2.5-fold) cells. Immunoblot analysis was performed for OSM (25 ng/mL) treatments at 24 hours for LOXL2 and Snail and 72 hours for E-cadherin and ERα. The response observed in C2 and OSM treated parental and EVctrl cells was expected for each protein analyzed. Both E-cadherin and ERα decreased at 72 hours while Snail and LOXL2 were upregulated at 24 hours. Key to note is that ERα was substantially downregulated by OSM expression in MCF7-Luc-flOSM C2, as well as in OSM treatment after 72 hours in parental and EV control cells. This has been shown before in MCF7 human breast cancer cells. [108] We were concerned that constitutive OSM expression would reduce ERα in MCF7-Luc-flOSM cells to a point where they would no longer express ER and would become ER-. To our excitement, MCF7-Luc-flOSM cells still express ER, though at a somewhat reduced level.

ER+ Mouse Model to Test LOXL2 Effect on OSM-mediated IDC Tumor Progression

As high levels of tumor-associated OSM expression have been associated with worse survival in ER+ breast cancer patients compared to ER- patients, it is clear that OSM has a more important role in ER+ breast cancer. [86, 108, 173] Therefore, we wanted to continue our studies in an ER+ mouse model of metastatic breast cancer. The successful establishment and characterization of MCF7-Luc-flOSM cells that overexpress OSM, along with the EVctrl vector control cells, gave us confidence to utilize them as our novel ER+ metastatic breast cancer mouse model. To inhibit LOXL2 in our mouse model, the pharmaceutical company Pharmaxis supplied one of the LOXL2/3-specific small molecule inhibitors (SMIs) that they had developed, named PXS-5283, which had

recently passed Phase I clinical trials. This SMI was used for our *in vivo* LOXL2 inhibition because of its better pharmacologic profile compared to PXS-5120, which had been used previously *in vitro*. Ideally, the SMI would have remained the same for *in vivo* studies; however, PXS-5120A's short half-life, poor target acquisition, and terrible oral bioavailability were enough reasons to make the switch (data not available). The structural formulas for PXS-5382 and PXS-5120A are similar and are represented by their skeletal structures **(Figure 3.2 A)**, with the differences between the SMIs circled in red and numbered. There are 3 areas that differ between PXS-5382 and PXS-5120A: i) the dimethylamine group (-N(CH3)2) from the dimethyl sulfonamide (-SO2N(CH3)2) bound to the phenyl ring is replaced with a methyl group (-CH3), ii) the 5-indole bound carboxyl group (-COOH) is replaced by a methyl group, and iii) a carbon atom from the indole located at 4-indole is replaced with a nitrogen. According to manufacturer, these differences do not appreciably impact on the inhibitory capability of PXS-5382, while greatly improving solubility, stability, and oral bioavailability *in vivo*. This allowed us to reduce the dosing frequency and gave us the option to use an oral method of SMI delivery versus IP injection. We also wanted confirmation that PXS-5382 retained the same or similar inhibition efficacy and selectivity for LOXL2. Research at Pharmaxis was performed using fluorometric activity assays, where purified proteins of the 5 lysyl oxidase were exposed to an 11-point serial dilution for each SMI and incubated for 30-minutes prior to analysis. The results were plotted and subsequent half-maximal inhibitory concentration (IC50) calculations were performed for PXS-5382, PXS-5120A, and βAPN (a well-known but non-selective pan-LOX SMI) and displayed as pIC50 values, which are negative log of IC50 values, where larger values correlate to stronger

inhibition **(Figure 3.2 B)**. The pIC50 values for PXS-5382 and PXS-5120A SMIs inhibition were nearly identical, with variation from 0.1 to 0.2 units. The LOXL2 pIC50 value remained ~2 units higher for PXS-5382, correlating to an ~100-fold higher IC50 concentration compared to all but LOXL3. These results confirmed the similarity between the SMI inhibitory profiles, giving no reason for concern moving forward with PXS-5382. Due to its great oral bioavailability a specialized chow was developed containing PXS-5382, formulated by Research Diets, Inc. This diet seemed like a great method to utilize for PXS-5382 treatment *in vivo*. To test the chow, a pilot study was conducted by Pharmaxis with mice that were fed the SMI infused chow diet for 14 days. On the last day, serum samples were collected 1-hour and 8-hours after the mice last ate **(Figure 3.2 C)**. The results showed that after 8 hours, there was ~50% less PXS-5382 compared to 1-hour, but the concentrations were all still above the 7.9 nM IC50 for LOXL2. The lowest (~121.1 nM) and highest (~500 nM) concentration were respectively ~15-fold and ~63-fold greater than the IC50. These results demonstrated PXS-5382 stability *in vivo* as well as oral bioavailability of the compound. The chow diet would maintain SMI concentration above LOXL2/3 IC50s but below the IC50s of other lysyl oxidases. Therefore, the chow diet would be used in our mouse model going forward, eliminating the need for daily IP injections of an anti-LOXL2 SMI that would have been required to maintain LOXL2 inhibition. For any concerns regarding the formulation of the PXS-5382 chow along with the control chow, a table is provided highlighting the entire contents of the mouse diet available from Research Diets, Inc. **(Table 3.1).** Further confidence in using PXS-5382 inhibitor is gained from the rigorous testing it underwent during Phase 1 clinical trials, which it passed, with Phase 2 trials set to start. PXS-5382

was rigorously tested for cytotoxicity as a result of the Phase I clinical trial, and patients showed no adverse side effects (data not available). Inhibition efficacy was analyzed in human subjects dosed orally with 100 mg PXS-5382 every 24-hours and measured by % inhibition by probing for SMI bound LOXL2 versus the total LOXL2 **(Figure 3.2 D)**. The results further confirmed the stability of PXS-5382 *in vivo* with a steady >85% LOXL2 enzymatic inhibition between doses after the 7-day mark. With PXS-5120A having minimal oral bioavailability, it would no doubt cause significant distress in the mice over the course of the experiment due to the daily IP injections, reducing the quality of life, and possibly resulting in early termination. The overall results made it clear that the switch from PXS-5120A should be made to PXS-5382, a LOXL2 SMI that has all the inhibitory qualities of the previous SMI with a pharmacokinetic profile that is ideal for *in vivo* research.

Utilizing an ER+ mouse model of breast cancer requires estrogen to be continuously present in the mice receiving the MCF7-Luc tumor cell injections in order for a tumor to develop properly *in vivo*. The absence of estrogen not only prevents the tumor from growing effectively, but it can completely hinder tumor development. To address this, we supplemented the drinking water for the mice with 4 mg/L of 17β-estradiol (E2), the most potent form of estrogen. This method has been proven to be effective in our lab and by others. [211, 212] Importantly, we ran a pilot study utilizing 6 mice that were injected with 2 x 10^6 MCF7-Luc-flOSM cells (a combination of 50% C1 and 50% C2 cells), which was compared against the parental MCF7-Luc cells because we did not have an established MCF7-Luc-EVctrl control cell line at the time. As the pilot was to determine whether the MCF7-Luc-flOSM colonies could promote metastasis, it

was not really necessary to have the vector control for comparison. After ~40 days post-injection, the health of the mice began to wane and their distress scores were all at the highest level and so the study was terminated. Analyzing the data, we were able to confirm that the mixed C1 and C2 MCF7-Luc-flOSM cell lines were more than capable of metastasizing. Of the 6 mice, 3 were injected with the MCF7-Luc-flOSM mixed tumor cells and 3 with a combination of 50% mixed tumor cells/ 50% Matrigel BME matrix. The MCF7-Luc-flOSM cells co-injected with 50% Matrigel BME matrix had larger tumors and faster tumor growth rates, with metastases present in the lungs in of all 3 mice (100%) (data not shown). The results from the group that did not receive Matrigel compared to the group that did, suggested that Matrigel promoted better tumor growth and was utilized in all tumor cell injections going forward. Given the results we gathered from our pilot study, we were confident that we had an ER+ metastatic breast cancer mouse model with which to move forward to test whether OSM-induced LOXL2 expression and subsequent ECM remodeling in MCF7-Luc cells significantly affects IDC progression and metastasis.

OSM-induced LOXL2 Promotes IDC Tumor Growth and Metastasis

Based on *in vitro* analysis of MCF7-Luc-flOSM C1, C2, and MCF7-Luc-EVctrl cells as well as pilot study results, the details of our mouse model were finalized. In total, forty 9-week-old immunocompromised nude athymic$^{<nu/nu>}$ female mice received tumor cells injected into the 4th mammary fat pad. The injections contained 2.0 x 10^6 of either MCF7-Luc-flOSM C2 or EVctrl cells (20 mice injected with each), composed of a 50% Matrigel BME matrix solution. MCF7-Luc-flOSM C2 was utilized instead of a 1:1 combination of C1 and C2. This was due to results obtained after the pilot experiment

was performed that showed a >2-fold higher LOXL2 expression in C2 when compared to C1. In addition, C2 expressed less OSM, reducing the potential risk of cytokine storm formation in the mice as the study progressed. [213] At day 10 post-tumor cell injection, palpable tumors were felt. Bioluminescent images were taken of the mice injected with MCF7-Luc-flOSM or EVctrl. The mice were sorted based on individual bioluminescent signal intensities (BLI) and placed into 4 total groups with comparable overall BLI of the 10 mice in each group. The groups were then treated with PXS-5382 LOXL2 SMI chow [PXS-5382] or control chow [vehicle]. Therefore, the final groups were: 1) MCF7-Luc-EVctrl [vehicle], 2) MCF7-Luc-EVctrl [PXS-5382], 3) MCF7-Luc-flOSM [vehicle], and 4) MCF7-Luc-flOSM [PXS-5382]. A diagram of the full mouse model, from start to finish, with names of each group and weekly procedures performed is found in **(Figure 3.3)**. After doing weekly measurements for the duration of the experiment, on day 46 the health of mice from the MCF7-Luc-flOSM + [vehicle] drastically waned, and therefore, endpoint procedures were initiated. Essential tissues and fluids were collected and stored, *ex vivo* imaging was performed for each mouse, and the pertinent data gathered throughout the course of the experiment was consolidated.

To make sure the mice were not suffering excessively, measures of mouse vitality were taken and recorded throughout the course of the study. This was done in part to confirm that mice in the study maintained good health, but also to show any trends or anomalies seen in individual mice, cages, or treatment groups that could skew the results. The vitality of mice is primarily determined by the weight measurements and fluctuations in mice over the course of the study, as measured 3x weekly, with any mouse < 20% start weight triggering euthanasia. Unfortunately, throughout the course of the study, two mice

died before they could be euthanized, but weight did not dip below 20% on last checkup. Mice are weighed using a gram scale that is sensitive enough to detect differences in weigh equal to or greater than 0.1 g, measured under the protection of an animal transfer tables airflow barrier. The mice appeared to enjoy the chow supplement, both PXS-5382 and control, as the average weight of the mice from each group increased as the experiment progressed from day 0 until the midpoint of the study, declining thereafter **(Figure 3.4 A, B)**. Overall, the weight fluctuations over time were expected minus the early deaths, and no significant changes were measured. The distress and/or pain the mice were experiencing was also measured and recorded 3x weekly and scored according to published mouse grimace scale guidelines. [208] The mice received scores of 0, 1, and 2 depending on the severity of the grimacing features such as nose and cheek bulge, ear positioning, and orbital tightness. One week of consecutive scores of 2 triggered the protocol for euthanizing mice. Until the final week of the study, only a few mice experienced issues at various points during experimentation, receiving scores of 1 and 1.5, but they would recover and score 0 within a week. The two mice that perished early both had MCF7-Luc-flOSM cell injections, one with vehicle and one with PXS-5382, and had scores of 1.5-2 prior, but neither were consistently at 2 for that long. Other than weight and pain score, these mice were removed from the rest of the study. In the final week, the number of mice that began grimacing increased and mice were no longer recovering, while all the mice in the untreated MCF7-Luc-flOSM [vehicle] group were scoring from 1 to 2 (data not shown). These results are normal for tumor metastasis studies, with the grimace scores at times correlating with the presence of metastatic lesions, and the MCF7-Luc-flOSM [vehicle] group was expected to show the earliest

signs requiring experiment termination. These results suggest that overall, the mice were not distressed beyond what was expected, given the circumstances, and the study was able to successfully conclude 46 days after tumor cell injections.

Of the goals we set out to accomplish through the mouse model study, one was to elucidate the impact that OSM-induced LOXL2 had on tumor growth. We determined the size of the tumors and their growth over the course of the study by using a digital caliper to get precise lengthwise and widthwise diameter measurements from each tumor, measurements taken 3x weekly. The tumor volumes in this *in vivo* study were calculated according to the accepted methodology for tumor volume calculation: volume = (width^2 x length)/2. [209] There were two instances in the mice, where two distinct lobes developed for the primary tumor; each lobe was measured separately and volumes were added. From each treatment group, the tumor volumes calculated for the mice on each day were averaged together resulting in 4 lines graphed to represent the average tumor volume (mm^3) over time from day 0 to day 46 **(Figure 3.4 C)**. By analyzing the tumor volume data, it was observed that ER+ MCF7-Luc-flOSM [vehicle] tumors grew significantly larger in volume compared to the MCF7-Luc-EVctrls, with tumors averaging ~175 mm^3 in volume at day 46 compared to ~15 mm^3 in MCF7-Luc-EVctrls either with or without PXS-5382. This means that the tumors were ~12-fold larger in mice with tumor cells expressing OSM at experimental end compared to mice with EV control cells. The growth of MCF7-Luc-flOSM tumors was significantly hampered by inhibition of LOXL2 enzymatic activity. PXS-5382 treatment reduced experimental end tumor volume from ~135 mm^3 to ~40 mm^3, a > 4-fold decrease in mice where OSM-

induced LOXL2 enzyme activity is inhibited compared to mice where OSM-induced LOXL2 is enzymatically active. These results suggest that LOXL2 plays a significant role in OSM-promoted tumor growth. The absence of OSM expression correlated with a reduced overall tumor growth potential regardless of LOXL2, as without OSM to induce LOXL2 expression, LOXL2 constitutively expressed by MCF7-Luc-EVctrl [vehicle] cells did not promote tumor growth. Overall, these results confirm that OSM-induced LOXL2 enzymatic activity is critical for OSM-promoted tumor growth, and that LOXL2 either needs to reach a certain concentration to promote tumor growth, or something related to OSM signaling potentiates the effectiveness of LOXL2 activity.

The most important outcome regarding our *in vivo* research was the impact that OSM-induced LOXL2 expression had on metastasis. This was of key importance because metastatic IDC severely reduces patient 5-year survival rates, and discovering novel mechanisms by which IDC cells metastasize is crucial. To determine the presence of metastatic lesions, the mice received luciferin by IP injection prior to being euthanized. The mice were dissected and their organs resected prior to *ex vivo* imaging, which constituted probing for traces of bioluminescent signal. *Ex vivo* bioluminescent images by treatment group are shown in Appendix B **(Supp. Figure B.4)**. For our analysis, the data from the *ex vivo* images were represented in two different ways. First, the number of mice in each group that had metastasis (both by total number and by organ location) was observed and listed in **(Figure 3.5 A)**. It is important to note that seven out of eight (7/8) MCF7-Luc-flOSM [vehicle] mice had metastasis, while when OSM-induced LOXL2 was blocked, only 1/8 MCF7-Luc-flOSM [PXS-5382] mice had metastasis. Second, the fraction of mice that had metastatic lesions in each group against the total number of

uncensored mice in each group was graphed **(Figure 3.5 B)**. The result from the data plotted by % Incidence of Metastasis in each treatment group clearly showed that: 1) OSM was a strong potentiator of metastatic IDC since the MCF7-Luc-EVctrl [vehicle] group only had metastases present in 1 out of 9 mice (11.11%), while the MCF7-Luc-flOSM [vehicle] group had them in 7 out of 8 mice (87%); and 2) LOXL2 enzymatic activity was critical in its involvement and had a significant impact on OSM-promoted metastasis, as observed in the MCF7-Luc-flOSM [PXS-5382] group where only 1 out of 8 mice (12.5%) of the mice had metastases compared to 87% for the untreated MCF7-Luc-flOSM [vehicle] group. These results confirm that OSM-induced LOXL2 and its enzymatic activity are significantly involved in promoting metastasis. Our previously published 3D invasion *in vitro* study had suggested that LOXL2 expression induced by OSM signaling and subsequent collagen I fiber crosslinking and alignment may be strong enough to play a significant role in OSM mediated metastasis. [146]

The results of our mouse study, corroborated with our previously published research on OSM-induced LOXL2 production and secretion, conclusively demonstrated that LOXL2 enzymatic activity catalyzed stromal ECM collagen I crosslinking and fiber alignment in the TME; and is therefore, a critical component in OSM-promoted metastasis of ER+ IDC cells. To confirm that our MCF7-Luc-flOSM mouse model retained its ER+ status for 46 days of *in vivo* tumor growth saturated with OSM, western blot analysis was performed on tumor tissue that was collected and lysed **(Figure 3.5 C)**. To make sure that the analysis was not skewed due to interference from mouse ECM tissues, a luciferase primary antibody was used to confirm that the majority of each sample came from tumor tissue and that the amount from sample to sample did not vary

too much. This was used as a control in addition to our total protein stain, commonly utilized to normalize proteins during immunoblotting**.** The immunoblot results showed that MCF7-Luc-flOSM tumor samples still expressed ERα, though there was an appreciable reduction in ERα protein when compared to EV controls. There was also, as expected, high levels of OSM expression and significantly more LOXL2 protein present in MCF7-Luc-flOSM tumor tissue. Together, this data demonstrates that OSM-induced LOXL2 expression remained strong in tumor cells and that the tumor maintained its ER+ status, though slightly reduced, after 46 days of *in vivo* tumor formation and OSM exposure. *Together, these results will allow us to write another manuscript on a novel new ER+ mouse model (MCF7-Luc-flOSM) that grows tumors quickly and metastasizes within 46 days.*

OSM-OSMR Signaling Pathways Promote LOXL2 Upregulation

After confirming the role OSM-induced LOXL2 played in tumor progression and metastasis, we next investigated the mechanism behind LOXL2 induction. Canonical OSM-OSMR signaling pathways were analyzed utilizing SMIs to inhibit the phosphorylation of ERK1/2, AKT, and STAT3; and therefore, turn off the downstream signaling effects of the MAPK, PI3K/AKT, and JAK/STAT3 pathways. For these experiments, we utilized MCF7 and MDA-MB-468 IDC cells that were exposed to a series of SMI concentrations, with a DMSO added to -OSM/ +OSM treatment to control for DMSO from SMI, for 2 hours prior incubation and then kept throughout the 24-hour treatment with rhOSM (25 ng/mL). The SMIs and their concentrations respectively in MCF7 cells were: PD0325901 [100, 150, 200 nM] for pERK1/pERK 2, GDC-00941 [100, 200, 300 nM] for pPI3K, and Stattic [1, 2, 3 μM] for pSTAT3. Slightly different

SMI concentrations were used with MDA-MB-468 cells; GDC-0941 [200, 300, 400 nM] and Stattic [2, 3, 4 μM]. MCF7 and MDA-MB-468 cells collected after 15-minute OSM treatment were lysed, and an immunoblot analysis was performed to determine pERK, pAKT, and pSTAT3 phospho-protein expression normalized against REVERT Total Protein stain. The results from this assay showed that OSM signaling activated all the pathways to varying degrees in each pathway, while each SMI inhibited their respective pathway as expected without any interference with the other pathways **(Supp. Figure 3.4)**. Next, OSM treatment was analyzed using the same immunoblot protocol as above but looking at LOXL2 protein expression after 24 hours. We observed increased LOXL2 protein expression in both cell lines treated with OSM, as expected, and as has been shown in our previous publication. [146] However, what was observed in the SMI treatments is that not just one of the pERK, pAKT, or pSTAT3 inhibited pathways prevented LOXL2 induction by OSM but they **all** did in MCF7 cells, according to reversal in OSM-induced LOXL2 protein expression for each pathway inhibited **(Figure 3.6 A-C)**. For the MDA-MB-468 cell line, the only pathway that prevented LOXL2 expression due to inhibition was the pSTAT3 pathway **(Figure 3.7 A-C)**. We also observed IDC cell viability and did not notice any of the SMIs significantly affecting cell detachment or viability (data not shown). These results suggested that OSM-induced LOXL2 expression in MDA-MB-468 IDC cells was upregulated by the pSTAT3 signal pathway. However, for the MCF7 IDC cell line there is a more complicated signaling interaction that is taking place. This is because inhibition of any one of the three pathways reduced LOXL2 expression down to baseline expression. The unexpected result led to brainstorming sessions comparing potential signal transducers or

transcription factors (TF) that could be activated by or even just marginally associated with all three pathways and activate LOXL2 expression.

Presence of c-Myc Transcription Factor Required for LOXL2 Induction

Our research above demonstrates that all three of the canonical OSM signaling pathways contribute to LOXL2 expression in MCF7 cells, while only pSTAT3 impacts LOXL2 expression in MDA-MB-468 cells. Due to the unexpected results gathered when the MCF7 cell line was analyzed, published research was scoured to determine if there was anything that could explain the inhibition of 3 different signaling pathways and completely prevent OSM-induced LOXL2 expression. The results suggested to us that there was a possible mediator protein or TF, which was shown to interact with each pathway resulting in the TF being upregulated, activated, or stabilized. A prospective target that emerged and had the potential to be responsible was identified as c-Myc, a well-known oncogenic factor. [114, 164, 165, 167, 169, 214] The mechanism proposed **(Figure 3.8)** involves pSTAT3 transcriptionally upregulating c-Myc expression. At the same time, pERK promotes the phosphorylation of c-Myc on its Serine 62 amino acid (referred to as p-c-Myc [Ser62]), thus extending Myc's half-life, while pAKT signaling prevents GSK-3 proteins from phosphorylating Myc at its Threonine 58 amino acid (p-c-Myc [Thr58]), thus preventing Myc degradation. To test our hypothesis, we analyzed the same MCF7 lysates gathered for the experiments above after 24-hour OSM treatment in order to determine the expression or c-Myc and the p-c-Myc variant associated with each pathway, in addition to LOXL2. The result of these assays showed that pERK and pSTAT3 pathway inhibition prevented the induction of c-Myc expression in addition LOXL2; however, pAKT pathway inhibition had no effect on c-Myc phosphorylation of

expression **(Figure 3.9 A-C)**. In MDA-MB-468 cells, we analyzed the pSTAT3-inhibited samples and found that c-Myc was also downregulated, as was LOXL2, though not as much c-Myc was induced by OSM **(Figure 3.9 D)**. This data, though not what was expected, demonstrated that c-Myc expression seemed to play at least some role in LOXL2 induction.

To take the c-Myc analysis one step further, a c-Myc SMI known as 10058-F4 that prevents transcriptional activity by blocking the dimerization of c-MYC/MAX was used at a series of concentrations [50, 60, 70, 80 μM]. In this experiment, MCF7 and MDA-MB-468 cells were incubated with 10058-F4 for 2 hours prior and throughout the 24-hour OSM treatment **(Figure 3.10 A, B)**. OSM-induced LOXL2 expression was inhibited in both of these cell lines when c-Myc activity was inhibited, and these results further suggest that the presence of c-Myc is important for LOXL2 expression, Taken together, our results demonstrate that c-Myc as a transcriptional factor likely plays a role in the induction of LOXL2 by OSM signaling, but it is likely one player in a complicated signaling mechanism in the ER+ MCF7 cell line. More research will be needed to determine what other factors could be at play.

Synergetic Impact of IL-1β Signaling on OSM-Induced LOXL2

In our attempt to further understand the interactions at play between proinflammatory cytokines and LOXL2, we observed that IL-1β treatment was the second most common inducer of LOXL2 expression amongst the four cytokines and six cell lines analyzed in Chapter 2. IL-1β and OSM are derived from two different families, IL-1 and IL-6, which have been shown to interact in a synergistic fashion by other labs as well as by a previous PhD student in our lab. [162, 163] Three cell lines in which OSM-

induced LOXL2 expression (MCF7, MDA-MB-468, and BT474) were further analyzed. Cells were treated with OSM (25 ng/mL), IL-1β (10 ng/mL), or a combination of both for 24 hours, and LOX2 expression was assessed by western blot analysis. Two of the three cell lines had strong synergistic reactions when OSM and IL-1β were treated in combination versus either one alone **(Figure 3.11 A-C)**. The only cell line in which the synergetic reaction was not significant was the MCF7 cell line. BT474 cells showed a drastic (>100-fold) synergistic increase in LOXL2 expression, compared to a ~10-fold increase with OSM alone and ~2-fold increase with IL-1β. These results confirm that there is a synergistic interaction between OSM and IL-1β in the expression of LOXL2, and there are likely more reactions like this to be discovered. Furthermore, the synergistic interaction between OSM and IL-1β in LOXL2 expression suggests that patients with high levels of both of these cytokines are at an even greater risk of metastasis due to LOXL2 overexpression.

Discussion

The novel research highlighted throughout this dissertation clearly reveals that in IDC cells, OSM-induced LOXL2 secreted into the TME significantly alters stromal ECM by crosslinking collagen I fibrils and promoting fiber density and alignment. In turn, the LOXL2-remodeled ECM promotes increased cellular 3D invasion in invasive ductal carcinoma. Importantly, using an *in vivo* ER+ mouse model, OSM-induced LOXL2 was observed to significantly impact IDC tumor growth, progression, and metastasis.

While previous research has shown that overexpression of LOXL2 promotes ECM remodeling and metastasis, these studies have relied on LOXL2-transformed cells that do not accurately reflect true LOXL2 regulation. Our research clearly showed *in vivo*

that LOXL2 enzyme activity significantly impacts OSM-promoted volumetric tumor growth compared to the LOXL2 transduction alone, where growth was not affected. [148, 149] Using our *in vivo* mouse model with flOSM and EVctrl transformed versions of the ER+ luminal A IDC cell line MCF7-Luc, we were able to assess the impact of OSM and LOXL2 expression on early IDC tumor progression, as well as metastasis. Our results show that LOXL2 has a significant impact on both, likely due to its ability to crosslink and align collagen I fibers, which underscores the importance of ECM structure in tumor progression. These results will guide future breast cancer research on inflammatory cytokines, since ECM remodeling by LOX family expression promoted by cytokine signaling was unknown prior to this research. Opening new avenues for advances in research due to collagen I fiber crosslinking and alignment strengthens the importance of ECM structure in tumor progression.

As we have previously shown (Chapter 2), [146] LOXL2 can enzymatically catalyze and initiate collagen I crosslinking and promote collagen fiber alignment and increased fiber density. The resulting orientation of the collagen fibers between cells radiating outward perpendicular to tumor surface into the TME becomes uniform and aligned directionally. This is, in part, due to fibers binding end-to-end like laid bricks and also in part due to physical forces exerted by motile cells and the tumor itself. This consolidation and alignment of fibers does not affect tumor cell speed but it importantly increases their velocity and conserves energy with aligned fibers forming paths efficiently connecting nearby tissue and/or vasculature, as opposed to directionless movement in a disorganized TME. Without LOXL2 enzymatic activity, the impact of OSM-promoted EMT is significantly reduced. This is likely due to the fact that even with

the acquisition of motility and a mesenchymal morphology, the stromal TME of the IDC does not have the proper ECM substrate characteristics needed for efficient tumor cell migration to other organs or nearby vasculature to promote metastatic events. This research taken together, highlights the important roles that LOXL2 activity, stromal collagen structure, and OSM signaling all play in IDC tumor progression and metastatic potentiation.

In our novel metastatic ER+ mouse model of breast cancer, the OSM secreting MCF7-Luc-flOSM cells yielded metastatic lesions in a relatively short period of time, with 7 of the 8 mice having at least one lesion detectable by BLI on day 46. The lesions were observed in the lung, bone, and in one mouse the stomach. This makes our model desirable compared to other orthotopic xenograft mouse models that utilize MCF7 or other slow growing, non-aggressive ER+ IDC cells that can take several months to show metastases or not metastasize at all. [215, 216] In fact, in many cases, researchers have resorted to using specialized NOD SCID gamma (NSG) mice that have a severely compromised immune response phenotype, and on average cost 3-times as much as nude athymic mice normally used for human xenograft *in vivo* studies. [33, 217] Therefore, our mouse model would be a beneficial and practical option for labs needing a metastatic ER+ mouse model that metastasizes on a short timescale and is less expensive than a NSG model, as long as OSM expression does not alter study dynamics or other interactions being studied.

The gene regulating TF c-Myc is a well-known proto-oncogene that has a central role in cell growth, proliferation, tumorigenesis and cell differentiation. [165, 167-169, 214] Additionally, c-Myc lies at the crossroads of multiple signal transduction pathways

including JAK/STAT, MAPK/ERK, and PI3K/AKT. These signaling pathways are regulated by numerous factors, but also canonically activated by OSM-OSMR signal transduction. With this in mind, the results shown in this chapter suggest that at minimum c-Myc expression is related to LOXL2 expression, and that c-Myc is necessary for OSM-induced LOXL2. Since we did not conclude that c-Myc was responsible in MDA-MB-468 cells, another novel player must be directly linked to LOXL2 induction if c-Myc is not. Further studies will be necessary to pin down the entire signaling mechanism at work that leads to OSM-induced LOXL2. Further signal transduction characterization of LOXL2 upregulation will allow breast cancer researchers to find better therapeutic targets to prevent IDC progression and metastasis.

Currently little research has been conducted on the potential for OSM and IL-1β signal transduction to promote synergistic gene expression, especially in breast cancer. Dr. Ken Tawara from our lab was able to confirm that IL-6 and VEGF expression were synergistically induced by OSM and IL-1β signaling activation. [162] Through my dissertation research on OSM-induced LOXL2 and subsequent effects, it was shown that LOXL2 expression is synergistic induced by OSM and IL-1β treatment. In fact, each of the three IDC cell lines tested had a synergistic interaction; however, in MCF7 cells the synergistic interaction was not large enough for the induction of LOXL2 expression to be statistically significant ($p = 0.32$) rather than additive. This is unlike in BT474 and MDA-MB-468 cells, where the synergy between OSM and IL-1 β was significantly more prominent. In BT474, the synergistic induction of LOXL2 by the combination of OSM and IL-1β was >100-fold that of no treatment, while OSM and IL-1β alone induced LOXL2 by ~15-fold and ~2-fold respectively. These results highlight the overwhelming

impact that synergistic OSM and IL-1β signaling can have on oncogene expression in IDC patients. It would be possible to use high levels of both of these cytokines as a new clinical biomarker combination that could alert doctors to these patients having a much greater risk of metastasis. With the poor efficacy of anti-inflammatory cytokine therapies previously tested in breast cancer patients, studies on cytokine signaling synergy, especially between OSM and IL-1β signaling, could lead to modified cytokine-inhibiting breast cancer therapeutics targeting synergistic pairs.

Conclusion

In summary, this dissertation research shows for the first time that the proinflammatory cytokine OSM is able to promote the expression of the ECM remodeling lysyl oxidase enzyme LOXL2. This occurred in the majority of IDC cells that have been tested, which leads us to believe this is a highly prevalent occurrence in breast cancer. OSM-induced LOXL2 is expressed at a high enough concentration to significantly promote collagen I fiber crosslinking, alignment, and IDC invasion. These modifications remodel the ECM in a manner that condenses stromal collagen I fibrils into thicker and thicker fibers that increases fiber density, which we showed qualitatively. OSM-induced LOXL2 increased IDC tumor growth and, most importantly, percent of mice with metastasis. In fact, tumor size was reduced ~4-fold and metastasis % dropped from 87.5% to 12.5%. These results seem to suggest that though EMT and VEGF secretion significantly factor into OSM-mediated metastasis, without proper ECM alterations in the stromal TME, the effects will not be fully realized. This provides us with valuable insight into the mechanisms involved in IDC metastasis, and what underlying processes are most critical to sever the link to tumor cell metastasis. This is

where focusing more on therapeutics that prevent ECM remodeling or can counter the alterations tumors make to the ECM is critical. If we can prevent these easy pathways for IDC cells, and also most all cancer cells, making it more difficult and energy consuming for the cancer cells in new metastatic research. With our examination of OSM signaling and c-Myc in LOXL2 highlighting the intricate nature of LOXL2 expression, methods for therapeutic LOXL2 inhibition could be developed with less unintended effects on other mechanisms. The synergistic impact of OSM in association with IL-1β on LOXL2 expression confirms previous research and proves that dual-targeted therapies against synergistic cytokines will be the most effective way to reduce oncogene expression. These fascinating mechanisms revealed affecting OSM-induced LOXL2 provide insight for multiple means of targeted drug inhibition against a protein interaction that has highly potent oncogenic effects in IDC that are significant in developing malignancy.

Future Directions

This research has led to quite a novel discovery. Until now, no one had demonstrated that OSM, IL-1β, or any other inflammatory cytokine could regulate the expression of LOXL2, or any lysyl oxidase, in breast cancer, or any other cancer. Additionally, OSM-induced LOXL2 exhibited an undeniable impact on IDC metastasis. This is likely achieved because OSM promotes EMT, leading to cellular detachment and motility, that when coordinated with OSM-induced LOXL2 enzymatic activity and subsequent collagen I crosslinking and fiber alignment, creates tracts for cells to travel on promoting directionality and efficiency to mobility provided by EMT. Further, OSM promotes VEGF secretion, which increases the presence of tumor vasculature and the possibility that IDC cells can reach and enter the circulatory system.

For future research the interaction between all three (EMT, collagen alignment, and angiogenesis) of these OSM-mediated methods of action that promote metastasis will be studied. Are these different mechanisms able to promote a significant number of metastatic formations on their own? Or are all of these pathways working in unison to bring about increased metastasis, and the loss of even one mechanism can significantly impact the overall metastatic potential of IDC cells. These questions will be answered in the future, in addition to what other types of cancers and isolated cell lines show similar OSM and IL-1β induction of LOXL2 and if so, does the interaction impact metastasis in the same way.

Another future direction involves determining the methods that lead to constitutive expression of LOXL2 in some IDC cells at excessive levels, high enough to need no further induction by outside signaling. This has been our hypothesis involving the TNBC and basal-like B cell line MDA-MB-231. These cells make 25-fold more LOXL2 than MCF7 cells without OSM treatment, and OSM and IL-1β together did not increase expression. With such high expression occurring naturally, there is enough LOXL2 to suggest that significant ECM remodeling takes place in the MDA-MB-231 TME, which is likely to play a crucial role in this cell line's aggressive phenotype and proclivity to metastasize.

The ultimate future goal would be to make a successful therapeutic to prevent OSM-induced LOXL2 or the effects of LOXL2 on ECM remodeling. This would be a goal that I would definitely like to take part in working on.

Chapter Three Figures

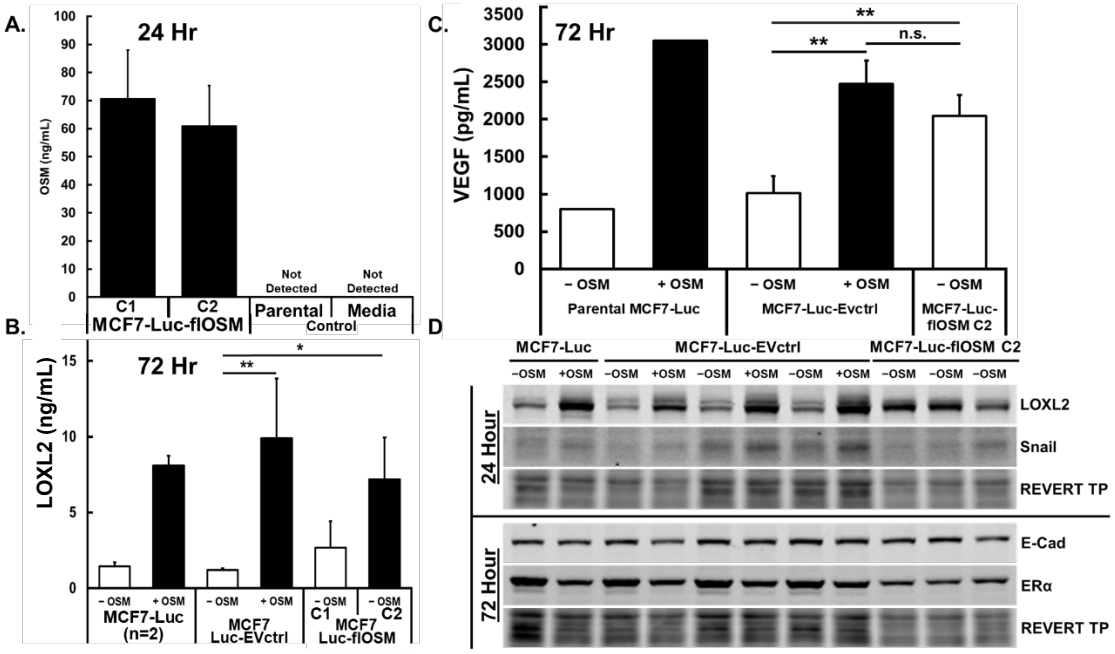

Figure 3.1 Transfected MCF7-Luc-flOSM and EVctrl Have Similar Protein Expression to Parental MCF7-Luc Cells.

All OSM treatments consisted of +/− rhOSM (25 ng/mL). In **A**, a quantitative OSM ELISA on the cellular CM from MCF7-Luc-flOSM C1 and C2 after 24-hour growth in fresh media demonstrates approximately 70 and 60 ng/mL of OSM secreted by C1 and C2 respectively, making both colonies viable for *in vivo* study. Parental cells and media control show undetectable levels of OSM. **B.** A quantitative LOXL2 ELISA shows MCF7-Luc-flOSM C1 and C2 OSM-induced LOXL2 compared to secreted LOXL2 from OSM treated parental and empty vector controls (EVctrl) after 72 hours. The data shows significant OSM induction of LOXL2 in the EVctrl as compared to parental MCF7-Luc cells, while MCF7-Luc-flOSM C2 produced more than 2.5-fold the LOXL2 that C1 did (7.19 ng/mL vs. 2.68 ng/mL). C2 also produced LOXL2 similar to EVctrl +OSM at 9.90 ng/mL, and also significantly more than −OSM expression. C2 was pushed forward with my research due to much higher LOXL2 expression and less overall OSM secreted compared to C1. **C.** Secreted VEGF expression was characterized by ELISA. MCF7-Luc-flOSM C2 CM after 72 hours was compared to parental and EVctrl, the induction patterns were similar to those for LOXL2 secretion. This means that C2 expressed significantly more VEGF than −OSM

treated EVctrl, but it was slightly less than +OSM treated EVctrl expression of VEGF. **D.** Immunoblot assay depicting LOXL2 and Snail expression after 24-hour +OSM treatment and E-cadherin and estrogen receptor (ERα) after 72-hour treatment. REVERT total protein stain is the loading control. Qualitative analysis of these proteins shows that parental MCF7-Luc +/−OSM expression is comparable to MCF7-Luc-EVctrl +/−OSM. Untreated MCF7-Luc-flOSM cells have elevated levels of OSM-induced protein expression for LOXL2 and Snail proteins at 24-hours, but a reduction in ERα and E-cadherin expression at 72-hours. The protein regulation both up and down was slightly less impactful compared to +OSM treated parental and EV control cells. (All experiments (n=3), except for parental (n=1-2) since it is used for references; not significant (n.s.) $p > 0.05$, * $p < 0.05$, ** $p < 0.01$ One-way ANOVA).

A.

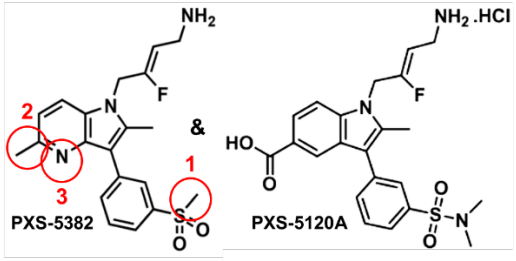

B.

	PXS-5382	PXS-5120	BAPN
	pIC50 ± SD		
LOX	6.0 ± 0.1	5.8 ± 0.1	5.7 ± 0.1
LOXL1	5.8 ± 0.2	5.7 ± 0.2	5.6 ± 0.1
LOXL2	8.1 ± 0.2	8.3 ± 0.2	6.4 ± 0.1
LOXL3	7.7 ± 0.1	7.8 ± 0.1	6.3 ± 0.1
LOXL4	6.9 ± 0.1	6.6 ± 0.1	6.5 ± 0.1

C.

Sample name	concentration (ng/mL)	concentration (nM)
PXS-5382-1 Hr-CHOW-PL-Animal-1	195.54	~500
PXS-5382-1 Hr-CHOW-PL-Animal-2	178.84	~457.3
PXS-5382-1 Hr-CHOW-PL-Animal-3	163.66	~418.5
PXS-5382-1 Hr-CHOW-PL-Animal-4	81.08	~207.3
PXS-5382-1 Hr-CHOW-PL-Animal-5	No volume	No volume
PXS-5382-8 Hr-CHOW-PL-Animal-1	84.64	~216.4
PXS-5382-8 Hr-CHOW-PL-Animal-2	106.96	~273.5
PXS-5382-8 Hr-CHOW-PL-Animal-3	62.49	~159.8
PXS-5382-8 Hr-CHOW-PL-Animal-4	47.37	~121.1

D.

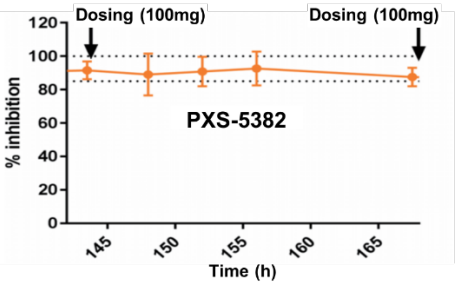

Figure 3.2 Mouse Model LOXL2 SMI is Well Characterized and Promotes Confidence in LOXL2 Enzymatic Inhibition.

A. Chemical structures for PXS-5382 and PXS-5120A (used in Chapter 2) are shown. Small composition differences between the two are circled in red for ease of reference. **B.** The pIC50, or the negative log of IC50, values for PXS-5382, PXS-5120A, and BAPN SMI are shown for each lysyl oxidase clarifying that PXS-5382 and PXS-5120A have similar enzymatic inhibition profiles against all the lysyl oxidases with the difference never more than 0.3. For LOXL2 pIC50 specifically, the difference was 0.2 with 8.1 for PXS-5382 and 8.3 for PXS-5120A, the difference being within the confidence intervals means that there is no statistical difference. The IC50 is equivalent to the molar

concentration of inhibitor needed for 50% inhibition in lysyl oxidase catalytic activity detected **C.** The table contains PXS-5382 concentrations in the form of molarity, in nano-moles (nM), and mass over volume, in nanograms per milliliter (ng/mL), determined by serum analysis from 4 mice. The data is from a pilot study where mice were fed only chow containing PXS-5382 for a week. At the end of the week the chow was replaced with regular feed and the mice were tested after 1 and 8 hours without PXS-5382 SMI. The serum SMI concentration was assessed in each mouse, and the concentrations are listed. The results show that in 8 hours approximately 50% of the PXS-5382 is eliminated; however, concentrations are well above the IC50 for LOXL2 inhibition with the lowest still 20x more than IC50. This confirms PXS-5382 *in vivo* stability and oral bioavailability; consequently, the PXS-5382 in the chow has been reduced by 50% to minimize LOXL3 interaction. **D.** The graph shows % of LOXL2 inhibition over time and in between PXS-5382 doses from Phase 1 clinical trial testing. In addition, PXS-5382 has been well characterized in in this trial and found nothing concerning cytotoxicity. Recently this SMI passed Phase 1 clinical trials, and the results have alleviated concerns regarding the efficacy and safety of this LOXL2 SMI *in vivo*. We confidently moved forward with this SMI in our ER+ mouse model for LOXL2 inhibition. (**A. B. D.** Taken from [Findlay 2019][138] & [Findlay 2020][139]; License granted for Copyright use, modified according to Copyright License guidelines).

Table 3.1 Formulation of the PXS-5382 SMI Chow (Formula 1) and Control Chow (D20011301) Peanut Flavored Rodent Diet. *Formulated According to Pharmaxis Recommendations*.

Rodent Diets With 10 kcal% Fat with Compounds/Peanut Flavor

Product #	D20011301		Formula 1	
%	gm	*kcal*	gm	*kcal*
Protein	19.0	*20*	19.0	*20*
Carbohydrate	66.6	*70*	66.6	*70*
Fat	4.2	*10*	4.2	*10*
Total		*100*		*100*
kcal/gm	3.81		3.81	
Ingredient	**gm**	***kcal***	**gm**	***kcal***
Casein	200	*800*	200	*800*
L-Cystine	3	*12*	3	*12*
Corn Starch	315	*1260*	315	*1260*
Maltodextrin 10	35	*140*	35	*140*
Sucrose	350	*1400*	350	*1400*
Cellulose, BW200	50	*0*	50	*0*
Soybean Oil	25	*225*	25	*225*
Lard	20	*180*	20	*180*
Mineral Mix S10026	10	*0*	10	*0*
DiCalcium Phosphate	13	*0*	13	*0*
Calcium Carbonate	5.5	*0*	5.5	*0*
Potassium Citrate, 1 H2O	16.5	*0*	16.5	*0*
Vitamin Mix V10001	10	*40*	10	*40*
Choline Bitartrate	2	*0*	2	*0*
PXS-5505	0	*0*	**0**	*0*
PXS-5382	0	*0*	**0.282**	*0*
Flavor, Peanut Powder	**10.7**	*0*	**10.7**	*0*
FD&C Yellow Dye #5	0.05	*0*	0	*0*
FD&C Red Dye #40	0	*0*	0	*0*
FD&C Blue Dye #1	0	*0*	0.05	*0*
Total	**1065.75**	***4057***	**1066.03**	***4057***
Compound, mg/kg diet	**0**		**265**	
% Flavor	**1.0**		**1.00372**	

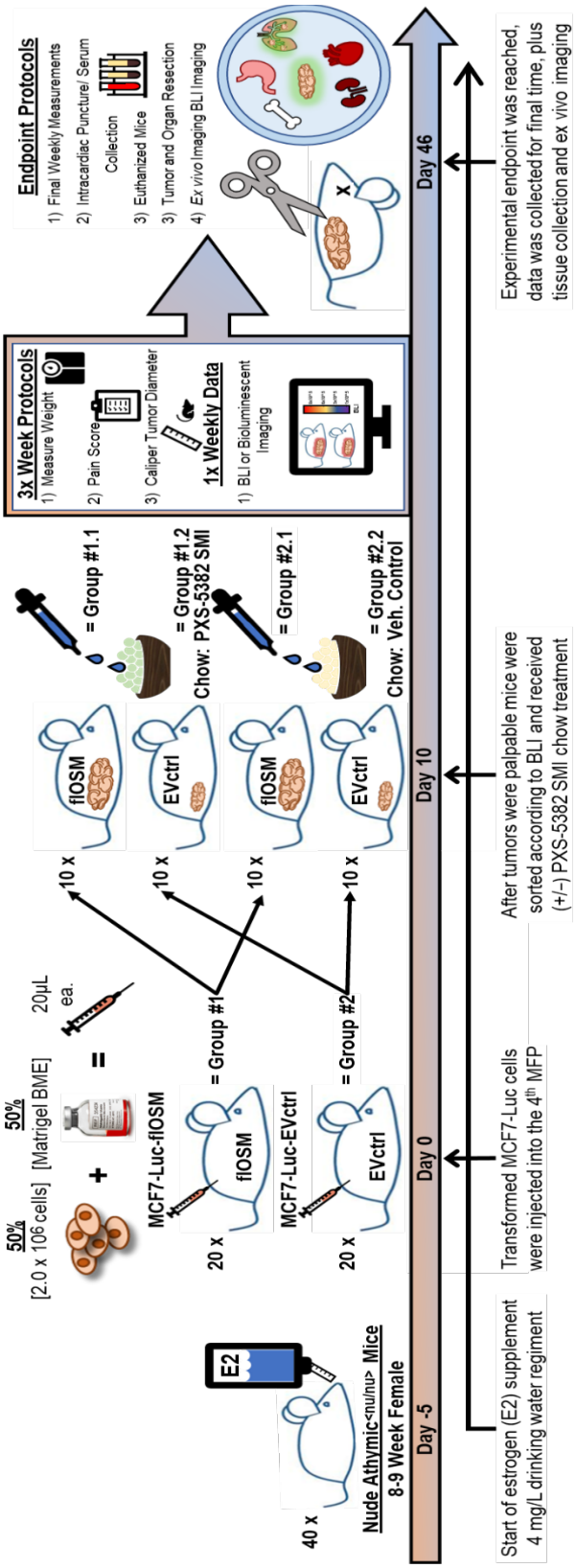

Figure 3.3 ER+ IDC Mouse Model for in vivo Tumor Progression and Metastasis.

This flow chart figure of our mouse model depicts the flow'of research from the 5 days prior to the start of tumor cell injections, where estrogen (E2) supplementation would provide a good initial concentration in the mice, to the day of where the 4th mammary fat pad will receive 2 million cells of either EV control or flOSM overexpressing MCF7-Luc cells to the final day of the study where terminal procedures must be performed, which includes: i) taking final weight and caliper measurements, ii) taking final live-mouse bioluminescent IVIS images, iii) anaesthetizing the mice with isoflurane gas, iv) drawing blood terminally by intracardiac puncture, v) euthanizing mice, vi) dissecting mice, and vii) resecting organs including tumor. After these procedures for each mouse, we concluded with *ex vivo* IVIS imaging, due to 200µL 100x luciferin IP injections given just before anaesthetization, we were able to image for metastasis by measuring bioluminescent signal in the resected organs.

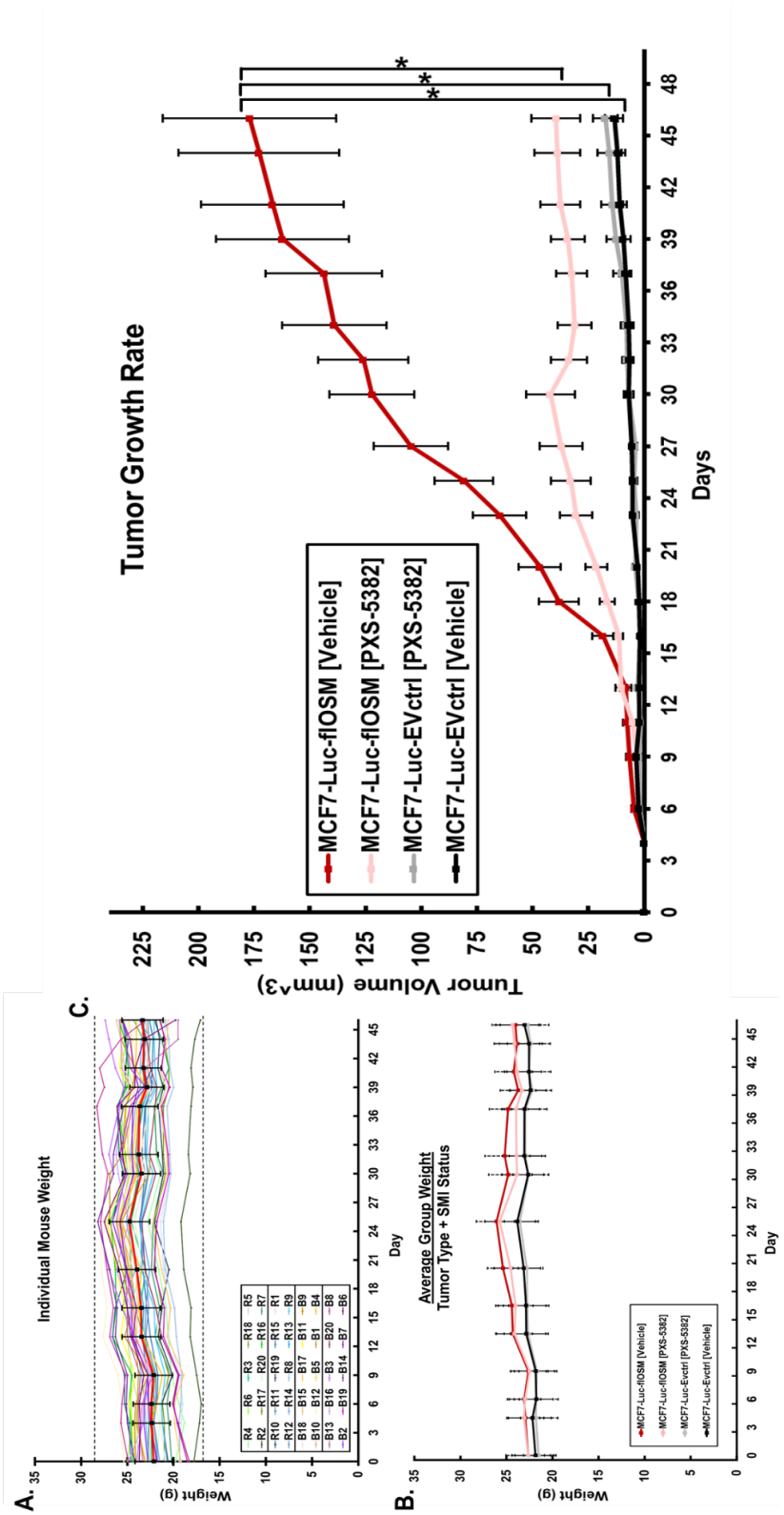

Figure 3.4 Mouse Weight Over Time and Tumor Size in Volume Over Time for MCF7-Luc Groups.

In **A.** The weekly weight measurements tallied with the graph depicting weight fluctuations for each mouse; the 40 mice are plotted separately with a line bisecting the datapoints. The black center line with error bars represents the average weight fluctuation of all the mice in the study. Two mice, B14 and B15, died before the conclusion of the study and so the corresponding lines end upon death. The data lines plotted for the mice were separated by color into 4 groups according to the treatment the 10 mice in that group received; with green hues stand for MCF7-Luc-EVctrl [Vehicle], blue hues stand for MCF7-Luc-EVctrl [PXS-5382], yellow-orange hues stand for MCF7-Luc-flOSM [PXS-5382], and violet hues stand for MCF7-Luc-flOSM [Vehicle]. The mice slightly gained weight in the first half of the study, peaking at the midpoint of the study, followed by a slow but steady decline. No mice needed to be sacrificed for falling below 80% original weight. **B.** This graph depicts the average weight of the mice in each group over time, until the study was terminated. The results show that there was not much of a difference between the average weight of mice, as well as small variations between weights, from each group. This suggests that the groups were eating properly and weight flux was not a concern **C.** The graph is a scatter plot with lines connecting consecutive days, error bars represent SEM, of the average tumor growth by way of volume, in millimeters cubed (mm^3), over time in days. Tumor growth curves represent the 4 groups of mice measurements were taken from the *in vivo* study, collected by caliper diameter measurements and calculated for tumor volume using the equation found in the M&M section under Analysis of Tumor Growth and Metastasis. MCF7-Luc-flOSM [Vehicle] tumors grew the largest and fastest, there is a significant increase in the size of the tumor compared to all 3 other groups from day 32 onwards, and LOXL2 expression is significantly involved in promoting larger tumors since LOXL2 inhibited mice had less than 1/3 the tumor volume. There is a notable size difference between the flOSM and EVctrl tumors overall, regardless of SMI exposure. This data shows that flOSM promotes increased tumor growth in ER+ MCF7 and the data suggests that tumor cells must have a greater doubling rate compared to EVctrl cells. (Each group (n=8+); * $p < 0.05$ RM Two-way ANOVA).

A.

	MCF7-Luc-EVctrl [Vehicle]	MCF7-Luc-EVctrl [PXS-5382]	MCF7-Luc-flOSM [Vehicle]	MCF7-Luc-flOSM [PXS-5382]
TOTAL	1/9	4/9	7/8	1/8
Lung	1/9	4/9	6/8	1/8
Bone	0/9	0/9	5/8	0/8
GI Tract	0/9	0/9	1/8	0/8
Brain	0/9	0/9	0/8	0/8
Kidney	0/9	0/9	0/8	0/8
Liver	0/9	0/9	0/8	0/8
Ovaries	0/9	0/9	0/8	0/8

B.

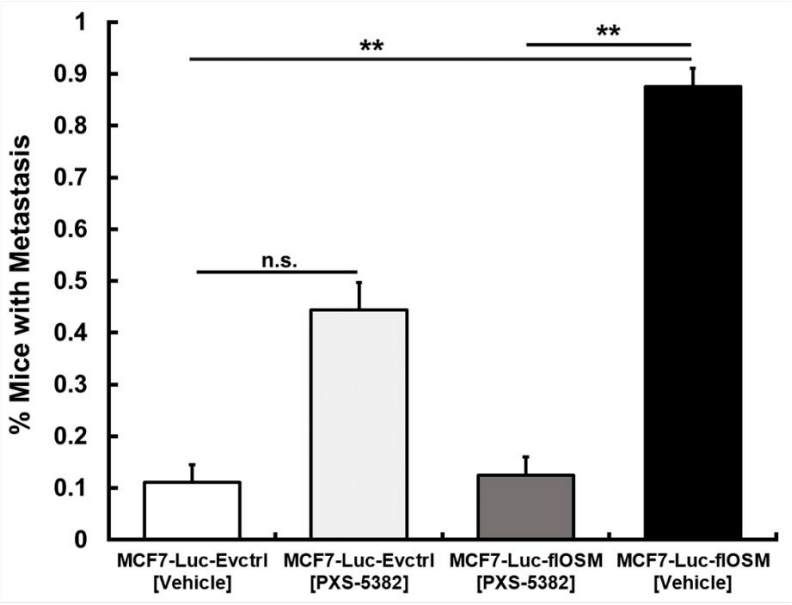

C.

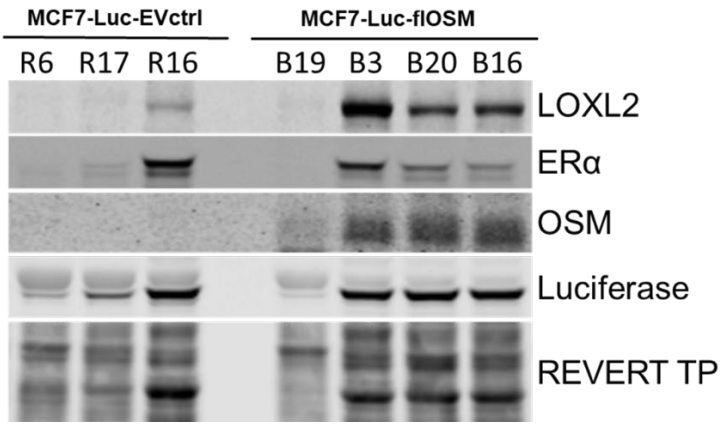

Figure 3.5 Number of Mice with Metastatic Lesions, and Organs With Them Present.

A. The table depicts each of the 4 groups of mice, with the fraction of mice positive for metastasis from the mouse study as well as the fraction that had the metastases located in specific organs. From the table the MCF7-Luc-flOSM [Vehicle] group had the most mice with metastases with 7 out of 8 or 87.5%, the majority of which had mets in both the lung and bone tissues. The MCF7-Luc-flOSM [PXS-5382] and MCF7-Luc-EVctrl [Vehicle] groups were similar in that only 1 mouse had metastases from each group, or 12.5% and 11.1% respectively, and both were found in the lungs. The MCF7-Luc-EVctrl [PXS-5382] group had 4 mice with metastases or 44.4% and again all were in the lungs. **B.** The data from the table is plotted to make a bar graph that is easily understood. The y-axis represents the fraction of mice with metastases from 0 to 1, multiply by 100% to get the percentage of mice with metastases per group. The data was analyzed by our professional statistician Laura Bond, the conclusion from the analysis is that there is a significant increase in metastasis between the flOSM [Vehicle] group and both the flOSM [PXS-5382] and the EVctrl [Vehicle] group while there is no significance compared to the EVctrl [PXS-5382] group. The EVctrl [PXS-5382] was also not significantly more metastatic than flOSM [PXS-5382] and EVctrl [Vehicle] groups. **C.** Tumor tissues collected and lysed from 4 mice receiving MCF7-Luc-flOSM IDC cell injections and 4 mice receiving MCF7-Luc-EVctrl IDC cells. They were analyzed by immunoblot assay for human LOXL2, OSM, ERα, and luciferase expression. We used a REVERT total protein stain as a loading control but due to the nature of the isolated tissues luciferase expression was also used as a loading control. This is because of the small tumors in the EV control group. Qualitative analysis confirms that we had 3 of our 4 flOSM samples composed mostly tumor tissue; however, only 1 of our 4 EV control samples were also mostly tumor tissue. Comparing the 3 flOSM tumor cells vs the EVctrl sample we noticed flOSM tumors produced high levels of LOXL2 while hOSM expression was present, which was not the case for the EV control. Furthermore, ERα expression was still present in the hOSM overexpressing MCF7-Luc cells, though reduced compared to the EVctrl. (Experimental groups are (flOSM n=8, EVctrl n=9); not significant (n.s.) $p > 0.05$, ** $p < 0.01$; Chi Squared test).

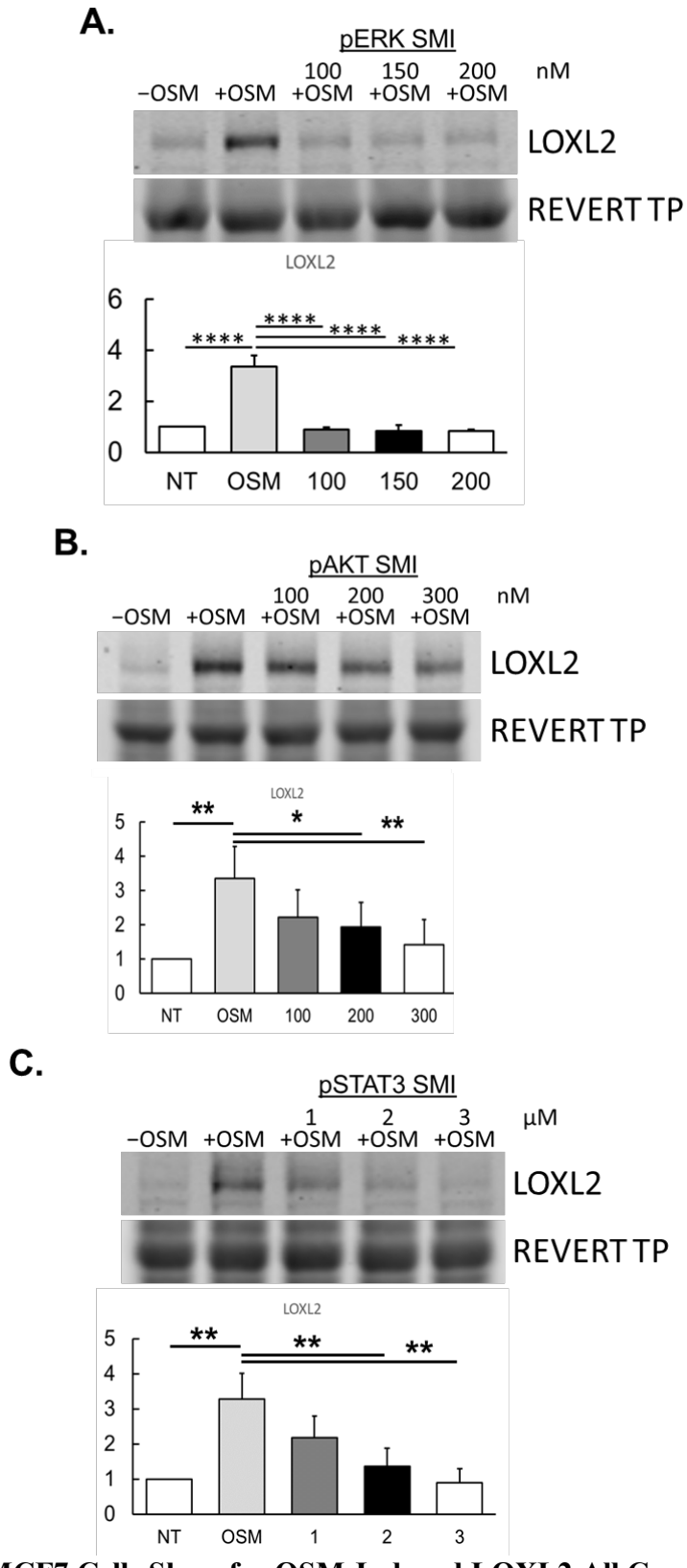

Figure 3.6 MCF7 Cells Show for OSM-Induced LOXL2 All Canonical Pathways are Critical for LOXL2 Induction.

A. MCF7 cells are incubated for 2-hours with a series of pERK SMI (PD0325901) concentrations 100 nM, 150 nM, and 200 nM before adding 25 ng/mL rhOSM treatment for 24-hours. **B.** MCF7 cells are incubated for 2-hours with a series of pAKT SMI (GDC-0941) concentrations 100 nM, 200 nM, and 300 nM before adding 25 ng/mL rhOSM treatment for 24-hours. **C.** MCF7 cells are incubated for 2-hours with a series of pSTAT3 SMI (Stattic) concentrations 1 μM, 2 μM, and 3 μM before adding 25 ng/mL rhOSM treatment for 24-hours. LOXL2 expression was analyzed by immunoblot assay and normalized to REVERT total protein stain loading control and compared against non OSM treated controls. We found that LOXL2 expression was significantly inhibited in every single canonical signaling pathway between OSM and OSMR, with pERK and pSTAT3 inhibition having strongest effect. To compare the results from each SMI tested we plotted the data on bar graph measuring fold change compared to non-treated controls. (All experiments (n=3); * $p < 0.05$, ** $p < 0.01$, **** $p < 0.0001$; One-way ANOVA).

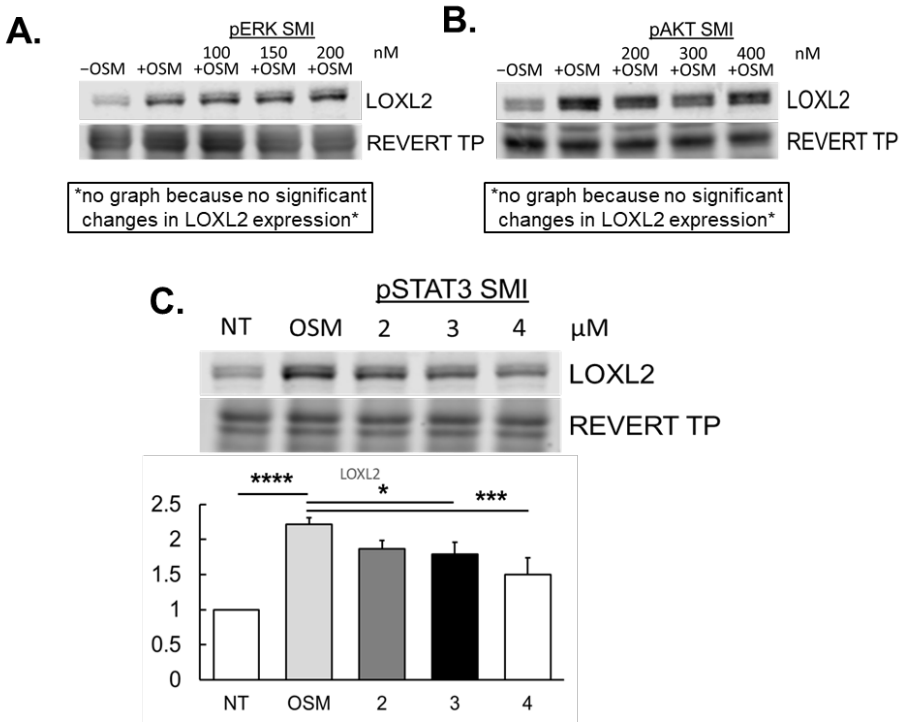

Figure 3.7 MDA-MB-468 Cells Show for OSM-Induced LOXL2 Only pSTAT3 is Critical for LOXL2 Induction.

A. MDA-MB-468 cells are incubated for 2-hours with a series of pERK SMI (PD0325901) concentrations 100 nM, 200 nM, and 300 nM before adding 25 ng/mL rhOSM treatment for 24-hours. **B.** MDA-MB-468 cells are incubated for 2-hours with a series of pAKT SMI (GDC-0941) concentrations 200 nM, 300 nM, and 400nM before adding 25 ng/mL rhOSM treatment for 24-hours. **C.** MDA-MB-468 cells are incubated for 2-hours with a series of pSTAT3 SMI (Stattic) concentrations 2 µM, 3 µM, and 4 µM before adding 25 ng/mL rhOSM treatment for 24-hours. LOXL2 expression was analyzed by immunoblot assay and normalized to REVERT total protein stain loading control and compared against non OSM treated controls. We observed that LOXL2 expression was only significantly inhibited by the pSTAT3 SMI. There was no observable change in LOXL2 expression due to pERK and pAKT inhibition so no graph was necessary; however, the relative expression from pSTAT3 SMI and OSM treated samples was graphed for comparison. (All experiments (n=3); * $p < 0.05$, *** $p < 0.001$, **** $p < 0.0001$; One-way ANOVA).

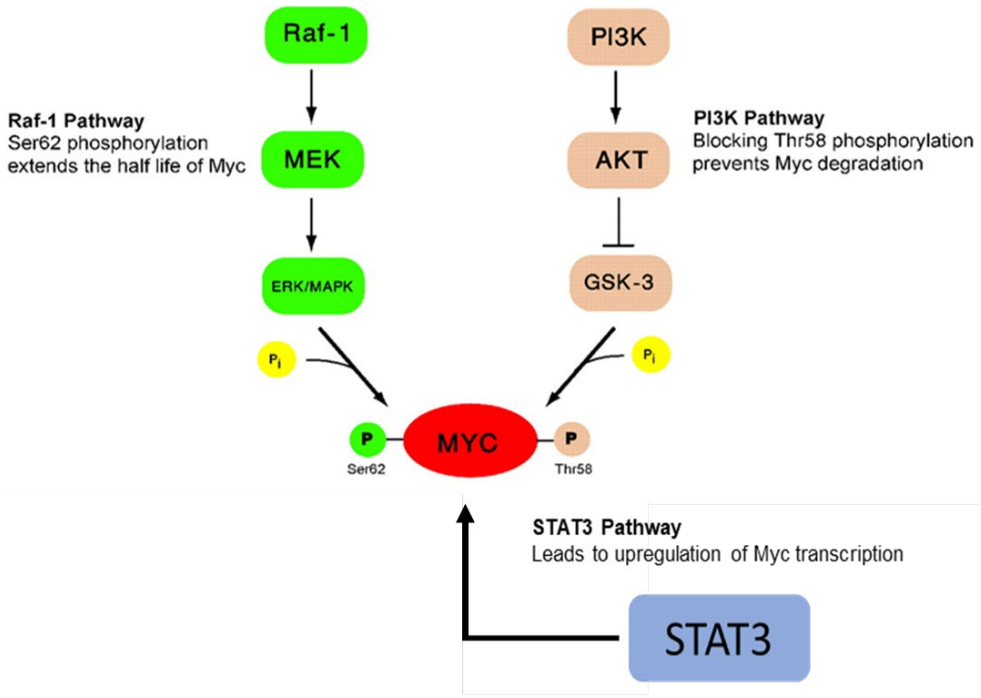

Figure 3.8 Proposed Mechanism for c-Myc Regulation by OSM Signal Pathway Activation.

The protein interactions diagramed illustrates the proposed transcription factor (TF) that the canonical OSM signal transduction pathways JAK-STAT3, PI3K-AKT, and MAPK-ERK1/2 converge on, which is the proto-oncogene c-Myc. Each of the pathways have a role in promoting increased c-Myc expression, suggesting this could be the downstream mediator for LOXL2 upregulation. In this interaction MAPK-ERK1/2 signal transduction leads to pERK promoting the phosphorylation of c-Myc at its Serine 62 amino acid or p-c-Myc [Ser62], which promotes an increase in c-Myc's half-life. The PI3K-AKT signal transduction pathway will lead to pAKT inhibition of the GSK-3 protein, not allowing GSK-3 to phosphorylate c-Myc at its Threonine 58 amino acid (p-c-Myc [Thr58]) which would cause c-Myc to be tagged for proteasomal degradation. The JAK-STAT3 signaling pathway leads to the pSTAT3 homodimer binding to the c-Myc promoter region, activating c-Myc gene transcription which ultimately leads to more c-Myc TF protein. (Taken from [Bachireddy 2005] [164]; License granted for Copyright use, modified according to Copyright License guidelines).

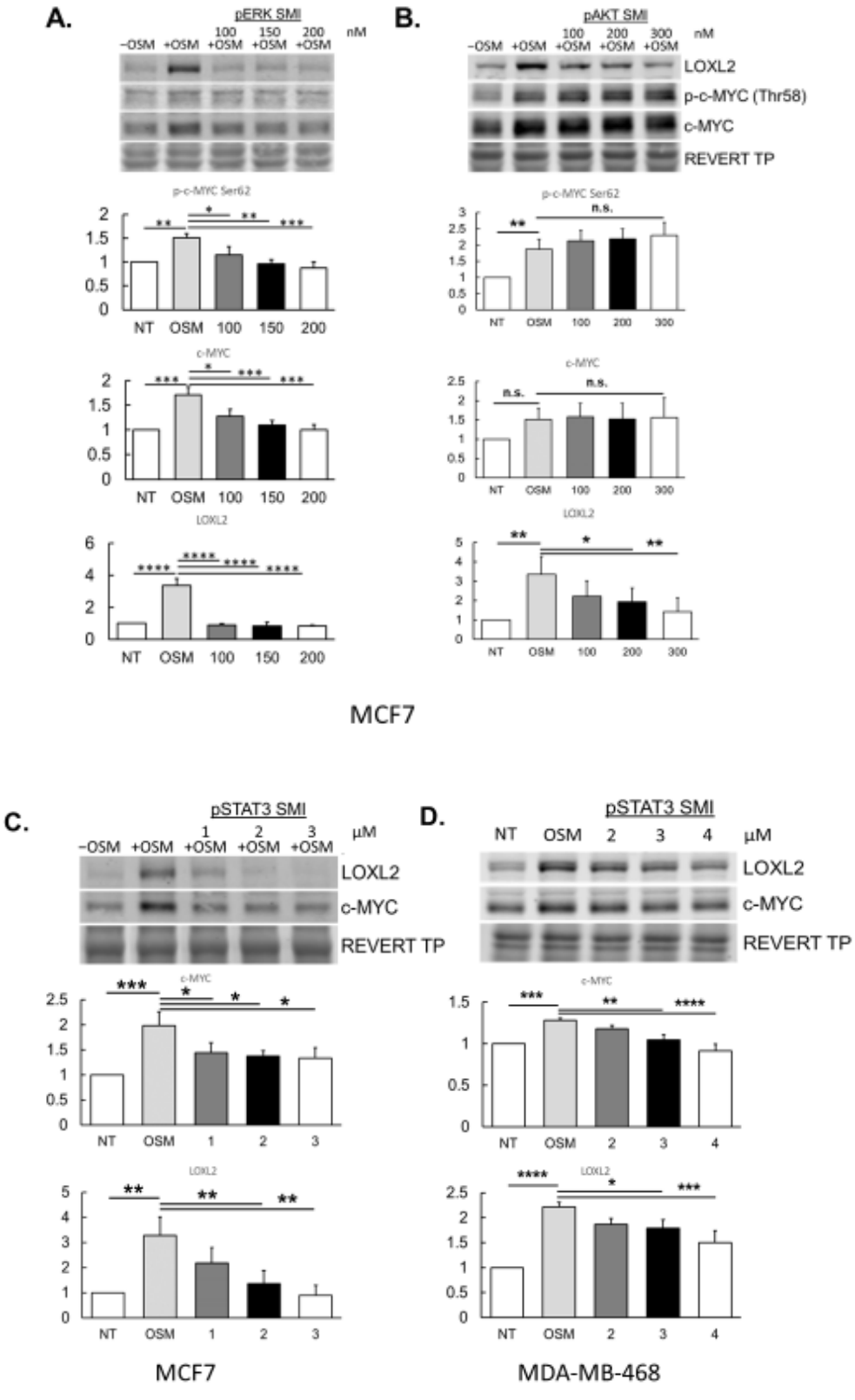

Figure 3.9 MCF7 Cells Seem to Rely on c-MYC for OSM-Induced LOXL2 in pERK and pSTAT3 pathway.

A. MCF7 cells are incubated for 2-hours with a series of pERK SMI (PD0325901) concentrations 100 nM, 150 nM, and 200 nM before adding 25 ng/mL rhOSM treatment for 24-hours. **B.** MCF7 cells are incubated for 2-hours with a series of pAKT SMI (GDC-0941) concentrations 100 nM, 200 nM, and 300 nM before adding 25 ng/mL rhOSM treatment for 24-hours. **C.** MCF7 cells are incubated for 2-hours with a series of pSTAT3 SMI (Stattic) concentrations 1 μM, 2 μM, and 3 μM before adding 25 ng/mL rhOSM treatment for 24-hours. **D.** MDA-MB-468 are incubated for 2-hours with a series of pSTAT3 SMI (Stattic) concentrations 2 μM, 3 μM, and 4 μM before adding 25 ng/mL rhOSM treatment for 24-hours. Afterwards lysates were collected and analyzed by immunoblot. The REVERT total protein stain was used as our loading control, and relative expression of LOXL2, c-Myc, and p-c-Myc Ser62 and Thr58 were compared against non-treated controls. The following results were graphed on the associated bar graph. We saw LOXL2 significantly upregulated by OSM treatment alone in all 4 experiemts. After that assessment we compared the OSM and signal pathway SMI treated cells against the OSM treatment and found that for LOXL2, c-Myc, p-c-Myc Ser62 for MCF7 cells with pERK SMI treatment, and p-c-Myc Thr58 for MCF7 cells with pAKT SMI treatment at the very least the highest concentration significantly reduced the expression of LOXL2, c-Myc, and for both p-c-Myc proteins. This data suggests that there is some sort of association between LOXL2 and c-Myc expression involved in the MCF7 cell lines. (All experiments (n=3); not significant (n.s.) $p > 0.05$, * $p < 0.05$, ** $p < 0.01$, *** $p < 0.001$ **** $p < 0.0001$; One-way ANOVA).

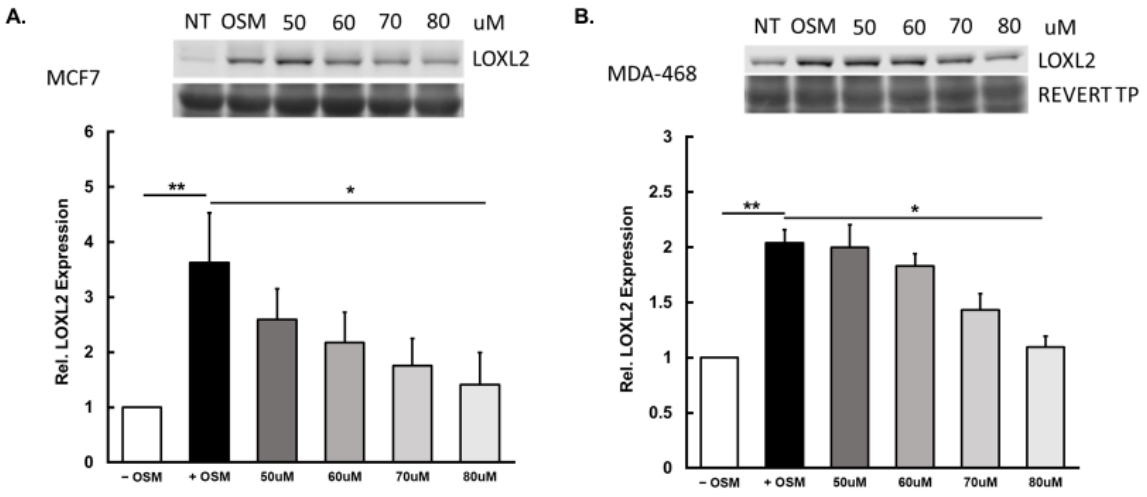

Figure 3.10 IDC Cells Depend on Presence of c-MYC for OSM-Induced LOXL2.

A. Immunoblot assays of MCF7 and MDA-MB-468 IDC cells treated with 25 ng/mL rhOSM and rhOSM with c-MYC SMI (10058-F4) at a series of concentrations 50 μM, 60 μM, 70 μM, 80 μM looking at LOXL2 expression. The REVERT total protein stain was used as a loading control, and relative expression was compared to no OSM treatment controls. **B.** The graphs represent the relative LOXL2 expression in Log2. This is done because the data was transformed to reduce the variance so that assumptions for ANOVA statistical analysis is met. There is a significant increase in LOXL2 expression with OSM treatment, but more importantly the c-Myc SMI caused a significant decrease in LOXL2 expression compared to OSM treatment. These results show that for both MCF7 and MDA-MB-468 cells, c-Myc transcriptional activity is required to either directly or indirectly. (All experiments (n=3); * $p < 0.05$, ** $p < 0.01$; One-way ANOVA).

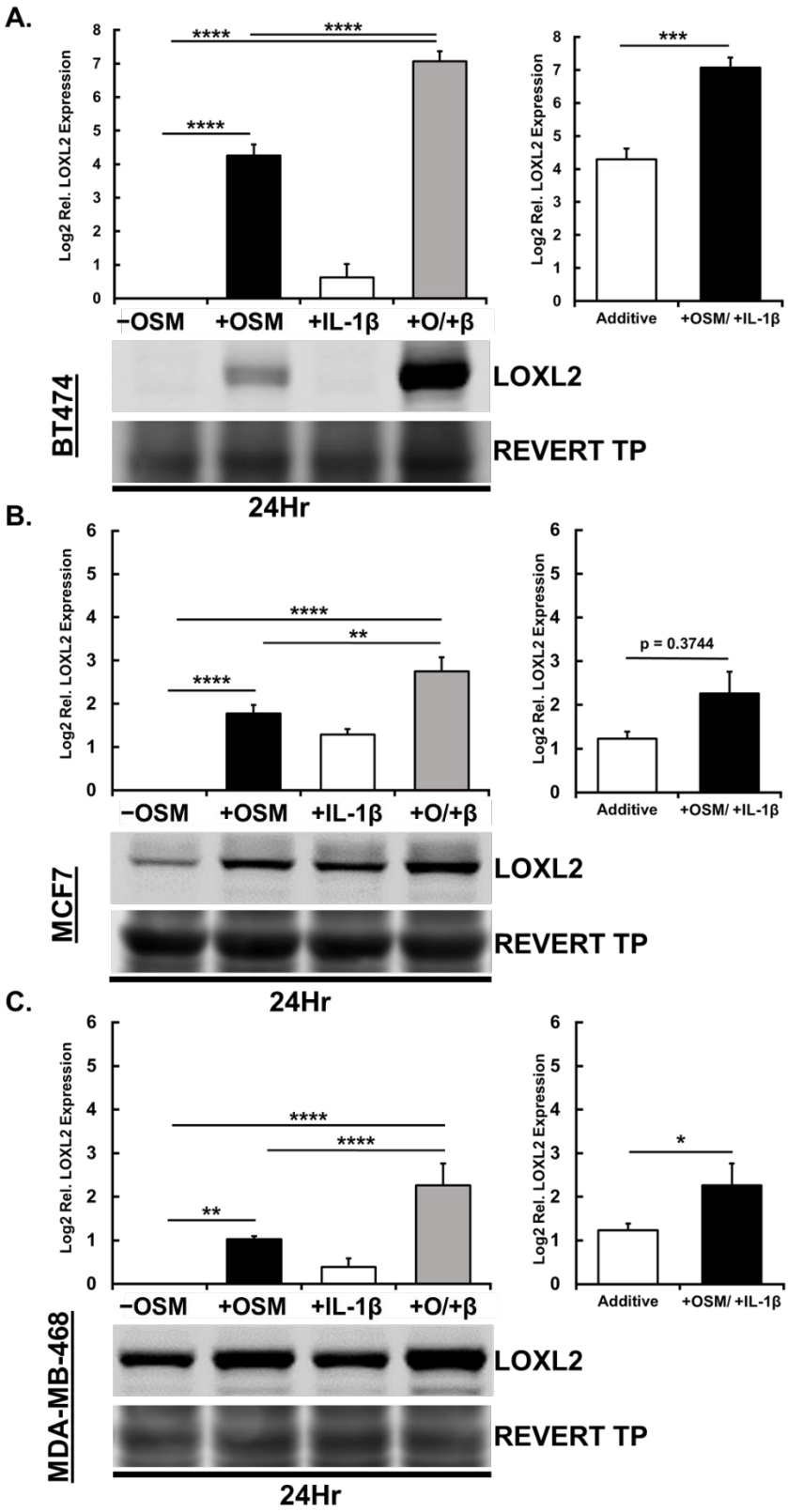

Figure 3.11 Synergistic Effect Between OSM-Induced LOXL2 and IL-1β-Induced LOXL2 Expression.

A. Immunoblot assays of BT474 IDC cells treated with 25 ng/mL rhOSM and/or 10 ng/mL rhIL-1β treated for 24-hours. The REVERT total protein stain was used as a loading control and the relative LOXL2 expression between various treatments was compared against the non-treated control. The expression of LOL2 is graphed in Log2 format to reduce variance to meet assumptions for ANOVA testing. The relative expression of OSM and IL-1β treatment combined is compared against inductions of OSM and IL-1β added together from individual treatments to determine synergistic interactions. The results show that OSM (~15-fold increase) and OSM/IL-1β (~100-fold increase) induced LOXL2 expression is significantly higher than no treatment and OSM/IL-1β significantly higher than OSM and though not depicted IL-1β treatment. The synergy plot also shows a large difference in LOXL2 that is very significant confirming synergistic interaction between OSM and IL-1β. **B.** The immunoblot assay was run the same way for MCF7 cells with same treatment times and controls, and Log2 graphed LOXL2 expression. The results show that OSM (~3.5-fold increase) IL-1β (~2.5-fold increase) and OSM/IL-1β (~7-fold increase) induced LOXL2 expression is significantly higher than no treatment and the combination is significantly higher than OSM treatment and IL-1β treatment, not depicted. The synergy plot shows slightly more LOXL2 in combined treatment; however, the synergistic interaction is not significantly greater than the sum of OSM and IL-1β and so not synergistic without a doubt. **C.** Immunoblot assays of MDA-MB-468 with same treatments and data analysis as for the previous cell lines. The same trend is observed in this cell line as the others, along with same treatments having comparisons that are significant. When analyzing the synergistic interaction there is indeed a statistically significant synergistic upregulation of LOXL2 with OSM and IL-1β. (All experiments (n=3); ** $p < 0.01$, *** $p < 0.001$, **** $p < 0.0001$; One-way ANOVA).

REFERENCES

1. Faguet, GB. 2015. *A brief history of cancer: Age-old milestones underlying our current knowledge database*. International Journal of Cancer. **136**(9): 2022-2036.

2. Hanahan, D and Weinberg, RA. 2011. *Hallmarks of cancer: The next generation*. Cell. **144**(5): 646-674.

3. Jones, PA and Baylin, SB. 2007. *The epigenomics of cancer*. Cell. **128**(4): 683-692.

4. Berdasco, M and Esteller, M. 2010. *Aberrant epigenetic landscape in cancer: How cellular identity goes awry*. Developmental Cell. **19**(5): 698-711.

5. Murphy, SL, Kochanek, KD, Xu, J and Arias, E. 2021. *Mortality in the united states, 2020*. NCHS data brief. 427): 1-8.

6. Abbafati, C, Abbas, KM, Abbasi, M, Abbasifard, M, Abbasi-Kangevari, M, Abbastabar, H, Abd-Allah, F, Abdelalim, A, Abdollahi, M, Abdollahpour, I, Abedi, A, Abedi, P, Abegaz, KH, Abolhassani, H, Abosetugn, AE, Aboyans, V, Abrams, EM, Abreu, LG, Abrigo, MRM, Abu Haimed, AK, et al. 2020. *Global burden of 369 diseases and injuries in 204 countries and territories, 1990-2019: A systematic analysis for the global burden of disease study 2019*. Lancet. **396**(10258): 1204-1222.

7. Siegel, RL, Miller, KD, Wagle, NS and Jemal, A. 2023. *Cancer statistics, 2023*. Ca-a Cancer Journal for Clinicians. **73**(1): 17-48.

8. Howlader, N, Noone, A, Krapcho, M, Miller, D, Brest, A, Yu, M, Ruhl, J, Tatalovich, Z, Mariotto, A, Lewis, D, Chen, H, Feuer, E and Cronin, K (editors). 2019. *SEER (Surveillance, Epidemiology, and End Results Program) Cancer Statistics Review from 1975-2016*. US Department of Health and Human Services, CDC, and NCI; Bethesda, MD. Submission of data: November 2018, Released on: April 2019, Last updated: April 2020. National Program of Cancer Registries and Surveillance, Epidemiology, and End Results Program [SEER*Stat Database]. (Website database). https://seer.cancer.gov/archive/csr/1975_2016/.

9. Bray, F, Ferlay, J, Soerjomataram, I, Siegel, RL, Torre, LA and Jemal, A. 2018. *Global cancer statistics 2018: Globocan estimates of incidence and mortality worldwide for 36 cancers in 185 countries*. Ca-a Cancer Journal for Clinicians. **68**(6): 394-424.

10. Yabroff, KR, Mariotto, A, Tangka, F, Zhao, J, Islami, F, Sung, H, Sherman, RL, Henley, SJ, Jemal, A and Ward, EM. 2021. *Annual report to the nation on the status of cancer, part 2: Patient economic burden associated with cancer care*. Jnci-Journal of the National Cancer Institute. **113**(12): 1670-1682.

11. Mariotto, AB, Enewold, L, Zhao, J, Zeruto, CA and Yabroff, KR. 2020. *Medical care costs associated with cancer survivorship in the united states*. Cancer Epidemiology Biomarkers & Prevention. **29**(7): 1304-1312.

12. Kuukasjarvi, T, Tanner, M, Pennanen, S, Karhu, R, Kallioniemi, OP and Isola, J. 1997. *Genetic changes in intraductal breast cancer detected by comparative genomic hybridization*. American Journal of Pathology. **150**(4): 1465-1471.

13. Harbeck, N, Penault-Llorca, F, Cortes, J, Gnant, M, Houssami, N, Poortmans, P, Ruddy, K, Tsang, J and Cardoso, F. 2019. *Breast cancer*. Nature Reviews Disease Primers. **5**(1): 66-97.

14. Giaquinto, AN, Sung, H, Miller, KD, Kramer, JL, Newman, LA, Minihan, A, Jemal, A and Siegel, RL. 2022. *Breast cancer statistics, 2022*. Ca-a Cancer Journal for Clinicians. **72**(6): 524-541.

15. Clough, KB, Lewis, JS, Couturaud, B, Fitoussi, A, Nos, C and Falcou, MC. 2003. *Oncoplastic techniques allow extensive resections for breast-conserving therapy of breast carcinomas*. Annals of Surgery. **237**(1): 26-34.

16. De La Fuente, FH, Fleitas, MG and Garcia, FM. 2009. *Reduction mammaplasty in breast cancer surgery*. Cirugia Espanola. **85**(3): 140-146.

17. Kumar, P and Aggarwal, R. 2016. *An overview of triple-negative breast cancer*. Archives of Gynecology and Obstetrics. **293**(2): 247-269.

18. Niklaus, NJ, Tokarchuk, I, Zbinden, M, Schlafli, AM, Maycotte, P and Tschan, MP. 2021. *The multifaceted functions of autophagy in breast cancer development and treatment*. Cells. **10**(6): 1447-1471.

19. Prat, A and Perou, CM. 2011. *Deconstructing the molecular portraits of breast cancer*. Molecular Oncology. **5**(1): 5-23.

20. Yoon, EC, Schwartz, C, Brogi, E, Ventura, K, Wen, H and Darvishian, F. 2019. *Impact of biomarkers and genetic profiling on breast cancer prognostication: A comparative analysis of the 8th edition of breast cancer staging system*. Breast Journal. **25**(5): 829-837.

21. Szymiczek, A, Lone, A and Akbari, MR. 2021. *Molecular intrinsic versus clinical subtyping in breast cancer: A comprehensive review*. Clinical Genetics. **99**(5): 613-637.

22. Siegel, RL, Miller, KD and Jemal, A. 2016. *Cancer statistics, 2016*. Ca-a Cancer Journal for Clinicians. **66**(1): 7-30.

23. Bolin, C, Tawara, K, Sutherland, C, Redshaw, J, Aranda, P, Moselhy, J, Anderson, R and Jorcyk, CL. 2012. *Oncostatin m promotes mammary tumor metastasis to bone and osteolytic bone degradation*. Genes & cancer. **3**(2): 117-130.

24. Grenier, A, Dehoux, M, Boutten, A, Arce-Vicioso, M, Durand, G, Gougerot-Pocidalo, MA and Chollet-Martin, S. 1999. *Oncostatin m production and regulation by human polymorphonuclear neutrophils*. Blood. **93**(4): 1413-1421.

25. Queen, MM, Ryan, RE, Holzer, RG, Keller-Peck, CR and Jorcyk, CL. 2005. *Breast cancer cells stimulate neutrophils to produce oncostatin m: Potential implications for tumor progression*. Cancer Research. **65**(19): 8896-8904.

26. Hergueta-Redondo, M, Palacios, J, Cano, A and Moreno-Bueno, G. 2008. *"New" molecular taxonomy in breast cancer*. Clinical & Translational Oncology. **10**(12): 777-785.

27. Alex, A, Bhandary, E and McGuire, KP. 2020. *Anatomy and physiology of the breast during pregnancy and lactation*. in Alipour, S and Omranipour, R (editors); *Diseases of the breast during pregnancy and lactation*, "Advances in experimental medicine and biology" series, Springer International Publishing Ag; Cham. pp. 3-7.

28. Uvnas-Moberg, K, Widstrom, AM, Werner, S, Matthiesen, AS and Winberg, J. 1990. *Oxytocin and prolactin levels in breast-feeding women. Correlation with milk yield and duration of breast-feeding*. Acta Obstetricia Et Gynecologica Scandinavica. **69**(4): 301-306.

29. Tucker, HA. 1979. *Endocrinology of lactation*. Seminars in Perinatology. **3**(3): 199-223.

30. Allred, DC. 2010. *Ductal carcinoma in situ: Terminology, classification, and natural history*. Journal of the National Cancer Institute. Monographs. **2010**(41): 134-138.

31. Tower, H, Ruppert, M and Britt, K. 2019. *The immune microenvironment of breast cancer progression*. Cancers. **11**(9): 1375-1390.

32. SastreGarau, X, Jouve, M, Asselain, B, VincentSalomon, A, Beuzeboc, P, Dorval, T, Durand, JC, Fourquet, A and Pouillart, P. 1996. *Infiltrating lobular carcinoma of the breast - clinicopathologic analysis of 975 cases with reference to data on conservative therapy and metastatic patterns*. Cancer. **77**(1): 113-120.

33. Sflomos, G, Battista, L, Aouad, P, De Martino, F, Scabia, V, Stravodimou, A, Ayyanan, A, Ifticene-Treboux, A, Bucher, P, Fiche, M, Ambrosini, G and Brisken, C. 2021. *Intraductal xenografts show lobular carcinoma cells rely on their own extracellular matrix and loxl1*. Embo Molecular Medicine. **13**(3): e13180-e13199.

34. Mamouch, F, Berrada, N, Aoullay, Z, El Khanoussi, B and Errihani, H. 2018. *Inflammatory breast cancer: A literature review.* World Journal of Oncology. **9**(5-6): 129-135.

35. Moutte, A, Chopin, N, Faure, C, Beurrier, F, Quoc, CH, Guinaudeau, F, Treilleux, I and Carrabin, N. 2016. *Surgical management of benign and borderline phyllodes tumors of the breast*. Breast Journal. **22**(5): 547-552.

36. Helwig, EB and Graham, JH. 1963. *Anogenital (extramammary) pagets disease - a clinicopathological study*. Cancer. **16**(3): 387-403.

37. Sorlie, T, Perou, CM, Tibshirani, R, Aas, T, Geisler, S, Johnsen, H, Hastie, T, Eisen, MB, van de Rijn, M, Jeffrey, SS, Thorsen, T, Quist, H, Matese, JC, Brown, PO, Botstein, D, Lonning, PE and Borresen-Dale, AL. 2001. *Gene expression patterns of breast carcinomas distinguish tumor subclasses with clinical implications*. Proceedings of the National Academy of Sciences of the United States of America. **98**(19): 10869-10874.

38. Yeo, SK and Guan, JL. 2017. *Breast cancer: Multiple subtypes within a tumor?* Trends in Cancer. **3**(11): 753-760.

39. Lim, E, Vaillant, F, Wu, D, Forrest, NC, Pal, B, Hart, AH, Asselin-Labat, ML, Gyorki, DE, Ward, T, Partanen, A, Feleppa, F, Huschtscha, LI, Thorne, HJ, Fox, SB, Yan, M, French, JD, Brown, MA, Smyth, GK, Visvader, JE and Lindeman, GJ. 2009. *Aberrant luminal progenitors as the candidate target population for basal tumor development in brca1 mutation carriers*. Nature Medicine. **15**(8): 907-913.

40. Henry-Tillman, RS and Klimberg, VS. 2000. *In situ breast cancer*. Current Treatment Options in Oncology. **1**(3): 199-209.

41. Sims, AH, Howell, A, Howell, SJ and Clarke, RB. 2007. *Origins of breast cancer subtypes and therapeutic implications*. Nature Clinical Practice Oncology. **4**(9): 516-525.

42. van de Vijver, MJ, He, YD, van 't Veer, LJ, Dai, H, Hart, AAM, Voskuil, DW, Schreiber, GJ, Peterse, JL, Roberts, C, Marton, MJ, Parrish, M, Atsma, D, Witteveen, A, Glas, A, Delahaye, L, van der Velde, T, Bartelink, H, Rodenhuis, S, Rutgers, ET, Friend, SH and Bernards, R. 2002. *A gene-expression signature as a predictor of survival in breast cancer*. New England Journal of Medicine. **347**(25): 1999-2009.

43. Malhotra, GK, Zhao, X, Band, H and Band, V. 2010. *Histological, molecular and functional subtypes of breast cancers*. Cancer Biol Ther. **10**(10): 955-960.

44. Siegal, GP, Barsky, SH, Terranova, VP and Liotta, LL. 1981. *Stages of neoplastic transformation of human breast tissue as monitored by dissolution of basement membrane components an immuno peroxidase study*. Invasion and Metastasis. **1**(1): 54-70.

45. Brown, B, Lindberg, K, Reing, J, Stolz, DB and Badylak, SF. 2006. *The basement membrane component of biologic scaffolds derived from extracellular matrix*. Tissue Engineering. **12**(3): 519-526.

46. Friedl, P and Brocker, EB. 2000. *The biology of cell locomotion within three-dimensional extracellular matrix*. Cellular and Molecular Life Sciences. **57**(1): 41-64.

47. Malik, R, Lelkes, PI and Cukierman, E. 2015. *Biomechanical and biochemical remodeling of stromal extracellular matrix in cancer*. Trends in Biotechnology. **33**(4): 230-236.

48. Levental, KR, Yu, HM, Kass, L, Lakins, JN, Egeblad, M, Erler, JT, Fong, SFT, Csiszar, K, Giaccia, A, Weninger, W, Yamauchi, M, Gasser, DL and Weaver, VM. 2009. *Matrix crosslinking forces tumor progression by enhancing integrin signaling*. Cell. **139**(5): 891-906.

49. Espinoza, JA, Jabeen, S, Batra, R, Papaleo, E, Haakensen, V, Wielenga, VT, Talman, MLM, Brunner, N, Borresen-Dale, AL, Gromov, P, Helland, A, Kristensen, VN and Gromova, I. 2016. *Cytokine profiling of tumor interstitial fluid of the breast and its relationship with lymphocyte infiltration and clinicopathological characteristics*. Oncoimmunology. **5**(12): e1248015-e1248029.

50. Wei, Y, Kim, TJ, Peng, DH, Duan, D, Gibbons, DL, Yamauchi, M, Jackson, JR, Le Saux, CJ, Calhoun, C, Peters, J, Derynck, R, Backes, BJ and Chapman, HA. 2017. *Fibroblast-specific inhibition of tgf-beta 1 signaling attenuates lung and tumor fibrosis*. Journal of Clinical Investigation. **127**(10): 3675-3688.

51. Tigges, J, Krutmann, J, Fritsche, E, Haendeler, J, Schaal, H, Fischer, JW, Kalfalah, F, Reinke, H, Reifenberger, G, Stuhler, K, Ventura, N, Gundermann, S, Boukamp, P and Boege, F. 2014. *The hallmarks of fibroblast ageing*. Mechanisms of Ageing and Development. **138**(1): 26-44.

52. Fisher, GJ, Varani, J and Voorhees, JJ. 2008. *Looking older - fibroblast collapse and therapeutic implications*. Archives of Dermatology. **144**(5): 666-672.

53. Zhu, RJ, Liu, CS and Gundersen, GG. 2018. *Nuclear positioning in migrating fibroblasts*. Seminars in Cell & Developmental Biology. **82**(1): 41-50.

54. Guihard, P, Danger, Y, Brounais, B, David, E, Brion, R, Delecrin, J, Richards, CD, Chevalier, S, Redini, F, Heymann, D, Gascan, H and Blanchard, F. 2012. *Induction of osteogenesis in mesenchymal stem cells by activated monocytes/macrophages depends on oncostatin m signaling*. Stem Cells. **30**(4): 762-772.

55. Tawara, K, Bolin, C, Koncinsky, J, Kadaba, S, Covert, H, Sutherland, C, Bond, L, Kronz, J, Garbow, JR and Jorcyk, CL. 2018. *Osm potentiates preintravasation events, increases ctc counts, and promotes breast cancer metastasis to the lung*. Breast Cancer Research. **20**(1): 53-71.

56. Deshmukh, SK, Srivastava, SK, Bhardwaj, A, Singh, AP, Tyagi, N, Marimuthu, S, Dyess, DL, Dal Zotto, V, Carter, JE and Singh, S. 2015. *Resistin and interleukin-6 exhibit racially-disparate expression in breast cancer patients, display molecular association and promote growth and aggressiveness of tumor cells through stat3 activation*. Oncotarget. **6**(13): 11231-11241.

57. Quail, DF and Joyce, JA. 2013. *Microenvironmental regulation of tumor progression and metastasis*. Nature Medicine. **19**(11): 1423-1437.

58. Kim, Y, Stolarska, MA and Othmer, HG. 2011. *The role of the microenvironment in tumor growth and invasion*. Progress in Biophysics & Molecular Biology. **106**(2): 353-379.

59. Kim, Y and Othmer, HG. 2013. *A hybrid model of tumor-stromal interactions in breast cancer*. Bulletin of Mathematical Biology. **75**(8): 1304-1350.

60. Araujo, AM, Abaurrea, A, Azcoaga, P, Lopez-Velazco, JI, Manzano, S, Rodriguez, J, Rezola, R, Egia-Mendikute, L, Valdes-Mora, F, Flores, JM, Jenkins, L, Pulido, L, Osorio-Querejeta, I, Fernandez-Nogueira, P, Ferrari, N, Viera, C, Martin-Martin, N, Tzankov, A, Eppenberger-Castori, S, Alvarez-Lopez, I, Urruticoechea, A, Bragado, P, Coleman, N, Palazon, A, Carracedo, A, Gallego-Ortega, D, Calvo, F, Isacke, CM, Caffarel, MM and Lawrie, CH. 2022. *Stromal oncostatin m cytokine promotes breast cancer progression by reprogramming the tumor microenvironment*. Journal of Clinical Investigation. **132**(7): e148667-e148685.

61. Insua-Rodriguez, J and Oskarsson, T. 2016. *The extracellular matrix in breast cancer*. Advanced Drug Delivery Reviews. **97**(1): 41-55.

62. Plotnikov, SV and Waterman, CM. 2013. *Guiding cell migration by tugging*. Current Opinion in Cell Biology. **25**(5): 619-626.

63. Das, M, Ithychanda, SS, Qin, J and Plow, EF. 2014. *Mechanisms of talin-dependent integrin signaling and crosstalk*. Biochimica Et Biophysica Acta-Biomembranes. **1838**(2): 579-588.

64. Barth, TFE, Rinaldi, N, Bruderlein, S, Mechtersheimer, G, Strater, J, Altevogt, P and Moller, P. 2002. *Mesothelial cells in suspension expose an enriched integrin repertoire capable of capturing soluble fibronectin and laminin*. Cell Communication and Adhesion. **9**(1): 1-14.

65. Emsley, J, Knight, CG, Farndale, RW, Barnes, MJ and Liddington, RC. 2000. *Structural basis of collagen recognition by integrin alpha 2 beta 1*. Cell. **101**(1): 47-56.

66. Senbanjo, LT and Chellaiah, MA. 2017. *Cd44: A multifunctional cell surface adhesion receptor is a regulator of progression and metastasis of cancer cells*. Frontiers in Cell and Developmental Biology. **5**(18): 1-6.

67. Witschen, PM, Chaffee, TS, Brady, NJ, Huggins, DN, Knutson, TP, LaRue, RS, Munro, SA, Tiegs, L, McCarthy, JB, Nelson, AC and Schwertfeger, KL. 2020. *Tumor cell associated hyaluronan-cd44 signaling promotes pro-tumor inflammation in breast cancer*. Cancers (Basel). **12**(5): 1325-1348.

68. Dutta, S, Warshall, C, Bandyopadhyay, C, Dutta, D and Chandran, B. 2014. *Interactions between exosomes from breast cancer cells and primary mammary epithelial cells leads to generation of reactive oxygen species which induce DNA damage response, stabilization of p53 and autophagy in epithelial cells*. Plos One. **9**(5): e97580-e97593.

69. Liao, Z, Chua, D and Tan, NS. 2019. *Reactive oxygen species: A volatile driver of field cancerization and metastasis*. Molecular Cancer. **266**(1): 53-59.

70. Petrova, V, Annicchiarico-Petruzzelli, M, Melino, G and Amelio, I. 2018. *The hypoxic tumour microenvironment*. Oncogenesis. **7**(10): 1-13.

71. Torres, S, Garcia-Palmero, I, Herrera, M, Bartolome, RA, Pena, C, Jesus Fernandez-Acenero, M, Padilla, G, Pelaez-Garcia, A, Lopez-Lucendo, M, Rodriguez-Merlo, R, Garcia de Herreros, A, Bonilla, F and Ignacio Casal, J. 2015. *Loxl2 is highly expressed in cancer-associated fibroblasts and associates to poor colon cancer survival*. Clinical Cancer Research. **21**(21): 4892-4902.

72. Pakshir, P, Noskovicova, N, Lodyga, M, Son, DO, Schuster, R, Goodwin, A, Karvonen, H and Hinz, B. 2020. *The myofibroblast at a glance*. Journal of Cell Science. **133**(13): 1-10.

73. Wu, L and Zhang, XHF. 2020. *Tumor-associated neutrophils and macrophages—heterogenous but not chaotic*. Frontiers in Immunology. **11**(553967): 1-18.

74. Kim, J and Bae, JS. 2016. *Tumor-associated macrophages and neutrophils in tumor microenvironment*. Mediators Inflamm. **2016**(6058147.

75. Brabletz, S, Schuhwerk, H, Brabletz, T and Stemmler, MP. 2021. *Dynamic emt: A multi-tool for tumor progression*. The EMBO Journal. **40**(18): e108647-e108669.

76. Gómez-Valenzuela, F, Escobar, E, Pérez-Tomás, R and Montecinos, VP. 2021. *The inflammatory profile of the tumor microenvironment, orchestrated by cyclooxygenase-2, promotes epithelial-mesenchymal transition*. Frontiers in Oncology. **11**(686792): 1-16.

77. Cano, A, Santamaria, PG and Moreno-Bueno, G. 2012. *Loxl2 in epithelial cell plasticity and tumor progression*. Future Oncology. **8**(9): 1095-1108.

78. Moon, HJ, Finney, J, Xu, L, Moore, D, Welch, DR and Mure, M. 2013. *Mcf-7 cells expressing nuclear associated lysyl oxidase-like 2 (loxl2) exhibit an epithelial-to-mesenchymal transition (emt) phenotype and are highly invasive in vitro*. Journal of Biological Chemistry. **288**(42): 30000-30008.

79. Wu, Y, Antony, S, Meitzler, JL and Doroshow, JH. 2014. *Molecular mechanisms underlying chronic inflammation-associated cancers*. Cancer Lett. **345**(2): 164-173.

80. Allen, MD and Jones, LJ. 2015. *The role of inflammation in progression of breast cancer: Friend or foe? (review)*. Int J Oncol. **47**(3): 797-805.

81. Giordano, SH and Hortobagyi, GN. 2003. *Inflammatory breast cancer: Clinical progress and the main problems that must be addressed*. Breast Cancer Research. **5**(6): 284-288.

82. Tecchio, C, Micheletti, A and Cassatella, MA. 2014. *Neutrophil-derived cytokines: Facts beyond expression*. Frontiers in Immunology. **5**(508): 1-7.

83. Butterfield, TA, Best, TM and Merrick, MA. 2006. *The dual roles of neutrophils and macrophages in inflammation: A critical balance between tissue damage and repair*. J Athl Train. **41**(4): 457-465.

84. Jorcyk, CL, Holzer, RG and Ryan, RE. 2006. *Oncostatin m induces cell detachment and enhances the metastatic capacity of t-47d human breast carcinoma cells*. Cytokine. **33**(6): 323-336.

85. Holzer, RG, Ryan, RE, Tommack, M, Schlekeway, E and Jorcyk, CL. 2004. *Oncostatin m stimulates the detachment of a reservoir of invasive mammary carcinoma cells: Role of cyclooxygenase-2*. Clinical & Experimental Metastasis. **21**(2): 167-176.

86. West, NR, Murphy, LC and Watson, PH. 2012. *Oncostatin m suppresses oestrogen receptor-alpha expression and is associated with poor outcome in human breast cancer*. Endocrine-Related Cancer. **19**(2): 181-195.

87. Baker, KJ, Houston, A and Brint, E. 2019. *Il-1 family members in cancer; two sides to every story*. Frontiers in Immunology. **10**(1197): 1-16.

88. Sansone, P, Storci, G, Tavolari, S, Guarnieri, T, Giovannini, C, Taffurelli, M, Ceccarelli, C, Santini, D, Paterini, P, Marcu, KB, Chieco, P and Bonafe, M. 2007. *Il-6 triggers malignant features in mammospheres from human ductal breast carcinoma and normal mammary gland*. Journal of Clinical Investigation. **117**(12): 3988-4002.

89. Sullivan, NJ, Sasser, AK, Axel, AE, Vesuna, F, Raman, V, Ramirez, N, Oberyszyn, TM and Hall, BM. 2009. *Interleukin-6 induces an epithelial-mesenchymal transition phenotype in human breast cancer cells*. Oncogene. **28**(33): 2940-2947.

90. Casneuf, T, Axel, AE, King, P, Alvarez, JD, Werbeck, JL, Verhulst, T, Verstraeten, K, Hall, BM and Sasser, AK. 2016. *Interleukin-6 is a potential therapeutic target in interleukin-6 dependent, estrogen receptor-ocpositive breast cancer*. Breast Cancer-Targets and Therapy. **8**(1): 13-27.

91. Guo, YQ, Xu, F, Lu, TJ, Duan, ZF and Zhang, Z. 2012. *Interleukin-6 signaling pathway in targeted therapy for cancer*. Cancer Treatment Reviews. **38**(7): 904-910.

92. Jorcyk, CL, Holzer, RG and Ryan, RE. 2006. *Oncostatin m induces cell detachment and enhances the metastatic capacity of t-47d human breast carcinoma cells*. Cytokine. **33**(6): 323-336.

93. Blanchard, F, Wang, YP, Kinzie, E, Duplomb, L, Godard, A and Baumann, H. 2001. *Oncostatin m regulates the synthesis and turnover of gp130, leukemia inhibitory factor receptor alpha, and oncostatin m receptor beta by distinct mechanisms*. Journal of Biological Chemistry. **276**(50): 47038-47045.

94. Hurst, SM, McLoughlin, RM, Monslow, J, Owens, S, Morgan, L, Fuller, GM, Topley, N and Jones, SA. 2002. *Secretion of oncostatin m by infiltrating neutrophils: Regulation of il-6 and chemokine expression in human mesothelial cells*. Journal of Immunology. **169**(9): 5244-5251.

95. Brown, TJ, Lioubin, MN and Marquardt, H. 1987. *Purification and characterization of cytostatic lymphokines produced by activated human t lymphocytes. Synergistic antiproliferative activity of transforming growth factor beta 1, interferon-gamma, and oncostatin m for human melanoma cells*. The Journal of Immunology. **139**(9): 2977-2983.

96. Ryan, RE, Martin, B, Mellor, L, Jacob, RB, Tawara, K, McDougal, OM, Oxford, JT and Jorcyk, CL. 2015. *Oncostatin m binds to extracellular matrix in a bioactive conformation: Implications for inflammation and metastasis*. Cytokine. **72**(1): 71-85.

97. Adrian-Segarra, JM, Schindler, N, Gajawada, P, Loerchner, H, Braun, T and Poeling, J. 2018. *The ab loop and d-helix in binding site iii of human oncostatin m (osm) are required for osm receptor activation*. Journal of Biological Chemistry. **293**(18): 7017-7029.

98. Chollangi, S, Mather, T, Rodgers, KK and Ash, JD. 2012. *A unique loop structure in oncostatin m determines binding affinity toward oncostatin m receptor and leukemia inhibitory factor receptor*. Journal of Biological Chemistry. **287**(39): 32848-32859.

99. Mosley, B, De Imus, C, Friend, D, Boiani, N, Thoma, B, Park, LS and Cosman, D. 1996. *Dual oncostatin m (osm) receptors: Cloning and characterization of an alternative signaling subunit conferring osm-specific receptor activation*. Journal of Biological Chemistry. **271**(51): 32635-32643.

100. Gearing, DP, Ziegler, SF, Comeau, MR, Friend, D, Thoma, B, Cosman, D, Park, L and Mosley, B. 1994. *Proliferative responses and binding properties of hematopoietic cells transfected with low-affinity receptors for leukemia inhibitory factor, oncostatin m, and ciliary neurotrophic factor*. Proceedings of the National Academy of Sciences. **91**(3): 1119-1123.

101. Wang, H, Lei, L, Hu, J and Li, Y. 2020. *Oncostatin m upregulates livin to promote keratinocyte proliferation and survival via erk and stat3 signalling pathways*. Experimental Physiology. **105**(7): 1151-1158.

102. Pastushenko, I and Blanpain, C. 2019. *Emt transition states during tumor progression and metastasis*. Trends in Cell Biology. **29**(3): 212-226.

103. Marhaba, R, Klingbeil, P, Nuebel, T, Nazarenko, I, Buechler, MW and Zoeller, M. 2008. *Cd44 and epcam: Cancer-initiating cell markers*. Curr Mol Med. **8**(8): 784-804.

104. Guo, L, Chen, C, Shi, M, Wang, F, Chen, X, Diao, D, Hu, M, Yu, M, Qian, L and Guo, N. 2013. *Stat3-coordinated lin-28-let-7-hmga2 and mir-200-zeb1 circuits initiate and maintain oncostatin m-driven epithelial-mesenchymal transition*. Oncogene. **32**(45): 5272-5282.

105. Pollack, V, Sarkoezi, R, Banki, Z, Feifel, E, Wehn, S, Gstraunthaler, G, Stoiber, H, Mayer, G, Montesano, R, Strutz, F and Schramek, H. 2007. *Oncostatin m-induced effects on emt in human proximal tubular cells: Differential role of erk signaling*. American Journal of Physiology-Renal Physiology. **293**(5): F1714-F1726.

106. West, NR, Murray, JI and Watson, PH. 2014. *Oncostatin-m promotes phenotypic changes associated with mesenchymal and stem cell-like differentiation in breast cancer*. Oncogene. **33**(12): 1485-1494.

107. Bryson, BL, Junk, DJ, Cipriano, R and Jackson, MW. 2017. *Stat3-mediated smad3 activation underlies oncostatin m-induced senescence*. Cell Cycle. **16**(4): 319-334.

108. Tawara, K, Scott, H, Emathinger, J, Ide, A, Fox, R, Greiner, D, LaJoie, D, Hedeen, D, Nandakumar, M, Oler, AJ, Holzer, R and Jorcyk, C. 2019. *Co-expression of vegf and il-6 family cytokines is associated with decreased survival in her2 negative breast cancer patients: Subtype-specific il-6 family cytokine-mediated vegf secretion*. Translational Oncology. **12**(2): 245-255.

109. Ruggiero, P, Bossù, P, Macchia, G, Del Grosso, E, Sabbatini, V, Bertini, R, Colagrande, A, Bizzarri, C, Maurizi, G, Di Cioccio, V, D'Andrea, G, Di Giulio, A, Frigerio, F, Grifantini, R, Grandi, G, Tagliabue, A and Boraschi, D. 1997. *Inhibitory activity of il-1 receptor antagonist depends on the balance between binding capacity for il-1 receptor type 1 and il-1 receptor type ii*. The Journal of Immunology. **158**(8): 3881-3887.

110. Shafik, NM, Mohamed, DA, Bedder, AE and El-Gendy, AM. 2015. *Significance of tissue expression and serum levels of angiopoietin-like protein 4 in breast cancer progression: Link to nf-κb /p65 activity and pro-inflammatory cytokines*. Asian Pacific journal of cancer prevention : APJCP. **16**(18): 8579-8587.

111. Campo, GM, Avenoso, A, D'Ascola, A, Scuruchi, M, Prestipino, V, Calatroni, A and Campo, S. 2012. *Hyaluronan in part mediates il-1beta-induced inflammation in mouse chondrocytes by up-regulating cd44 receptors*. Gene. **494**(1): 24-35.

112. Castaño, Z, San Juan, BP, Spiegel, A, Pant, A, DeCristo, MJ, Laszewski, T, Ubellacker, JM, Janssen, SR, Dongre, A, Reinhardt, F, Henderson, A, Del Rio, AG, Gifford, AM, Herbert, ZT, Hutchinson, JN, Weinberg, RA, Chaffer, CL and McAllister, SS. 2018. *Il-1β inflammatory response driven by primary breast cancer prevents metastasis-initiating cell colonization*. Nat Cell Biol. **20**(9): 1084-1097.

113. Lappano, R, Talia, M, Cirillo, F, Rigiracciolo, DC, Scordamaglia, D, Guzzi, R, Miglietta, AM, De Francesco, EM, Belfiore, A, Sims, AH and Maggiolini, M. 2020. *The il1β-il1r signaling is involved in the stimulatory effects triggered by hypoxia in breast cancer cells and cancer-associated fibroblasts (cafs)*. Journal of Experimental & Clinical Cancer Research. **39**(1): 153-175.

114. Shchors, K, Shchors, E, Rostker, F, Lawlor, ER, Brown-Swigart, L and Evan, GI. 2006. *The myc-dependent angiogenic switch in tumors is mediated by interleukin 1 beta*. Genes & Development. **20**(18): 2527-2538.

115. Stamenkovic, I. 2003. *Extracellular matrix remodelling: The role of matrix metalloproteinases*. Journal of Pathology. **200**(4): 448-464.

116. Naba, A, Clauser, KR, Lamar, JM, Carr, SA and Hynes, RO. 2014. *Extracellular matrix signatures of human mammary carcinoma identify novel metastasis promoters*. Elife. **3**(1): e01308-e01331.

117. Paulsson, M. 1992. *Basement-membrane proteins - structure, assembly, and cellular interactions*. Critical Reviews in Biochemistry and Molecular Biology. **27**(1-2): 93-127.

118. Albrechtsen, R, Wewer, UM and Liotta, LA. 1986. *Basement-membranes in human cancer*. Pathology Annual. **21**(1): 251-276.

119. Grossman, M, Ben-Chetrit, N, Zhuravlev, A, Afik, R, Bassat, E, Solomonov, I, Yarden, Y and Sagi, I. 2016. *Tumor cell invasion can be blocked by modulators of collagen fibril alignment that control assembly of the extracellular matrix*. Cancer Research. **76**(14): 4249-4258.

120. Werb, Z and Lu, P. 2015. *The role of stroma in tumor development*. Cancer Journal. **21**(4): 250-253.

121. Conklin, MW and Keely, PJ. 2012. *Why the stroma matters in breast cancer insights into breast cancer patient outcomes through the examination of stromal biomarkers*. Cell Adhesion & Migration. **6**(3): 249-260.

122. Heppner, KJ, Matrisian, LM, Jensen, RA and Rodgers, WH. 1996. *Expression of most matrix metalloproteinase family members in breast cancer represents a tumor-induced host response*. American Journal of Pathology. **149**(1): 273-282.

123. Naba, A, Clauser, KR, Hoersch, S, Liu, H, Carr, SA and Hynes, RO. 2012. *The matrisome: In silico definition and in vivo characterization by proteomics of normal and tumor extracellular matrices*. Molecular & Cellular Proteomics. **11**(4): 1-18.

124. Erler, JT and Weaver, VM. 2009. *Three-dimensional context regulation of metastasis*. Clinical & Experimental Metastasis. **26**(1): 35-49.

125. Peng, DH, Ungewiss, C, Tong, P, Byers, LA, Wang, J, Canales, JR, Villalobos, PA, Uraoka, N, Mino, B, Behrens, C, Wistuba, II, Han, RI, Wanna, CA, Fahrenholtz, M, Grande-Allen, KJ, Creighton, CJ and Gibbons, DL. 2017. *Zeb1 induces loxl2-mediated collagen stabilization and deposition in the extracellular matrix to drive lung cancer invasion and metastasis*. Oncogene. **36**(14): 1925-1938.

126. Liu, Y, Keikhosravi, A, Mehta, GS, Drifka, CR and Eliceiri, KW. 2017. *Methods for quantifying fibrillar collagen alignment*. Fibrosis: Methods and Protocols. **1627**(1): 429-451.

127. Sander, LM. 2014. *Modeling contact guidance and invasion by cancer cells*. Cancer Research. **74**(17): 4588-4596.

128. Bredfeldt, JS, Liu, Y, Conklin, MW, Keely, PJ, Mackie, TR and Eliceiri, KW. 2014. *Automated quantification of aligned collagen for human breast carcinoma prognosis*. Journal of pathology informatics. **5**(1): 28-28.

129. Thangapazham, RL, Darling, TN and Meyerle, J. 2014. *Alteration of skin properties with autologous dermal fibroblasts*. International Journal of Molecular Sciences. **15**(5): 8407-8427.

130. Maller, O, Martinson, H and Schedin, P. 2010. *Extracellular matrix composition reveals complex and dynamic stromal-epithelial interactions in the mammary gland*. Journal of Mammary Gland Biology and Neoplasia. **15**(3): 301-318.

131. Frantz, C, Stewart, KM and Weaver, VM. 2010. *The extracellular matrix at a glance*. Journal of Cell Science. **123**(24): 4195-4200.

132. Bruce, SA. 1991. *Ultrastructure of dermal fibroblasts during development and aging - relationship to invitro senescence of dermal fibroblasts*. Experimental Gerontology. **26**(1): 3-16.

133. Ochiai, Y, Itoh, K, Sakurai, E, Adachi, M and Tanaka, Y. 2006. *Substrate selectivity of monoamine oxidase a, monoamine oxidase b, diamine oxidase, and semicarbazide-sensitive amine oxidase in cos-1 expression systems*. Biol Pharm Bull. **29**(12): 2362-2366.

134. Rucker, RB, Kosonen, T, Clegg, MS, Mitchell, AE, Rucker, BR, Uriu-Hare, JY and Keen, CL. 1998. *Copper, lysyl oxidase, and extracellular matrix protein cross-linking*. American Journal of Clinical Nutrition. **67**(5): 996S-1002S.

135. Moon, HJ, Finney, J, Ronnebaum, T and Mure, M. 2014. *Human lysyl oxidase-like 2*. Bioorganic Chemistry. **57**(1): 231-241.

136. Grau-Bove, X, Ruiz-Trillo, I and Rodriguez-Pascual, F. 2015. *Origin and evolution of lysyl oxidases*. Scientific Reports. **5**(10568): 1-11.

137. Vallet, SD, Guéroult, M, Belloy, N, Dauchez, M and Ricard-Blum, S. 2019. *A three-dimensional model of human lysyl oxidase, a cross-linking enzyme*. ACS Omega. **4**(5): 8495-8505.

138. Findlay, AD, Foot, JS, Buson, A, Deodhar, M, Jarnicki, AG, Hansbro, PM, Liu, G, Schilter, H, Turner, CI, Zhou, W and Jarolimek, W. 2019. *Identification and optimization of mechanism-based fluoroallylamine inhibitors of lysyl oxidase-like 2/3*. Journal of Medicinal Chemistry. **62**(21): 9874-9889.

139. Findlay, A, Turner, C and Hamprecht, D. 2020. *Inhibition of loxl2 and other lysyl oxidase (like) enzymes: Intervention at the core of fibrotic pathology*. [Ch. 5] in Brenneman, J and Iyer, MR (editors); *Anti-fibrotic drug discovery*, 1st edition. "Drug discovery" series, Vol. **73**. The Royal Society of Chemistry; London, UK. pp. 145-164.

140. Erasmus, M, Samodien, E, Lecour, S, Cour, M, Lorenzo, O, Dludla, P, Pheiffer, C and Johnson, R. 2020. *Linking loxl2 to cardiac interstitial fibrosis*. International Journal of Molecular Sciences. **21**(16): 5913-5931.

141. Ursin, G, Hovanessian-Larsen, L, Parisky, YR, Pike, MC and Wu, AH. 2005. *Greatly increased occurrence of breast cancers in areas of mammographically dense tissue*. Breast Cancer Research. **7**(5): R605-R608.

142. Boyd, NF, Dite, GS, Stone, J, Gunasekara, A, English, DR, McCredie, MRE, Giles, GG, Tritchler, D, Chiarelli, A, Yaffe, MJ and Hopper, JL. 2002. *Heritability of mammographic density, a risk factor for breast cancer*. New England Journal of Medicine. **347**(12): 886-894.

143. Akiri, G, Sabo, E, Dafni, H, Vadasz, Z, Kartvelishvily, Y, Gan, N, Kessler, O, Cohen, T, Resnick, M, Neeman, M and Neufeld, G. 2003. *Lysyl oxidase-related protein-1 promotes tumor fibrosis and tumor progression in vivo*. Cancer Res. **63**(7): 1657-1666.

144. Boyd, NF, Lockwood, GA, Byng, JW, Tritchler, DL and Yaffe, MJ. 1998. *Mammographic densities and breast cancer risk*. Cancer Epidemiology Biomarkers & Prevention. **7**(12): 1133-1144.

145. Hollosi, P, Yakushij, JK, Fong, KSK, Csiszar, K and Fong, SFT. 2009. *Lysyl oxidase-like 2 promotes migration in noninvasive breast cancer cells but not in normal breast epithelial cells*. International Journal of Cancer. **125**(2): 318-327.

146. Dinca, SC, Greiner, D, Weidenfeld, K, Bond, L, Barkan, D and Jorcyk, CL. 2021. *Novel mechanism for osm-promoted extracellular matrix remodeling in breast cancer: Loxl2 upregulation and subsequent ecm alignment*. Breast Cancer Research. **23**(56): 1-18.

147. Ahn, SG, Dong, SM, Oshima, A, Kim, WH, Lee, HM, Lee, SA, Kwon, SH, Lee, JH, Lee, JM, Jeong, J, Lee, HD and Green, JE. 2013. *Loxl2 expression is associated with invasiveness and negatively influences survival in breast cancer patients*. Breast Cancer Research and Treatment. **141**(1): 89-99.

148. Barker, HE, Chang, J, Cox, TR, Lang, G, Bird, D, Nicolau, M, Evans, HR, Gartland, A and Erler, JT. 2011. *Loxl2-mediated matrix remodeling in metastasis and mammary gland involution*. Cancer Research. **71**(5): 1561-1572.

149. Chang, J, Lucas, MC, Leonte, LE, Garcia-Montolio, M, Singh, LB, Findlay, AD, Deodhar, M, Foot, JS, Jarolimek, W, Timpson, P, Erler, JT and Cox, TR. 2017. *Pre-clinical evaluation of small molecule loxl2 inhibitors in breast cancer*. Oncotarget. **8**(16): 26066-26078.

150. Wong, CC-L, Tse, AP-W, Huang, Y-P, Zhu, Y-T, Chiu, DK-C, Lai, RK-H, Au, SL-K, Kai, AK-L, Lee, JM-F, Wei, LL, Tsang, FH-C, Lo, RC-L, Shi, J, Zheng, Y-P, Wong, C-M and Ng, IO-L. 2014. *Lysyl oxidase-like 2 is critical to tumor microenvironment and metastatic niche formation in hepatocellular carcinoma*. Hepatology. **60**(5): 1645-1658.

151. Wu, SF, Zheng, QD, Xing, XX, Dong, YY, Wang, YH, You, Y, Chen, RX, Hu, C, Chen, J, Gao, DM, Zhao, Y, Wang, ZM, Xue, TC, Ren, ZG and Cui, JF. 2018. *Matrix stiffness-upregulated loxl2 promotes fibronectin production, mmp9 and cxcl12 expression and bmdcs recruitment to assist pre-metastatic niche formation*. Journal of Experimental & Clinical Cancer Research. **37**(99): 1-12.

152. Weidenfeld, K, Schif-Zuck, S, Abu-Tayeh, H, Kang, K, Kessler, O, Weissmann, M, Neufeld, G and Barkan, D. 2016. *Dormant tumor cells expressing loxl2 acquire a stem-like phenotype mediating their transition to proliferative growth*. Oncotarget. **7**(44): 71362-71377.

153. Chang, J, Nicolau, MM, Cox, TR, Wetterskog, D, Martens, JWM, Barker, HE and Erler, JT. 2013. *Loxl2 induces aberrant acinar morphogenesis via erbb2 signaling*. Breast Cancer Research. **15**(4): R67-R85.

154. Moreno-Bueno, G, Salvador, F, Martin, A, Floristan, A, Cuevas, EP, Santos, V, Montes, A, Morales, S, Castilla, MA, Rojo-Sebastian, A, Martinez, A, Hardisson, D, Csiszar, K, Portillo, F, Peinado, H, Palacios, J and Cano, A. 2011. *Lysyl oxidase-like 2 (loxl2), a new regulator of cell polarity required for metastatic dissemination of basal-like breast carcinomas*. Embo Molecular Medicine. **3**(9): 528-544.

155. Wang, YH, Xu, XT, Zhao, P, Tong, B, Wei, ZF and Dai, Y. 2016. *Escin ia suppresses the metastasis of triple-negative breast cancer by inhibiting epithelial-mesenchymal transition via down-regulating loxl2 expression*. Oncotarget. **7**(17): 23684-23699.

156. Cuevas, EP, Eraso, P, Mazon, MJ, Santos, V, Moreno-Bueno, G, Cano, A and Portillo, F. 2017. *Loxl2 drives epithelial-mesenchymal transition via activation of ire1-xbp1 signalling pathway*. Scientific Reports. **7**(1): 44988-44999.

157. Peinado, H, Iglesias-de la Cruz, MD, Olmeda, D, Csiszar, K, Fong, KSK, Vega, S, Nieto, MA, Cano, A and Portillo, F. 2005. *A molecular role for lysyl oxidase-like 2 enzyme in snail regulation and tumor progression*. Embo Journal. **24**(19): 3446-3458.

158. Han, W, Chen, S, Yuan, W, Fan, Q, Tian, J, Wang, X, Chen, L, Zhang, X, Wei, W, Liu, R, Qu, J, Jiao, Y, Austin, RH and Liu, L. 2016. *Oriented collagen fibers direct tumor cell intravasation*. Proceedings of the National Academy of Sciences of the United States of America. **113**(40): 11208-11213.

159. Yaffe, MJ. 2008. *Mammographic density - measurement of mammographic density*. Breast Cancer Research. **10**(209): 1-10.

160. Roeder, BA, Kokini, K, Sturgis, JE, Robinson, JP and Voytik-Harbin, SL. 2002. *Tensile mechanical properties of three-dimensional type i collagen extracellular matrices with varied microstructure*. Journal of Biomechanical Engineering-Transactions of the Asme. **124**(2): 214-222.

161. Roell, KR, Reif, DM and Motsinger-Reif, AA. 2017. *An introduction to terminology and methodology of chemical synergy—perspectives from across disciplines*. Frontiers in Pharmacology. **8**(158): 1-11.

162. Tawara, K, Scott, H, Emathinger, J, Wolf, C, LaJoie, D, Hedeen, D, Bond, L, Montgomery, P and Jorcyk, C. 2019. *High expression of osm and il-6 are associated with decreased breast cancer survival: Synergistic induction of il-6 secretion by osm and il-1beta*. Oncotarget. **10**(21): 2068-2085.

163. Bernard, C, Merval, R, Lebret, M, Delerive, P, Dusanter-Fourt, I, Lehoux, S, Creminon, C, Staels, B, Maclouf, J and Tedgui, A. 1999. *Oncostatin m induces interleukin-6 and cyclooxygenase-2 expression in human vascular smooth muscle cells - synergy with interleukin-1 beta*. Circulation Research. **85**(12): 1124-1131.

164. Bachireddy, P, Bendapudi, PK and Felsher, DW. 2005. *Getting at myc through ras*. Clinical Cancer Research. **11**(12): 4278-4281.

165. Dang, CV. 2012. *Myc on the path to cancer*. Cell. **149**(1): 22-35.

166. Choi, JW, Schroeder, MA, Sarkaria, JN and Bram, RJ. 2014. *Cyclophilin b supports myc and mutant p53-dependent survival of glioblastoma multiforme cells*. Cancer Research. **74**(2): 484-496.

167. Armelin, HA, Armelin, MCS, Kelly, K, Stewart, T, Leder, P, Cochran, BH and Stiles, CD. 1984. *Functional-role for c-myc in mitogenic response to platelet-derived growth-factor*. Nature. **310**(5979): 655-660.

168. Gartel, AL, Ye, X, Goufman, E, Shianov, P, Hay, N, Najmabadi, F and Tyner, AL. 2001. *Myc represses the p21(waf1/cip1) promoter and interacts with sp1/sp3*. Proc Natl Acad Sci U S A. **98**(8): 4510-4515.

169. Fallah, Y, Brundage, J, Allegakoen, P and Shajahan-Haq, AN. 2017. *Myc-driven pathways in breast cancer subtypes*. *Biomolecules*.

170. Heinrich, PC, Behrmann, I, Haan, S, Hermanns, HM, Muller-Newen, G and Schaper, F. 2003. *Principles of interleukin (il)-6-type cytokine signalling and its regulation*. Biochemical Journal. **374**(1): 1-20.

171. Liu, JW, Hadjokas, N, Mosley, B, Estrov, Z, Spence, MJ and Vestal, RE. 1998. *Oncostatin m-specific receptor expression and function in regulating cell proliferation of normal and malignant mammary epithelial cells*. Cytokine. **10**(4): 295-302.

172. Junk, DJ, Bryson, BL, Smigiel, JM, Parameswaran, N, Bartel, CA and Jackson, MW. 2017. *Oncostatin m promotes cancer cell plasticity through cooperative stat3-smad3 signaling*. Oncogene. **36**(28): 4001-4013.

173. Douglas, AM, Grant, SL, Goss, GA, Clouston, DR, Sutherland, RL and Begley, CG. 1998. *Oncostatin m induces the differentiation of breast cancer cells*. International Journal of Cancer. **75**(1): 64-73.

174. Tawara, K, Bolin, C, Sutherland, C, Anderson, RL and Jorcyk, CL. 2011. *A role for oncostatin m in breast cancer metastasis to bone*. Clinical & Experimental Metastasis. **28**(2): 190-191.

175. Bonnans, C, Chou, J and Werb, Z. 2014. *Remodelling the extracellular matrix in development and disease*. Nature Reviews Molecular Cell Biology. **15**(12): 786-801.

176. Li, J, Lau, GKK, Chen, LL, Dong, SS, Lan, HY, Huang, XR, Li, Y, Luk, JM, Yuan, YF and Guan, XY. 2011. *Interleukin 17a promotes hepatocellular carcinoma metastasis via nf-kb induced matrix metalloproteinases 2 and 9 expression*. Plos One. **6**(7): e21816-e21825.

177. Tsai, CY, Wang, CS, Tsai, MM, Chi, HC, Cheng, WL, Tseng, YH, Chen, CY, Lin, CD, Wu, JI, Wang, LH and Lin, KH. 2014. *Interleukin-32 increases human gastric cancer cell invasion associated with tumor progression and metastasis*. Clinical Cancer Research. **20**(9): 2276-2288.

178. Ma, JH, Qin, L and Li, X. 2020. *Role of stat3 signaling pathway in breast cancer*. Cell Communication and Signaling. **18**(33): 1-13.

179. Barry-Hamilton, V, Spangler, R, Marshall, D, McCauley, S, Rodriguez, HM, Oyasu, M, Mikels, A, Vaysberg, M, Ghermazien, H, Wai, C, Garcia, CA, Velayo, AC, Jorgensen, B, Biermann, D, Tsai, D, Green, J, Zaffryar-Eilot, S, Holzer, A, Ogg, S, Thai, D, Neufeld, G, Van Vlasselaer, P and Smith, V. 2010. *Allosteric inhibition of lysyl oxidase-like-2 impedes the development of a pathologic microenvironment*. Nature Medicine. **16**(9): 1009-U1107.

180. Kirschmann, DA, Seftor, EA, Fong, SFT, Nieva, DRC, Sullivan, CM, Edwards, EM, Sommer, P, Csiszar, K and Hendrix, MJC. 2002. *A molecular role for lysyl oxidase in breast cancer invasion*. Cancer Research. **62**(15): 4478-4483.

181. Blockhuys, S and Wittung-Stafshede, P. 2017. *Roles of copper-binding proteins in breast cancer*. International Journal of Molecular Sciences. **18.4**(871): 1-10.

182. Csiszar, K. 2001. *Lysyl oxidases: A novel multifunctional amine oxidase family*. Progress in Nucleic Acid Research and Molecular Biology. **70**(1): 1-32.

183. Kober, KI, Cano, A, Geraud, C, Sipila, K, Mobasseri, SA, Philippeos, C, Pisco, AO, Stannard, A, Martin, A, Salvador, F, Santos, V, Boutros, M, Rognoni, E and Watt, FM. 2018. *Loxl2 is dispensable for dermal development, homeostasis and tumour stroma formation*. Plos One. **13**(6): e0199679-e0199697.

184. Virtanen, P, Gommers, R, Oliphant, TE, Haberland, M, Reddy, T, Cournapeau, D, Burovski, E, Peterson, P, Weckesser, W, Bright, J, van der Walt, SJ, Brett, M, Wilson, J, Millman, KJ, Mayorov, N, Nelson, ARJ, Jones, E, Kern, R, Larson, E, Carey, CJ, Polat, I, Feng, Y, Moore, EW, VanderPlas, J, Laxalde, D, Perktold, J, Cimrman, R, Henriksen, I, Quintero, EA, Harris, CR, Archibald, AM, Ribeiro, ANH, Pedregosa, F, van Mulbregt, P and SciPy, C. 2020. *Scipy 1.0: Fundamental algorithms for scientific computing in python*. Nature Methods. **17**(3): 261-272.

185. Hothorn, T and Lausen, B. 2003. *On the exact distribution of maximally selected rank statistics*. Computational Statistics & Data Analysis. **43**(2): 121-137.

186. Aranda, PS, LaJoie, DM and Jorcyk, CL. 2012. *Bleach gel: A simple agarose gel for analyzing rna quality*. Electrophoresis. **33**(2): 366-369.

187. Palamakumbura, AH and Trackman, PC. 2002. *A fluorometric assay for detection of lysyl oxidase enzyme activity in biological samples*. Analytical Biochemistry. **300**(2): 245-251.

188. Barritault, D, Expertbezancon, A, Guerin, MF and Hayes, D. 1976. *Use of acetone precipitation in isolation of ribosomal-proteins*. European Journal of Biochemistry. **63**(1): 131-135.

189. Suzuki, K, Bose, P, Leong-Quong, RY, Fujita, DJ and Riabowol, K. 2010. *Reap: A two minute cell fractionation method*. BMC research notes. **3**(294): 1-6.

190. de Jong, OG, van Balkom, BWM, Gremmels, H and Verhaar, MC. 2016. *Exosomes from hypoxic endothelial cells have increased collagen crosslinking activity through up-regulation of lysyl oxidase-like 2*. Journal of Cellular and Molecular Medicine. **20**(2): 342-350.

191. Barker, HE, Bird, D, Lang, G and Erler, JT. 2013. *Tumor-secreted loxl2 activates fibroblasts through fak signaling*. Molecular Cancer Research. **11**(11): 1425-1436.

192. Brightman, AO, Rajwa, BP, Sturgis, JE, McCallister, ME, Robinson, JP and Voytik-Harbin, SL. 2000. *Time-lapse confocal reflection microscopy of collagen fibrillogenesis and extracellular matrix assembly in vitro*. Biopolymers. **54**(3): 222-234.

193. Kaufman, LJ, Brangwynne, CP, Kasza, KE, Filippidi, E, Gordon, VD, Deisboeck, TS and Weitz, DA. 2005. *Glioma expansion in collagen i matrices: Analyzing collagen concentration-dependent growth and motility patterns*. Biophysical Journal. **89**(1): 635-650.

194. Lan, YW, Theng, SM, Huang, TT, Choo, KB, Chen, CM, Kuo, HP and Chong, KY. 2017. *Oncostatin m-preconditioned mesenchymal stem cells alleviate bleomycin-induced pulmonary fibrosis through paracrine effects of the hepatocyte growth factor*. Stem Cells Translational Medicine. **6**(3): 1006-1017.

195. Kamiya, A, Kinoshita, T, Ito, Y, Matsui, T, Morikawa, Y, Senba, E, Nakashima, K, Taga, T, Yoshida, K, Kishimoto, T and Miyajima, A. 1999. *Fetal liver development requires a paracrine action of oncostatin m through the gp130 signal transducer*. Embo Journal. **18**(8): 2127-2136.

196. Akoglu, H. 2018. *User's guide to correlation coefficients*. Turkish Journal of Emergency Medicine. **18**(3): 91-93.

197. Neve, RM, Chin, K, Fridlyand, J, Yeh, J, Baehner, FL, Fevr, T, Clark, L, Bayani, N, Coppe, JP, Tong, F, Speed, T, Spellman, PT, DeVries, S, Lapuk, A, Wang, NJ, Kuo, WL, Stilwell, JL, Pinkel, D, Albertson, DG, Waldman, FM, McCormick, F, Dickson, RB, Johnson, MD, Lippman, M, Ethier, S, Gazdar, A and Gray, JW. 2006. *A collection of breast cancer cell lines for the study of functionally distinct cancer subtypes*. Cancer Cell. **10**(6): 515-527.

198. Wagnerand, M and Wiig, H. 2015. *Tumor interstitial fluid formation, characterization, and clinical implications*. Frontiers in Oncology. **5**(115): 1-12.

199. Underhill-Day, N and Heath, JK. 2006. *Oncostatin m (osm) cytostasis of breast tumor cells: Characterization of an osm receptor beta-specific kernel*. Cancer Research. **66**(22): 10891-10901.

200. May, CD, Sphyris, N, Evans, KW, Werden, SJ, Guo, W and Mani, SA. 2011. *Epithelial-mesenchymal transition and cancer stem cells: A dangerously dynamic duo in breast cancer progression*. Breast Cancer Research. **13**(202): 1-10.

201. Kim, Y-M, Kim, E-C and Kim, Y. 2011. *The human lysyl oxidase-like 2 protein functions as an amine oxidase toward collagen and elastin*. Molecular Biology Reports. **38**(1): 145-149.

202. Shukla, VC, Higuita-Castro, N, Nana-Sinkam, P and Ghadiali, SN. 2016. *Substrate stiffness modulates lung cancer cell migration but not epithelial to mesenchymal transition*. Journal of Biomedical Materials Research Part A. **104**(5): 1182-1193.

203. Kucia-Tran, JA, Tulkki, V, Smith, S, Scarpini, CG, Hughes, K, Araujo, AM, Yan, KYM, Botthof, J, Perez-Gomez, E, Quintanilla, M, Cuschieri, K, Caffarel, MM and Coleman, N. 2016. *Overexpression of the oncostatin-m receptor in cervical squamous cell carcinoma is associated with epithelial-mesenchymal transition and poor overall survival*. British Journal of Cancer. **115**(2): 212-222.

204. Li, Q, Zhu, J, Sun, F, Liu, L, Liu, X and Yue, Y. 2011. *Oncostatin m promotes proliferation of ovarian cancer cells through signal transducer and activator of transcription 3*. International Journal of Molecular Medicine. **28**(1): 101-108.

205. Smith, DA, Kiba, A, Zong, Y and Witte, ON. 2013. *Interleukin-6 and oncostatin-m synergize with the pi3k/akt pathway to promote aggressive prostate malignancy in mouse and human tissues*. Molecular Cancer Research. **11**(10): 1159-1165.

206. Wang, M-L, Pan, C-M, Chiou, S-H, Chen, W-H, Chang, H-Y, Lee, OK-S, Hsu, H-S and Wu, C-W. 2012. *Oncostatin m modulates the mesenchymal-epithelial transition of lung adenocarcinoma cells by a mesenchymal stem cell-mediated paracrine effect*. Cancer Research. **72**(22): 6051-6064.

207. Ikenaga, N, Peng, ZW, Vaid, KA, Liu, SB, Yoshida, S, Sverdlov, DY, Mikels-Vigdal, A, Smith, V, Schuppan, D and Popov, YV. 2017. *Selective targeting of lysyl oxidase-like 2 (loxl2) suppresses hepatic fibrosis progression and accelerates its reversal*. Gut. **66**(9): 1697-1708.

208. Langford, DJ, Bailey, AL, Chanda, ML, Clarke, SE, Drummond, TE, Echols, S, Glick, S, Ingrao, J, Klassen-Ross, T, LaCroix-Fralish, ML, Matsumiya, L, Sorge, RE, Sotocinal, SG, Tabaka, JM, Wong, D, van den Maagdenberg, A, Ferrari, MD, Craig, KD and Mogil, JS. 2010. *Coding of facial expressions of pain in the laboratory mouse*. Nature Methods. **7**(6): 447-U452.

209. Tomayko, MM and Reynolds, CP. 1989. *Determination of subcutaneous tumor size in athymic (nude) mice*. Cancer Chemotherapy and Pharmacology. **24**(3): 148-154.

210. Angelici, B, Mailand, E, Haefliger, B and Benenson, Y. 2016. *Synthetic biology platform for sensing and integrating endogenous transcriptional inputs in mammalian cells*. Cell Reports. **16**(9): 2525-2537.

211. Li, YS, Zhang, HY, Zhao, Y, Wang, CY, Cheng, ZG, Tang, LN, Gao, YL, Liu, FR, Li, JB, Li, Y, Geng, NX, Rui, X, Teng, YE, Liu, YP, Cao, L, Kumar, R, Jin, F and Li, F. 2019. *A mandatory role of nuclear pak4-lifr axis in breast-to-bone metastasis of er alpha-positive breast cancer cells*. Oncogene. **38**(6): 808-821.

212. Levin-Allerhand, JA, Sokol, K and Smith, JD. 2003. *Safe and effective method for chronic 17 beta-estradiol administration to mice*. Contemporary Topics in Laboratory Animal Science. **42**(6): 33-35.

213. Hoermann, G, Cerny-Reiterer, S, Herrmann, H, Blatt, K, Bilban, M, Gisslinger, H, Gisslinger, B, Müllauer, L, Kralovics, R, Mannhalter, C, Valent, P and Mayerhofer, M. 2012. *Identification of oncostatin m as a jak2 v617f-dependent amplifier of cytokine production and bone marrow remodeling in myeloproliferative neoplasms*. Federation of American Societies for Experimental Biology Journal. **26**(2): 894-906.

214. Junk, DJ, Bryson, BL and Jackson, MW. 2014. *Hijak'd signaling; the stat3 paradox in senescence and cancer progression*. Cancers. **6**(2): 741-755.

215. Hu, L, Zhu, YT, Qi, C and Zhu, Y-J. 2009. *Identification of smyd4 as a potential tumor suppressor gene involved in breast cancer development*. Cancer Research. **69**(9): 4067-4072.

216. Johnson, CH, Manna, SK, Krausz, KW, Bonzo, JA, Divelbiss, RD, Hollingshead, MG and Gonzalez, FJ. 2013. *Global metabolomics reveals urinary biomarkers of breast cancer in a mcf-7 xenograft mouse model*. Metabolites. **3**(3): 658-672.

217. Iorns, E, Drews-Elger, K, Ward, TM, Dean, S, Clarke, J, Berry, D, El Ashry, D and Lippman, M. 2012. *A new mouse model for the study of human breast cancer metastasis*. Plos One. **7**(10): e47995-e48003.

APPENDIX A

Chapter 2 Supplemental Figures

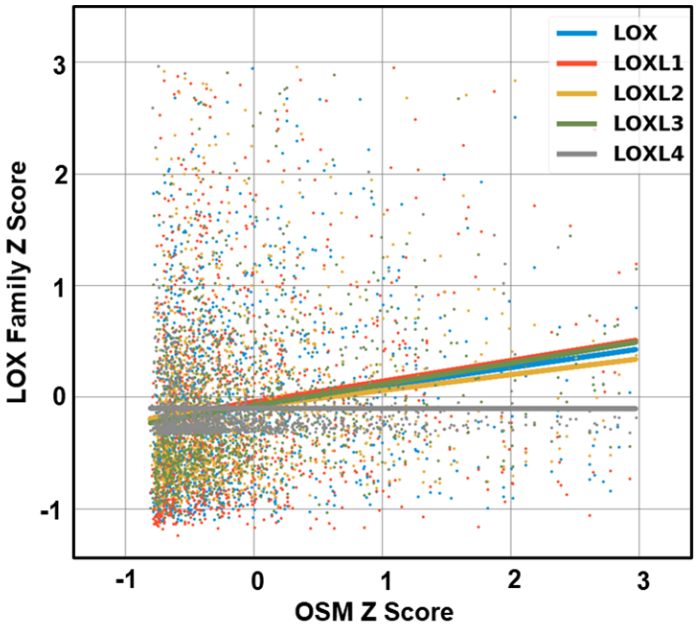

Protein	Patients	Pearson Coeff.	P-Value	Slope	95% CI
LOX	n=1048	0.1496	$3.09*10^{-07}$	0.166	0.1 – 0.23
LOXL1	n=1051	0.151	$2.22*10^{-07}$	0.186	0.12 – 0.26
LOXL2	n=1044	0.139	$2.02*10^{-06}$	0.142	0.08 – 0.2
LOXL3	n=1050	0.209	$5.34*10^{-13}$	0.191	0.14 – 0.24
LOXL4	n=1048	-0.002	0.951	-0.001	-0.03 – 0.03

Supp Figure A.1 OSM mRNA Expression Positively Correlates to Lysyl Oxidase mRNA Expression in Breast Cancer Biopsies.

The Cancer Genome Atlas (TCGA) breast cancer patient RNA-Seq database was used to compare lysyl oxidase family (LOX and LOXL1-4) mRNA expression to OSM mRNA expression in breast cancer patients. All the lysyl oxidase mRNA had a significant positive correlation to OSM mRNA, except for LOXL4, which had no correlation. The table below the plot details the n-value, Pearson coefficient and its P-value, linear regression slope and its 95% CI for all lysyl oxidases being analyzed. (Log Rank Test/ Least Squares Regression).

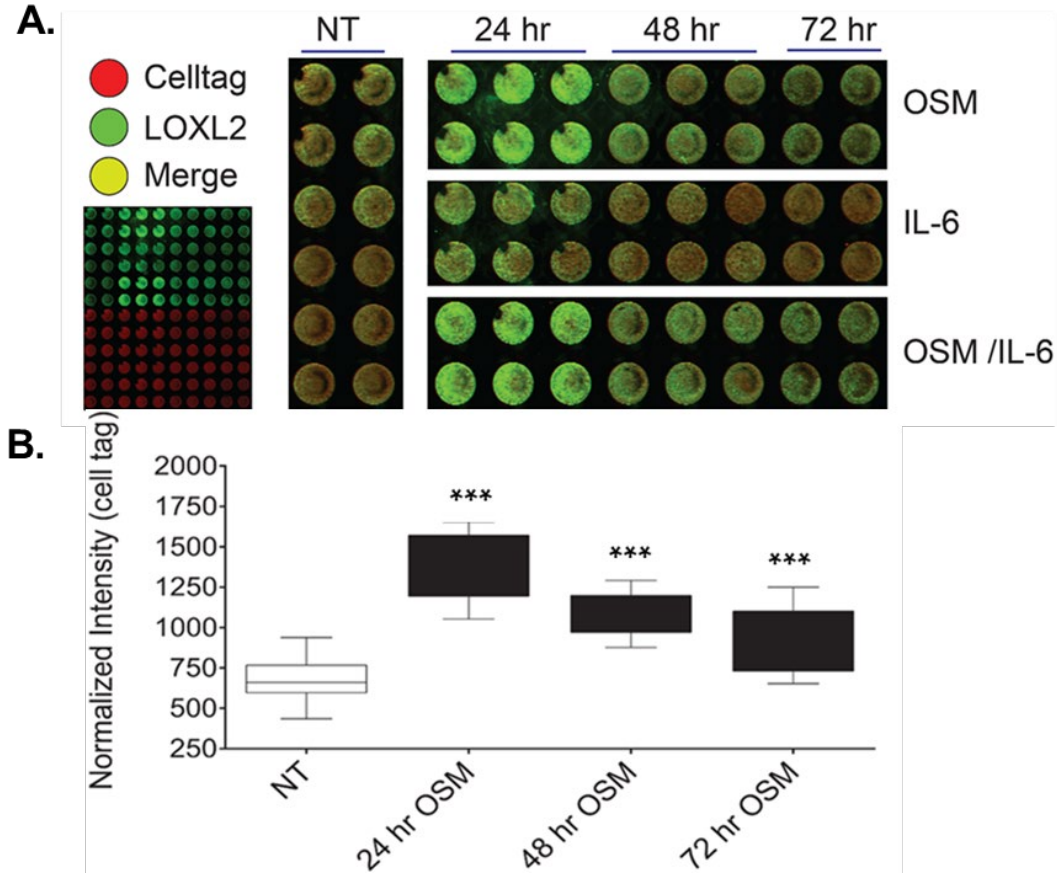

Supp Figure A.2 Optimal OSM-Induced LOXL2 Protein Expression is Achieved at 24 Hours.

In **A.** Image of Cell Tag normalization (red) and LOXL2 fluorescence (green) derived from In-cell Western analysis of MCF7 cells exposed to OSM for 24, 48, and 72 hours. The results highlight that OSM-induced LOXL2 is greatest after 24 hours post treatment. **B.** Graphical box-and-whisker plot representation of the level of LOXL2 protein fluorescence detected as compared to the non-treated controls, Cell Tag is used to normalize the data. (n=3; *** $p<0.001$; Student's t-test).

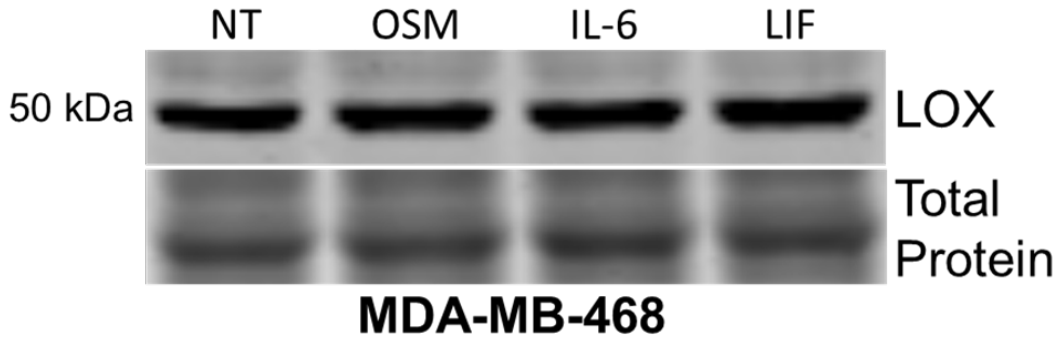

Supp Figure A.3 MDA-MB-468 Cells have High LOX Expression, not Suitable for LOXL2 Analysis.

Immunoblot analysis of MDA-MB-468 cell lysates after 24 hour OSM, IL-6, and LIF treatment does not change LOX expression, yet constitutively high levels of LOX protein is present. This presents problems as LOX enzymatic activity will mask and skew the results of the enzymatic activity of LOXL2 in this cell line. Therefore, moving forward MCF7 cells were utilized to determine the effect OSM-induced LOXL2 has on the ECM. (n=3).

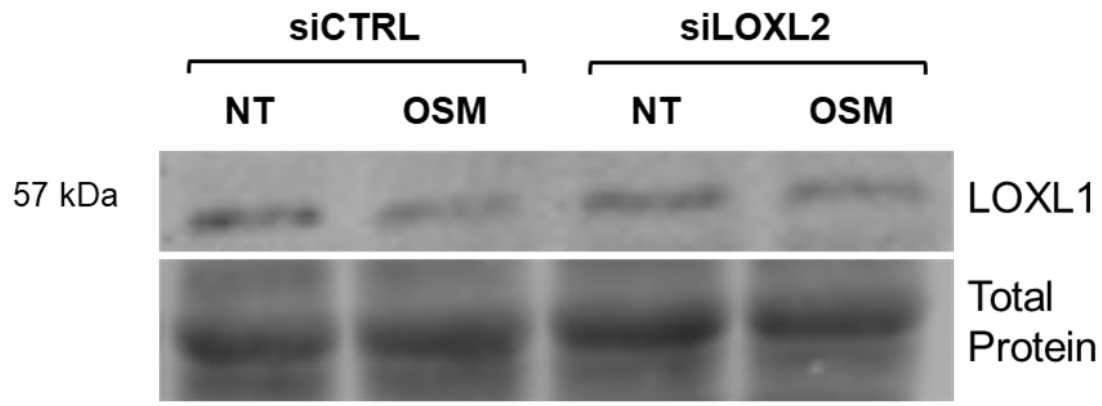

Supp Figure A.4 Inhibition of LOXL2 with siLOXL2 did not Promote Any Off Target LOXL1 inhibition.

Immunoblot analysis of MCF7 lysates collected after 48 hours of siCTRL and siLOXL2 transfection and 24 hours of OSM treatment. Treatment with OSM did not induce the expression of LOXL1, the only other lysyl oxidase detectable in MCF7 cells analyzed. The siLOXL2 exposed MCF7 cells showed no alteration in LOXL1 expression when compared against samples exposed to the siCTRL. Continued LOXL1 expression confirms that LOXL2 is the only lysyl oxidase mRNA that is targeted by the siLOXL2, this is because no other lysyl oxidase is detectable by immunoblot in MCF7 cells. (n=3).

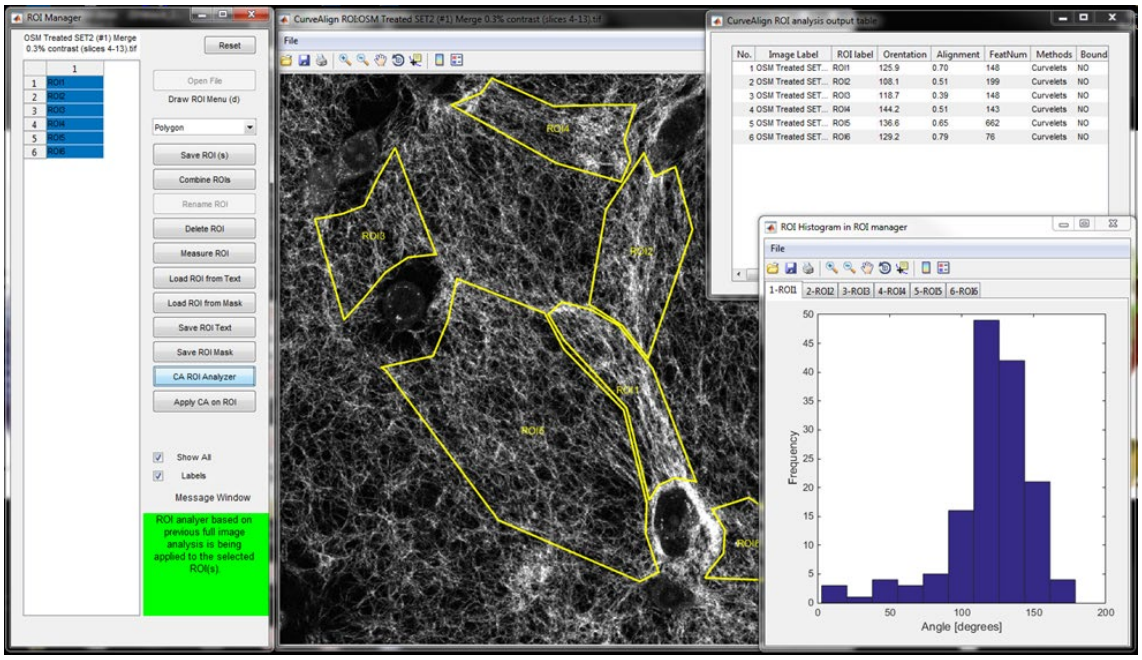

Supp Figure A.5 Representative Image of ROI Formation for Alignment Quantification of Collagen I Fibers.

To attain the relevant alignment data necessary, we created ROI's that encompassed bundles of fibers oriented in-between individual MCF7 cells, and perpendicular to the cell surface. CurveAlign4.0 full image analysis only looks at global alignment in images without ROI's; the ROIs are necessary because of the random MCF7 cell distribution and direction of alignment confuses the software. Attempts were made to follow natural curvature of fibers when forming ROI's. All experimental results are an aggregate of 4 technical replicates for each biological sample. (n=3).

APPENDIX B

Chapter 3 Supplemental Figures

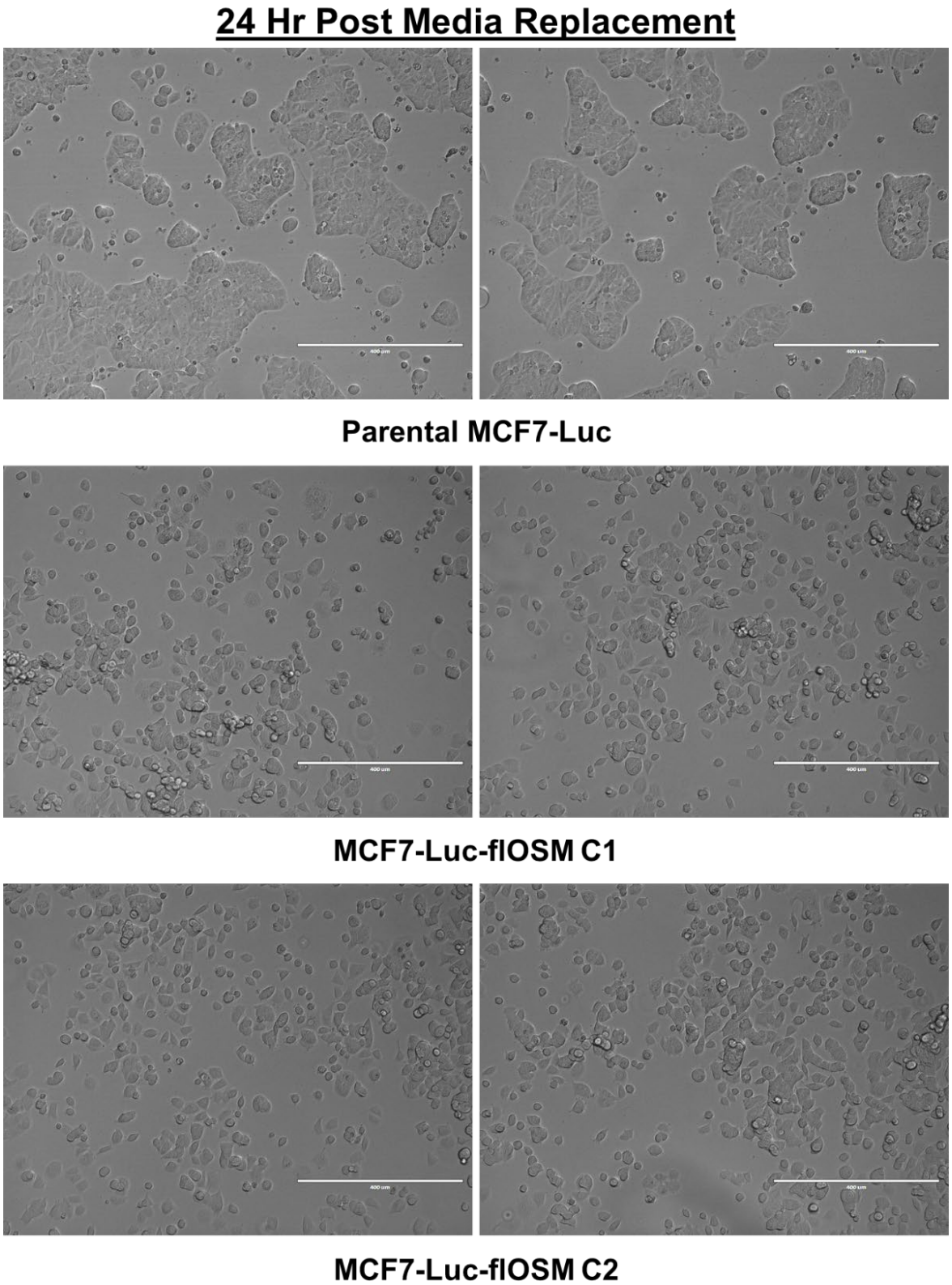

Supp Figure B.1 Morphology for MCF7-Luc-flOSM C1 and C2 Compared Against Untreated Parental MCF7-Luc.

Phenotype imaging using EVOS imaging station to determine the morphology of the transformed MCF7-Luc-flOSM colonies C1 and C2 with 250, 000 cells plated into a 12-well plate and with 1 mL of fresh media added and left to incubate for 24-hour incubation. The resulting morphology was compared against parental MCF7-Luc cells with no treatment but in 24-hour incubation in media, or with 25 ng/mL rhOSM treatment for 24-hours (not shown). C1 and C2 both have the morphology of MCF7-Luc cells that are treated with OSM for 24-hours or longer, this confirms that the cells behave as they should by reacting to OSM being constituently secreted in a similar manner to being treated with endogenous OSM. C1 and C2 were imaged while in freshly changed media as well to compare if their morphology reverts back towards the parental line did occur (not shown). (Each colony was imaged 2x for plating (n=3) of each colony or parental control).

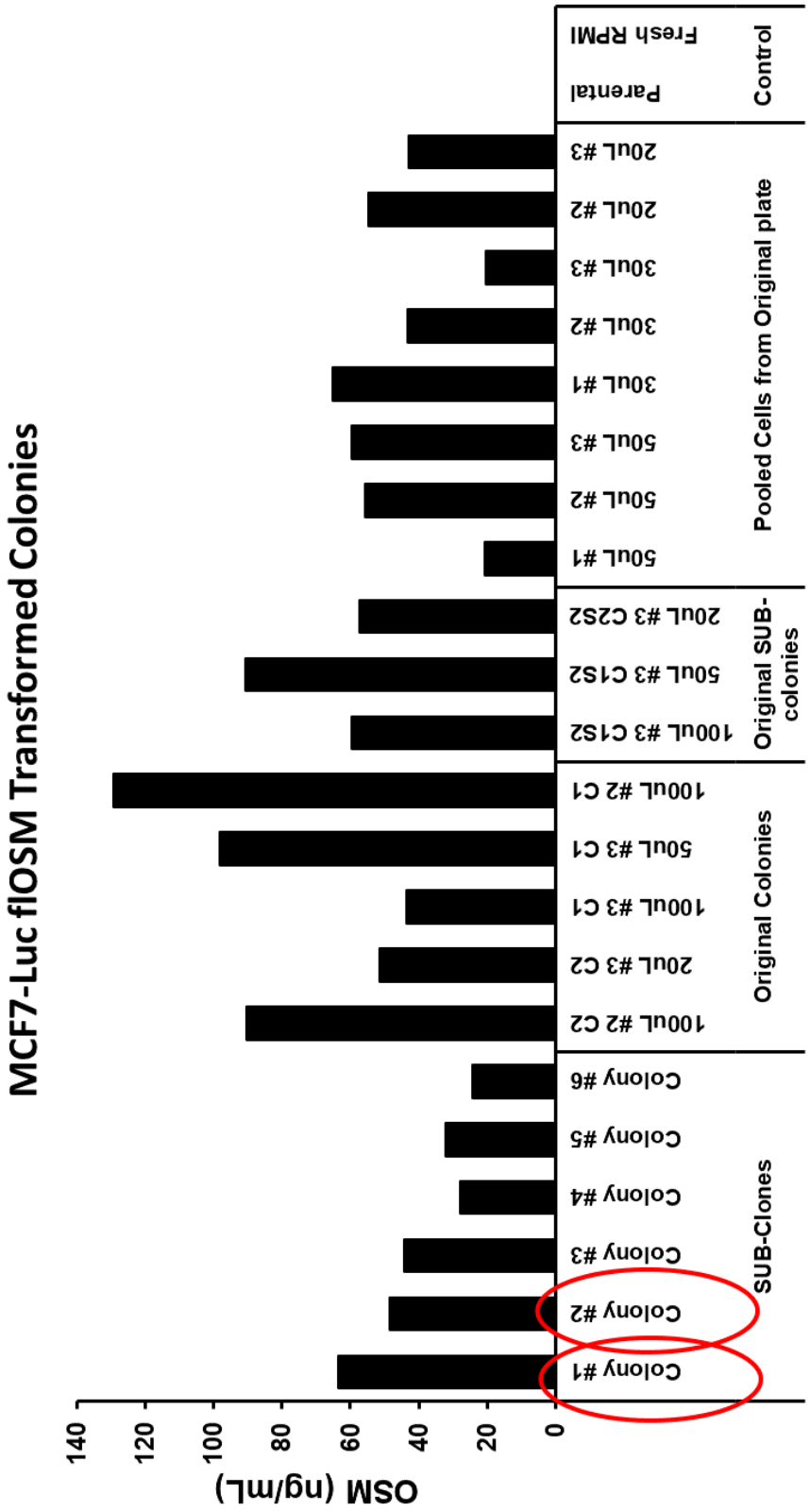

Supp Figure B.2 OSM Secreted by MCF7-Luc-flOSM Colonies with C1 and C2 Circled in Red.

Viable MCF7-Luc-flOSM colonies were isolated after being exposed to selection media for 30 to 60 days. Seeded at 250, 000 cells per well, in a 12-well plate with 1mL of media we incubated the cells for 24-hours prior to collecting the CM and running an OSM ELISA assays to determine concentration of secreted OSM and compare across the colonies. These colonies vary from pools of cells from the original transduction plate, to cell colonies that have been through several passes of isolation. Each pass cells forming a patch or clump of cells that was separate from neighboring cells would be scraped and transferred to a new well, this process was repeated 2 more times for Colony #1 through #6. The other colonies are labelled according to volume in (μL) of lentiviral particles added to the starting 96-well plate. The results depicted on the graph are all preliminary results and colonies expressed a range of OSM cytokines, from ~30 to ~130 ng/uL of OSM. C1 and C2 utilized in our Chapter 3 experiments were chosen because they produced an amount of OSM that hovered around 50 ng/mL. Though double the exogenous rhOSM we treat with, *in vivo* the concentration would be reduced due to proteases and other protein and cellular interactions that are not present *in vitro*. (All experiments n=1).

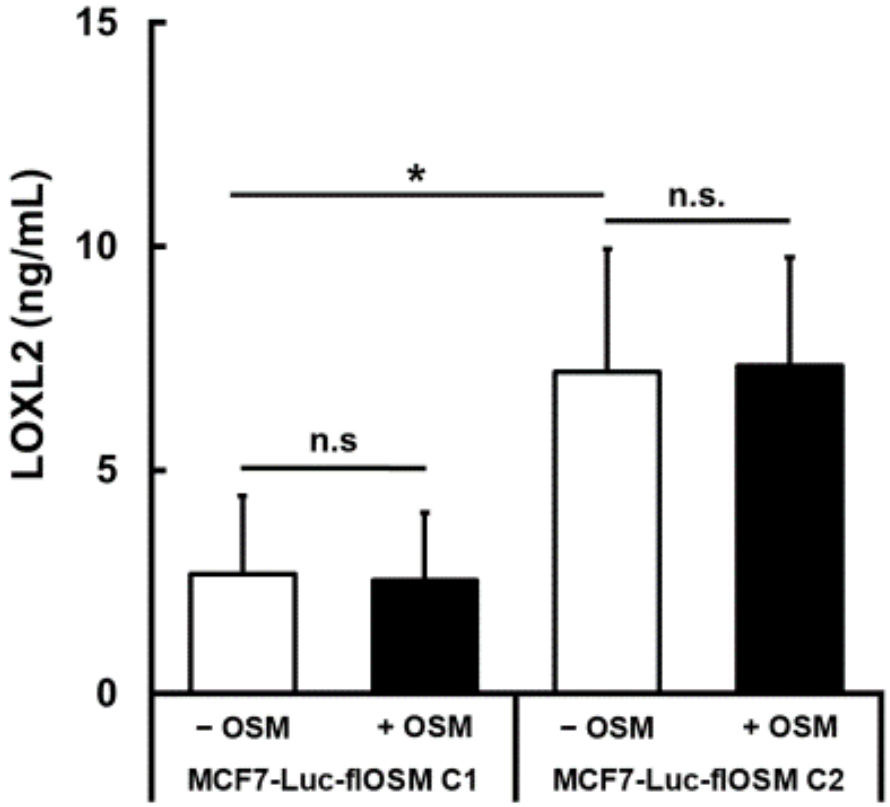

Supp Figure B.3 Endogenous rhOSM Added to MCF7-Luc-flOSM Colonies Could not Further Promote Gene Expression.

To confirm that MCF7-Luc-flOSM C1 and C2 secreted flOSM was effectively interacting with OSMR and transduction of the signal was efficient, LOXL2 expression and secretion was analyzed. To confirm constitutive OSM efficacy C1 and C2 were both plated at 250, 000 cells / well of a 12-well with 1 mL fresh complete media that were either left to produce constitutive OSM or treated with an additional 25 ng/mL of rhOSM. Collecting the CM, a LOXL2 quantitative ELISA was performed and the results were graphed showing that rhOSM did not increase LOXL2 secretion, indicating that the OSM produced by the MCF7-Luc-flOSM colonies was similarly effective at OSM signaling. (All experiments (n=3); not significant (n.s.) $p > 0.05$, * $p < 0.05$; One-way ANOVA).

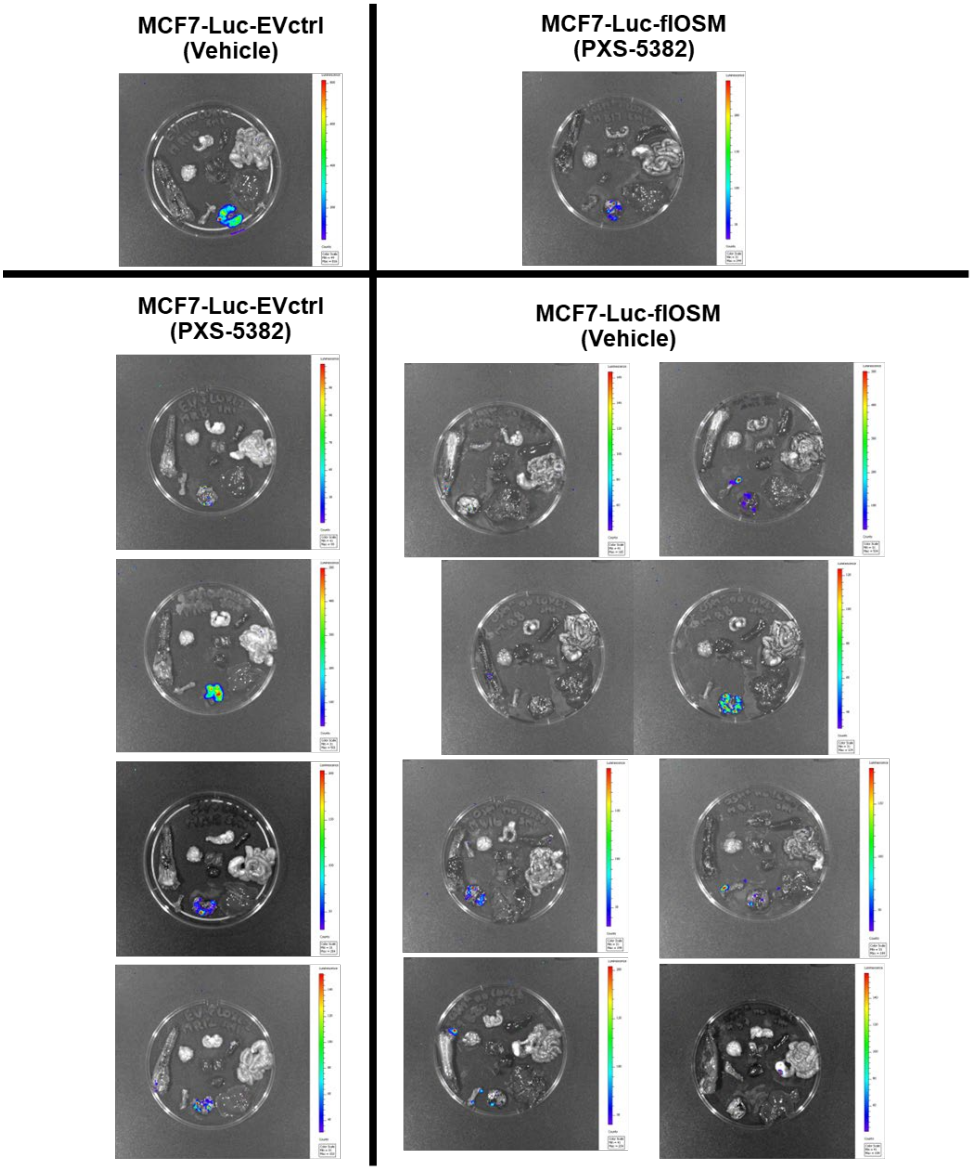

Supp Figure B.4 Raw Resected Organ *Ex Vivo* Bioluminescent Images.

The images in this figure are representative of all the bioluminescent images (BLI) that were taken during *ex vivo* imaging at the termination of Chapter 3 *in vivo* mouse model study. The images that were taken and show no bioluminescence were omitted for space, however the images are available for those curious. The metastases are resolved by the bioluminescent signal in each image, where blue end of spectrum correlates to a weaker signal intensity and red hues the stronger signal. The spread and intensity must be taken together to get the best idea of the amount of tumor cells present in each metastasis. The mice with metastases are separated according to the group from which they derive with 1

mouse with metastases in MCF7-Luc-flOSM [PXS-5382] and MCF7-Luc-EVctrl [Vehicle] groups. The MCF7-Luc-EVctrl [PXS-5382] group had 4 mice with metastasis detectable by BLI, while the MCF7-Luc-flOSM [Vehicle] group had the most mice with metastases detectable by BLI. (*Ex vivo* groups n=8 for flOSM, and n=9 for EVctrl).

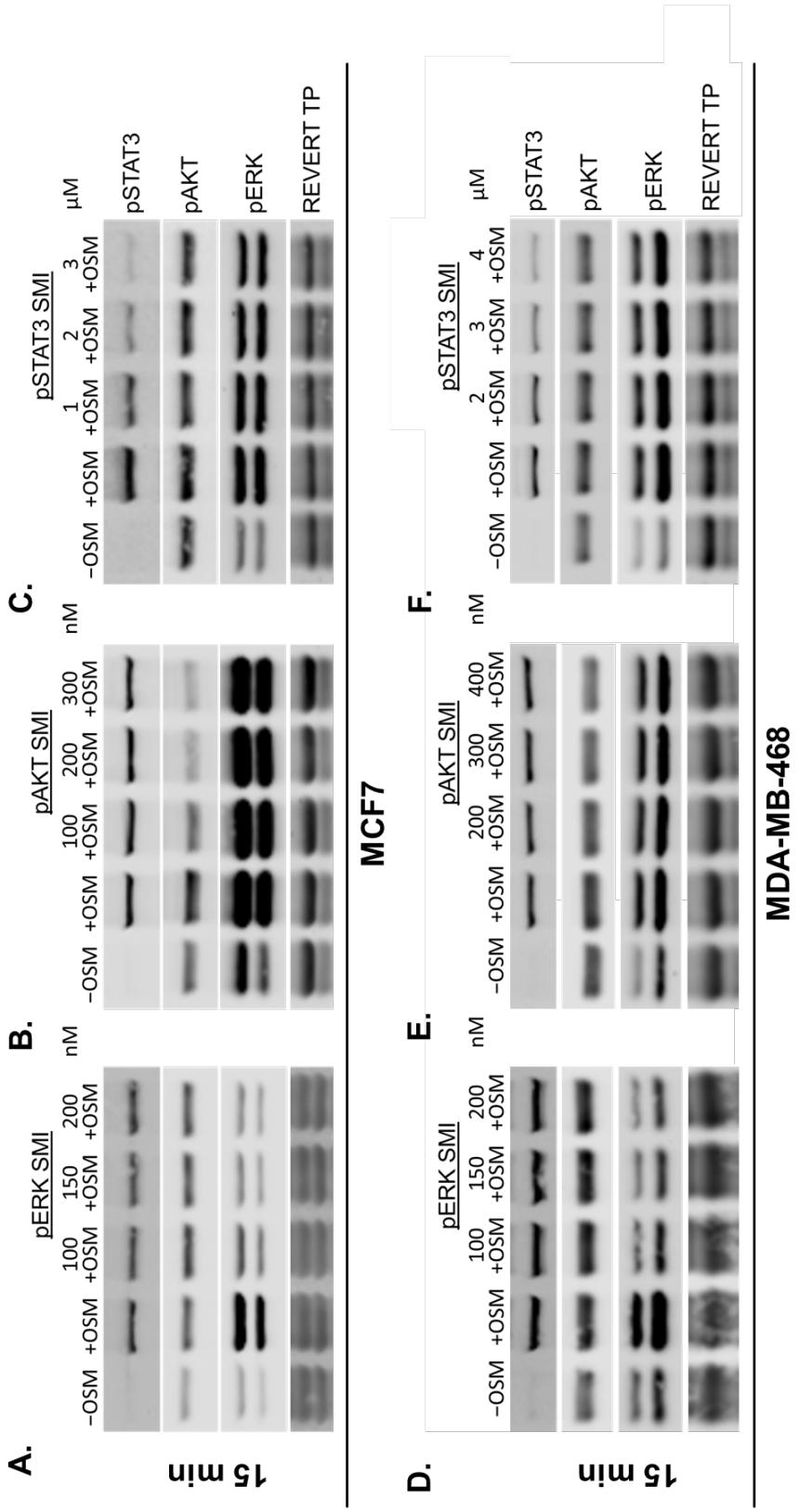

Supp Figure B.5 OSM Signaling Pathway Inhibitors Prevent Their Respective Phospho-Proteins from Phosphorylation and Activation.

A. MCF7 cells are incubated for 2-hours with a series of pERK SMI (PD0325901) concentrations 100 nM, 150 nM, and 200 nM before adding 25 ng/mL rhOSM treatment for 15-min. **B.** MCF7 cells are incubated for 2-hours with a series of pAKT SMI (GDC-0941) concentrations 100 nM, 200 nM, and 300 nM before adding 25 ng/mL rhOSM treatment for 15-min. **C.** MCF7 cells are incubated for 2-hours with a series of pSTAT3 SMI (Stattic) concentrations 1 μM, 2 μM, and 3 μM before adding 25 ng/mL rhOSM treatment for 15-min. **D.** MDA-MB-468 cells are incubated for 2-hours with a series of pERK SMI (PD0325901) concentrations 100 nM, 200 nM, and 300 nM before adding 25 ng/mL rhOSM treatment for 15-min. **E.** MDA-MB-468 cells are incubated for 2-hours with a series of pAKT SMI (GDC-0941) concentrations 200 nM, 300 nM, and 400nM before adding 25 ng/mL rhOSM treatment for 15-min. **F.** MDA-MB-468 cells are incubated for 2-hours with a series of pSTAT3 SMI (Stattic) concentrations 2 μM, 3 μM, and 4 μM before adding 25 ng/mL rhOSM treatment for 15-min. The immunoblots performed to determine whether the OSM canonical signal pathways were inhibited by the SMI's for pERK, pAKT, and pSTAT3 signal transduction. The results for pERK, pAKT, and pSTAT3 protein expression show that Each inhibitor worked in the inhibition of each respective pathway. (All experiments n=3).